Production of cold molecules via magnetically tunable Feshbach resonances

Thorsten Köhler and Krzysztof Góral

Clarendon Laboratory, Department of Physics, University of Oxford, Parks Road, Oxford OX1 3PU, United Kingdom

Paul S. Julienne

Atomic Physics Division, National Institute of Standards and Technology, 100 Bureau Drive Stop 8423, Gaithersburg, Maryland 20899-8423, USA

(Published 1 December 2006)

Magnetically tunable Feshbach resonances were employed to associate cold diatomic molecules in a series of experiments involving both atomic Bose and two-spin-component Fermi gases. This review illustrates theoretical concepts of both the particular nature of the highly excited Feshbach molecules produced and the techniques for their association from unbound atom pairs. Coupled-channels theory provides a rigorous formulation of the microscopic physics of Feshbach resonances in cold gases. Concepts of dressed versus bare energy states, universal properties of Feshbach molecules, and the classification in terms of entrance- and closed-channel-dominated resonances are introduced on the basis of practical two-channel approaches. Their significance is illustrated for several experimental observations, such as binding energies and lifetimes with respect to collisional relaxation. Molecular association and dissociation are discussed in the context of techniques involving linear magnetic-field sweeps in cold Bose and Fermi gases and pulse sequences leading to Ramsey-type interference fringes. Their descriptions in terms of Landau-Zener, two-level mean-field, as well as beyond mean-field approaches are reviewed in detail, including the associated ranges of validity.

DOI: 10.1103/RevModPhys.78.1311 PACS number(s): 03.75.Ss, 34.50.−s, 05.30.Jp

CONTENTS

I. INTRODUCTION

Resonances in general refer to the energy-dependent enhancement of interparticle collision cross sections due to the existence of a metastable state. Since the beginning of quantum mechanics, such phenomena have been the subject of numerous studies in nuclear (Blatt and Weisskopf, 1952) as well as atomic and molecular physics (Child, 1974; Bransden and Joachain, 2003). The metastable state may be described in terms of tunneling across a potential energy barrier or coupling a bound level of a subsystem to its environment (Rice, 1933; Fano, 1935, 1961; Feshbach, 1958, 1962). These scenarios are referred to as shape and Feshbach resonances, respectively.

In the context of cold atomic gases, collision phenomena associated with Feshbach resonances were first predicted for systems of spin-polarized hydrogen and deuterium (Stwalley, 1976; Uang and Stwalley, 1980) as well as lithium (Uang *et al.*, 1981) in the presence of magnetic fields. The associated resonance energies depend on the field strength via the Zeeman effect in the hyperfine levels. This research has gained new experimental perspectives since the achievement of Bose-Einstein condensation (Bose, 1924; Einstein, 1924, 1925) of dilute alkali atom vapors (Anderson *et al.*, 1995; Bradley *et al.* 1995, 1997; Davis *et al.*, 1995). Contrary to conventional gases, such atomic clouds with densities five orders of magnitude less than air and sub-μK temperatures give rise to binary collision energies close to the threshold between scattering and molecular binding. In this extraordinary regime, magnetically tunable Feshbach resonances can be employed to manipulate the interatomic forces determined by the scattering length (Tiesinga *et al.*, 1993), as well as for the production of diatomic molecules at rest (Timmermans *et al.*, 1999b).

Both techniques were demonstrated in several experiments with widespread applications throughout the physics of cold gases. Figure 1 illustrates the manipulation of the scattering length a in a ^{23}Na Bose-Einstein condensate exposed to a spatially homogeneous magnetic field of variable strength B (Inouye *et al.*, 1998). The pole in Fig. 1 at about 907 G[1] is due to the near degeneracy of the energy associated with a Feshbach resonance and the threshold. Such a singularity, usually referred to as a zero-energy resonance (Taylor, 1972),[2] allows the scattering length, in principle, to assume all values between $-\infty$ and ∞. Cold gases with such widely tunable interactions were subsequently realized for several species of alkali atoms, such as ^{85}Rb (Courteille *et al.*, 1998; Roberts *et al.*, 1998) and ^{133}Cs (Vuletic *et al.*, 1998; Chin *et al.*, 2003). Their applications involve the Bose-Einstein condensation of ^{85}Rb (Cornish *et al.*, 2000) and ^{133}Cs (Weber *et al.*, 2003) as well as studies of condensate collapse with negative scattering lengths

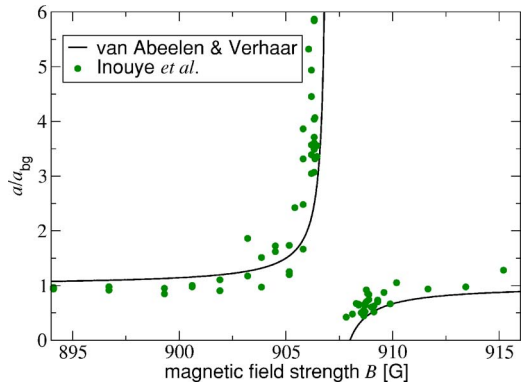

FIG. 1. (Color online) Order-of-magnitude variation of the scattering length a as a function of the magnetic-field strength B in the vicinity of the 907 G (90.7 mT) zero-energy resonance of ^{23}Na. Circles refer to measurements using sodium Bose-Einstein condensates (Inouye *et al.*, 1998), while the solid curve indicates associated theoretical predictions (van Abeelen and Verhaar, 1998). The scattering length is normalized to its asymptotic value a_{bg} away from the singularity at B_0=907 G. Adapted by permission from Macmillan Publishers Ltd: Nature (London) (Inouye *et al.*, 1998), copyright, 1998.

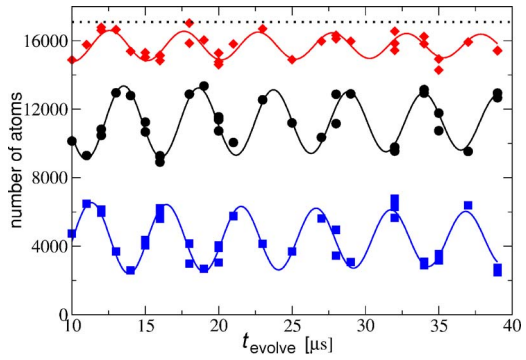

FIG. 2. (Color online) Ramsey fringes between atomic and molecular components produced from a Bose-Einstein condensate of 17 100 ^{85}Rb atoms (Donley *et al.*, 2002) via a sequence of magnetic-field pulses in the vicinity of the 155 G zero-energy resonance. Circles and squares are the number of particles in the remnant condensate and in an atomic burst consisting of correlated pairs with a comparatively high relative velocity, respectively. Diamonds indicate the total amount of particles in both of these components. The difference with respect to the total number of atoms (dotted line) indicates the production of undetected Feshbach molecules. Fringes are shown as a function of the delay time of the interferometer t_{evolve}, in which the atomic and molecular states acquire their phase difference. The fringe frequency provides an accurate measure of the binding energy (Claussen *et al.*, 2003). Adapted by permission from Macmillan Publishers Ltd: Nature (London) (Donley *et al.*, 2002), copyright, 2002.

[1]The Standard International unit for magnetic field is Tesla, whereas most of the papers quoted in this review use Gauss as the unit. Consequently, we use G here, where 1 G=10^{-4} T.

[2]In the context of cold gases, a singularity of the scattering length is also often referred to simply as a Feshbach resonance.

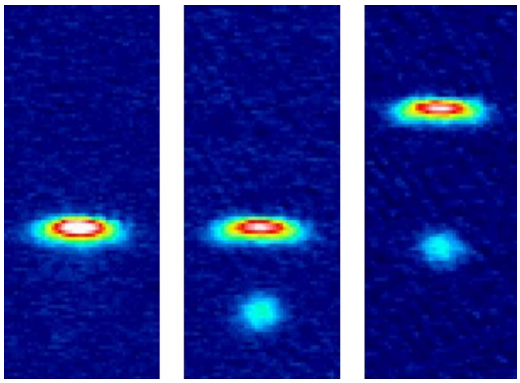

FIG. 3. (Color online) A molecular component of about 3000 dimers is out-coupled from a dilute cloud of 25 000 ground-state cesium atoms using Stern-Gerlach separation in an inhomogeneous magnetic field (Herbig *et al.*, 2003). Left and middle images are situations in which the magnetic field is calibrated such that it exactly compensates for the gravitational force acting on atoms in gases without and with a molecular component, respectively. Due to their magnetic moment difference of $-0.57\mu_{\mathrm{Bohr}}$ ($\mu_{\mathrm{Bohr}}=9.274\,009\,49\times10^{-24}$ J/T is the Bohr magneton) with respect to separated atoms, Feshbach molecules in the middle image drop below the atomic cloud, which is levitated and centered at the same position as in the left reference image. Conversely, the right image shows levitation of molecules and upward acceleration of separated atoms using a suitably adjusted inhomogeneous magnetic field.

(Roberts *et al.*, 2000a; Donley *et al.*, 2001).

Quite generally, the zero-energy resonance position coincides exactly with the field strength at which the energy of a diatomic vibrational bound state becomes degenerate with the threshold for dissociation into an atom pair at rest. For positive scattering lengths, this Feshbach molecular state describes a stable molecule in the absence of background gas collisions that ceases to exist at the position of the singularity. In the context of two-body systems involving the same species of atoms, such a bound state is usually referred to as a dimer. The relation between collision resonances above threshold and bound states below it links the manipulation of interactions to the molecular conversion of separated atom pairs.

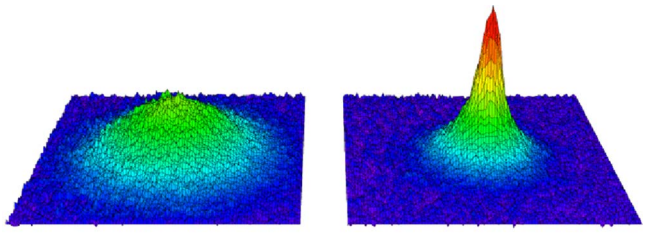

FIG. 4. (Color online) Density distributions of dilute thermal (left image) and partially Bose-Einstein condensed (right image) gases of $^{40}K_2$ Feshbach molecules (Greiner *et al.*, 2003). Both molecular vapors were produced using linear magnetic-field sweeps across the 202 G zero-energy resonance. The initial two-spin-component clouds of 470 000 and 250 000 Fermi atoms were prepared above (250 nK) and below (79 nK) the associated critical temperatures for condensation, respectively. The condensate fraction in the right image is 12%. Adapted by permission from Macmillan Publishers Ltd: Nature (London) (Greiner *et al.*, 2003), copyright, 2003.

Production of cold dimers was first demonstrated (Fioretti *et al.*, 1998; Nikolov *et al.*, 1999; Takekoshi *et al.*, 1999; Wynar *et al.*, 2000) via photoassociation of atoms (Weiner *et al.*, 1999). This achievement was followed by studies of condensed gases of ^{85}Rb exposed to time-dependent magnetic-field variations consisting of pulse pairs in the vicinity of the 155 G zero-energy resonance (Donley *et al.*, 2002). These experiments temporarily probed the strong interaction regime where the size of the scattering length was comparable to the average interatomic distance. Such perturbations led to the three distinct components of the gas illustrated in Fig. 2. The oscillatory behavior of their occupations as a function of the time delay between the pulses implied an interpretation in terms of Ramsey interference fringes due to a superposition state of separated atoms and Feshbach molecules.

According to Fig. 2, the pulse sequence allowed a conversion of up to about 16% of ^{85}Rb atoms into Feshbach molecules. Subsequent experiments improved the production efficiency using magnetic-field sweeps from negative to positive scattering lengths across a zero-energy resonance. This technique was applied to cold gases consisting of incoherent two-spin-component mixtures of either ^{40}K or ^{6}Li atoms (Cubizolles *et al.*, 2003; Jochim *et al.*, 2003a; Regal *et al.*, 2003a; Strecker *et al.*, 2003) as well as Bose-Einstein condensates of ^{133}Cs, ^{87}Rb, and ^{23}Na (Herbig *et al.*, 2003; Xu *et al.*, 2003; Dürr *et al.*, 2004). In these experiments, new schemes for the detection of Feshbach molecules were developed. These techniques involve radio-frequency (rf) photodissociation, atom loss and recovery, as well as the spatial separation of molecules from the remnant atomic cloud followed by their dissociation using magnetic-field sweeps. Separation of Feshbach molecules from an atomic gas, for instance, may be achieved via the Stern-Gerlach approach of Fig. 3 (Herbig *et al.*, 2003; Dürr, Volz, Marte, and Rempe, 2004; Chin *et al.*, 2005), probing the magnetic moments of dimers at magnetic fields away from the zero-energy resonance.

Near resonance their large spatial extent associated with a loose bond (Köhler, Gasenzer, and Burnett, 2003; Köhler, Gasenzer, Julienne, and Burnett, 2003) can lead to a remarkable stability of Feshbach molecules with respect to inelastic collisions in the environment of a two-spin-component Fermi gas (Petrov *et al.*, 2004, 2005b). The lifetimes of such dimers, ranging from about 100 ms in the case of $^{40}K_2$ (Regal *et al.*, 2004a) to several seconds in $^{6}Li_2$ gases (Cubizolles *et al.*, 2003; Jochim *et al.*, 2003a), were sufficient for the observation of their Bose-Einstein condensation. This achievement was based on either the magnetic-field sweep technique illustrated in Fig. 4 (Greiner *et al.*, 2003) or evaporative cooling of a molecular cloud (Jochim *et al.*, 2003b; Zwierlein *et al.*, 2003). Such pioneering experiments gave rise to an on-

going series of studies[3] probing the crossover from Bardeen-Cooper-Schrieffer (BCS) pairing at negative scattering lengths to molecular Bose-Einstein condensation (Eagles, 1969; Leggett, 1980; Nozières and Schmitt-Rink, 1985; Randeria, 1995).

This article reviews the theoretical background of the exotic species of highly excited Feshbach molecules produced as well as their formation in the environment of a cold gas.

Section II introduces the concept of universality of weakly bound dimers, their relevant length and energy scales, as well as the general form of their wave functions. This discussion integrates near-resonant Feshbach molecules into the general class of quantum halo systems whose classic examples are the deuteron of nuclear physics and the $^4He_2$ dimer molecule. More details about such exotic two-particle states as well as their extensions to few-body systems have been given in a recent review (Jensen *et al.*, 2004).

Section III discusses the concepts of diatomic scattering and molecular physics that are particular to Feshbach resonances in cold gases. Section III.A introduces the microscopic origin of resonance interactions illustrated in Fig. 1, scattering channels and rigorous coupled channels theory (Stoof *et al.*, 1988; Mies *et al.*, 1996), as well as the relation between zero-energy resonances and molecular energy spectra. Several aspects of the rigorous method are well recovered in terms of two-channel approaches whose general concepts, such as the two-channel Hamiltonian and the metastable Feshbach resonance state, are discussed in Sec. III.B. On this basis, Sec. III.C introduces the bare and dressed bound and continuum energy levels. The universal properties of Feshbach molecules near resonance are derived in Sec. III.D. Their physical significance is illustrated in Sec. III.E for several experimentally relevant examples, such as molecular binding energies and lifetimes of dimers in cold Fermi and Bose gases. The size of the magnetic-field range associated with universality implies a distinction between entrance- and closed-channel-dominated zero-energy resonances, whose physical origin is discussed in Sec. III.F. Implementations of two-channel approaches are given in Sec. III.G, describing properties of Feshbach molecules close to as well as away from zero-energy resonances. Their applications involve the Stern-Gerlach separation of dimers shown in Fig. 3. Characteristic parameters relevant to two-channel approaches, such as, for instance, the magnetic moments associated with Feshbach resonances of several atomic species, are summarized in Tables IV and V.

Section IV reviews dynamical approaches describing the production and dissociation of cold Feshbach molecules via linear magnetic-field sweeps across zero-energy resonances. It outlines on the basis of the discrete energy spectrum of a trapped atom pair the adiabatic transfer from quasicontinuum to dimer states. Molecular association of an atom pair via linear magnetic-field sweeps falls into the category of dynamical two-body problems whose solutions can be represented in an analytic form (Demkov and Osherov, 1968; Macek and Cavagnero, 1998). A derivation of the associated transition amplitudes in Sec. IV.A provides the foundation for subsequent applications of the Landau-Zener approach (Landau, 1932; Zener, 1932). These involve predicting the final populations of the quasicontinuum to dimer state transfer in tight atom traps, as well as fast sweep limits of molecule production in cold Bose and two-spin-component Fermi gases. Such conversion efficiencies can be sensitive to the quantum statistics associated with identical atoms whose effects are discussed in Sec. IV.B. The opposite saturation limits of molecule production via magnetic-field sweeps in cold gases have been a subject of ongoing research requiring dynamical descriptions of many-particle systems. Among such methods, the two-level mean-field approach to Bose-Einstein condensates (Timmermans *et al.*, 1999b) is outlined in detail, including its relation to the associated Landau-Zener theory (Mies *et al.*, 2000; Góral *et al.*, 2004). Intuitive as well as quantitative methods in the context of molecular Bose-Einstein condensation illustrated in Fig. 4 are reviewed in Sec. IV.C, outlining the concept of an adiabatic production of dimers via magnetic-field sweeps in cold gases with a significant momentum spread. Section IV.D discusses the theory of Feshbach molecular dissociation, demonstrating the accuracy of analytic treatments of linear magnetic-field sweeps across zero-energy resonances.

Section V addresses the production of dimers via nonlinear magnetic-field variations, illustrated, for instance, in Fig. 2 in the context of Ramsey interferometry with atoms and Feshbach molecules. The description of these experiments requires general theoretical concepts, such as a precise treatment of molecular populations in gases, which are obscured in many applications involving linear magnetic-field sweeps. Section V.A gives an intuitive explanation for observations of the Ramsey fringes of Fig. 2 using a two-body approach. The general observable describing the number of molecules in the environment of a gas (Köhler, Gasenzer, and Burnett, 2003) is introduced in Sec. V.B. This includes simple applications to the fast sweep limits of dimer production in Bose and two-spin-component Fermi gases. Section V.C addresses the description of the Ramsey interferometry experiments in terms of dynamical beyond mean-field approaches (Holland *et al.*, 2001; Köhler and Burnett, 2002).

Section VI concludes this review and provides an outlook on related research, such as *p*-wave and optical Feshbach resonances, cold dipolar and ground-state molecules, as well as extensions to few-body physics and studies of Efimov's effect.

[3]See, for example, Loftus *et al.*, 2002; O'Hara *et al.*, 2002; Bartenstein *et al.*, 2004; Bourdel *et al.*, 2004; Chin, Bartenstein, *et al.*, 2004; Kinast *et al.*, 2004; Regal *et al.*, 2004b; Zwierlein *et al.* 2004, 2005; Partridge *et al.*, 2005.

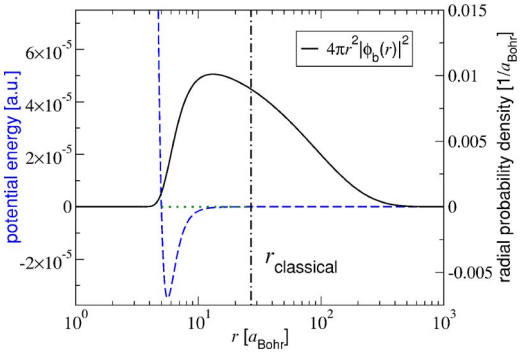

FIG. 5. (Color online) Helium dimer interaction potential (dashed curve) (Tang *et al.*, 1995) and radial probability density of the $^4He_2$ molecule (solid curve). Dotted and dot-dashed lines are the bound-state energy $E_b=-4.2\times10^{-9}$ a.u. (1 a.u. $=4.359\,744\,17\times10^{-18}$ J is the atomic unit of energy) and classical turning point $r_{\text{classical}}=27a_{\text{Bohr}}$ ($a_{\text{Bohr}}=0.052\,917$ nm is the Bohr radius), respectively. The interatomic distance r is given on a logarithmic scale.

II. WEAKLY BOUND DIATOMIC MOLECULES

Weakly bound diatomic molecules are special cases of low-energy halo systems (Jensen *et al.*, 2004). These remarkable quantum states are characterized by a large mean separation between the constituent particles that greatly exceeds the outer classical turning point $r_{\text{classical}}$ determined by their binding energy and their attractive interaction. Halos are, therefore, quite distinct from spatially extended quasiclassical states, such as the Rydberg levels associated with the long-range Coulomb potential. Due to their nonclassical but comparatively simple nature, two-body halos have played a significant role in the present understanding of composite few-particle systems. Classic examples are the deuteron in nuclear physics (Blatt and Weisskopf, 1952) as well as the weakly bound helium dimer $^4He_2$ molecule (Luo *et al.*, 1993; Schöllkopf and Toennies, 1994), whose typical halo wave function is illustrated in Fig. 5. We note that the modulus of the bound-state energy of this halo molecule with respect to the dissociation threshold, i.e., the zero of energy in Fig. 5, is negligibly small compared to the well depth of the pair interaction. The ^4He atoms are separated by distances larger than the classical turning point $r_{\text{classical}}$ with a probability of about 80%. Such distances greatly exceed the intuitive force range associated with the potential well.

The characteristic long range of isotropic diatomic halo molecules, such as the helium dimer, is determined mainly by a single parameter of the interaction potential, the *s*-wave scattering length a. Whenever the interatomic interaction supports a weakly bound halo state, the scattering length is positive. In accordance with effective range theory (Schwinger, 1947a, 1947b; Bethe, 1949), the length scale a may be interpreted in terms of a hypothetical hard sphere radius that mimics the scattering properties of the real microscopic potential in the limit of zero collision energy. This radius is closely related to the bound-state energy of a weakly bound diatomic halo molecule, which is well approximated by

$$E_b=-\hbar^2/ma^2. \tag{1}$$

Here m is twice the reduced mass of the atom pair, which in the case of identical particles coincides with the mass of a single atom. At interatomic distances r large compared to the classical turning point $r_{\text{classical}}$, the associated isotropic bound-state wave function assumes the following general form:

$$\phi_b(r)=\frac{1}{\sqrt{2\pi a}}\frac{e^{-r/a}}{r}. \tag{2}$$

This wave function gives the mean distance between the atoms, i.e., the bond length of the molecule, as

$$\langle r\rangle=4\pi\int_0^\infty r^2dr|\phi_b(r)|^2=a/2. \tag{3}$$

For the typical example of the helium dimer in Fig. 5, the solution of the stationary two-body Schrödinger equation with a realistic pair interaction (Tang *et al.*, 1995) predicts $\langle r\rangle=5.1$ nm, while the estimate of Eq. (3) yields $\langle r\rangle=5.2$ nm. For comparison, measurements based on the diffraction of a helium molecular beam from a microfabricated material transmission grating (Grisenti *et al.*, 2000) determined the bond length of $^4He_2$ to be $\langle r\rangle=5.2(4)$ nm.

A dependence of physical quantities, such as those of Eqs. (1) and (2), only on the scattering length rather than the details of the microscopic forces is usually referred to as universality. The relation between Eqs. (1) and (2) follows immediately from the stationary Schrödinger equation $H_{2B}\phi_b(r)=E_b\phi_b(r)$, using the general two-body Hamiltonian associated with the relative motion of an atom pair,

$$H_{2B}=-\frac{\hbar^2}{m}\nabla^2+V(r). \tag{4}$$

A typical realistic molecular potential $V(r)$ (Tang *et al.*, 1995) is depicted in Fig. 5 for the helium dimer example. Its behavior in the limit of large interatomic distances is dominated by the van der Waals interaction,

$$V(r)\underset{r\to\infty}{\sim}-C_6/r^6. \tag{5}$$

The constant C_6 is known as the van der Waals dispersion coefficient. In accordance with Eq. (5), the outer classical turning point of the relative motion of an atom pair with the energy E_b of Eq. (1) is given by

$$r_{\text{classical}}=[a(2l_{\text{vdW}})^2]^{1/3}. \tag{6}$$

Here l_{vdW} is a characteristic range associated with the van der Waals interaction between atoms, usually referred to as the van der Waals length,

$$l_{\text{vdW}}=\tfrac{1}{2}(mC_6/\hbar^2)^{1/4}. \tag{7}$$

A characteristic property of diatomic halo molecules is that their spatial extent, determined by the scattering length a, greatly exceeds $r_{\text{classical}}$, thus implying the con-

dition $a \gg l_{\mathrm{vdW}}$ for their existence. In the range of such typically large interatomic distances $r \gg l_{\mathrm{vdW}}$, the stationary Schrödinger equation for a halo molecule reduces to its interaction-free counterpart, i.e.,

$$E_b \phi_b(r) \underset{r\to\infty}{\sim} -(\hbar^2/m)\nabla^2 \phi_b(r), \tag{8}$$

whose unit-normalized solution associated with the bound-state energy of Eq. (1) is given by Eq. (2).

The universal properties of Eqs. (1) and (2) and length scales a and l_{vdW} associated with diatomic halo systems characterize, in the same manner, the helium dimer as well as highly excited long-range Feshbach molecules. Any other details of their binary interactions are obscured by the large spatial extent of the bound states. The size of the scattering length, however, which determines the long range of these states depends sensitively on the microscopic potential whose detailed structure varies among different species.

III. FESHBACH RESONANCES

Interatomic collisions in cold gases are characterized by de Broglie wavelengths much larger than the van der Waals length of the microscopic potential. Similarly to the universal properties of diatomic halo molecules, such a separation of length scales implies that the associated low-energy interactions are determined mainly by the s-wave scattering length a. Feshbach resonances provide an opportunity of manipulating these interatomic forces by exposing a cold gas of alkali atoms to a spatially homogeneous magnetic field of strength B. Based on microscopic physics, this section describes the concept of magnetic tuning of the scattering length and the associated cross section (given, for instance, by $8\pi a^2$ in the case of identical Bose atoms) as well as its relation to molecular state properties.

A. Molecular physics of resonances

Resonance enhancement of collision cross sections depends on the existence of metastable states. The two-body molecular physics of such neutral-atom Feshbach resonance states is the subject of this subsection. This involves the microscopic origin of interatomic interactions as well as the atomic and molecular symmetries that permit classification of scattering channels and molecular bound and metastable energy levels. Such a basic understanding of low-energy neutral-atom scattering and bound states provides the foundation for the practical two-channel approaches found in subsequent subsections.

1. Interatomic interactions

The helium atom has a $^1S_0$ configuration with no unpaired electron, and the interaction of two such atoms is represented by the single molecular Born-Oppenheimer potential illustrated in Fig. 5. Such a system is too simple to have a magnetically tunable resonance state. It is therefore necessary to consider the experimentally relevant case of $^2S_{1/2}$ atom pairs of the same species. The unpaired electron spins $\mathbf{s}_1$ and $\mathbf{s}_2$ from each atom can be coupled to a total spin $\mathbf{S}=\mathbf{s}_1+\mathbf{s}_2$ with the associated quantum numbers $S=0$ or 1. States with $S=0$ or 1 are called singlet or triplet states, respectively. The electronic part of the interatomic interaction is represented, as for the simplest molecule H_2 (Pauling, 1939), by singlet and triplet molecular Born-Oppenheimer potentials of $^1\Sigma_g^+$ and $^3\Sigma_u^+$ symmetry corresponding, to $2S+1=1$ and 3, respectively. Here the notation Σ refers to zero projection of the electronic orbital angular momentum on the interatomic axis. The label + indicates that the electronic wave function is left unchanged upon reflection in a plane containing the nuclei. Finally, g and u are associated with the *gerade* (even) and *ungerade* (odd) symmetry upon inversion through the geometric center of the molecule, respectively. Consequently, the latter symmetry is absent when the atoms are of different species.

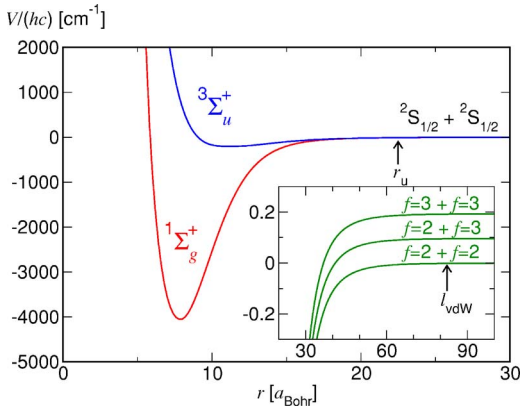

FIG. 6. (Color online) The $^1\Sigma_g^+$ and $^3\Sigma_u^+$ Born-Oppenheimer potential-energy curves for the Rb_2 dimer molecule correlating with two separated $^2S_{1/2}$ Rb atoms. An energy E associated with the wave-number unit $E/hc=1$ cm^{-1} corresponds to $E/h=29.979$ GHz. Inset: The long-range adiabatic potentials (Mies *et al.*, 1996, 2000) on a much smaller energy scale with the zero field ($B=0$) hyperfine structure of the ^{85}Rb isotope with $E_{\mathrm{hf}}/h=3.035$ GHz. Arrows show the van der Waals length l_{vdW} of Eq. (7) and the uncoupling distance r_u, where the hyperfine energy E_{hf} is the difference between the $^3\Sigma_u^+$ and $^1\Sigma_g^+$ Born-Oppenheimer potential curves. The ^{87}Rb isotope has the same Born-Oppenheimer potential-energy curves, but the long-range curves would be different with atomic levels $f=1$ and 2 and $E_{\mathrm{hf}}/h=6.835$ GHz.

Figure 6 shows potential-energy curves $V_S(r)$ for $S=0$ and 1 for two Rb atoms as an illustrative case. Similar potentials exist for any pair of like alkali-metal atoms, and if the *gerade* and *ungerade* symmetry labels g and u are dropped, for pairs of unlike alkali-metal atoms. For the case of two S-state atoms, the long-range form of the potential is the van der Waals dispersion with the lead term $-C_6/r^6$ of Eq. (5), which is identical for $^1\Sigma_g^+$ and $^3\Sigma_u^+$ potentials. The splitting between these two potentials results from the difference in chemical bonding interactions when charge clouds of the two at-

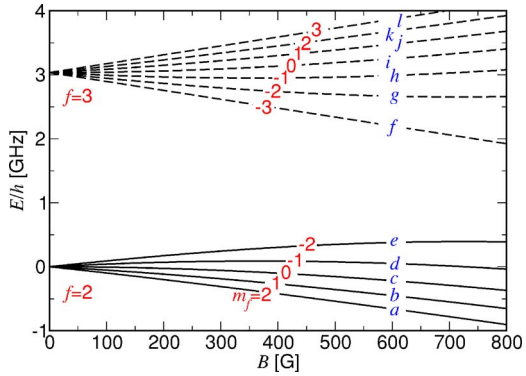

FIG. 7. (Color online) Zeeman levels of the ^{85}Rb $^2S_{1/2}$ atom vs the magnetic-field strength B. Solid and dashed curves are the $f=2$ and 3 multiplets, respectively. The projection quantum numbers m_f and the alphabetic labels a, b, c,… are shown.

oms overlap at small interatomic distances, $r<1$ nm. The long-range form of this splitting is associated with the electron exchange interaction, which decreases exponentially as r increases. This interaction is attractive for the $^1\Sigma_g^+$ state and repulsive for the $^3\Sigma_u^+$ state.

More diatomic states need to be accounted for when the atomic nuclear spin quantum number i is nonzero. At zero magnetic field, i.e., $B=0$, unpaired electrons in each atom with total electronic angular momentum $\mathbf{j}$ can interact with the nuclear spin $\mathbf{i}$ to produce the hyperfine levels of total angular momentum $\mathbf{f}=\mathbf{j}+\mathbf{i}$. For alkali-metal atoms in their electronic ground states, the identity $\mathbf{j}=\mathbf{s}$ gives the total angular momentum quantum number to be either $f=i-\frac{1}{2}$ or $i+\frac{1}{2}$. The difference in energy between these two hyperfine levels is the hyperfine splitting E_{hf}. If f is an integer, the atom will be a composite boson, whereas if f is half an odd integer, the atom will be a composite fermion. Interaction with a magnetic field will further split the energy of each f state into its Zeeman components. Figure 7 illustrates the B-dependent energy levels of ^{85}Rb, a bosonic isotope. In the limit of high magnetic-field strengths, the Zeeman energy of the unpaired electron becomes large compared to E_{hf}. Consequently, f will no longer be a good quantum number. Rotation about the magnetic-field axis, however, is a symmetry transformation. This implies that m_f, the quantum number associated with the projection of the total angular momentum onto this axis, is conserved. Figure 7 also shows that the Zeeman levels of a ^{85}Rb atom do not anticross in a range of magnetic fields up to a few hundred G. As for notation, it is therefore often convenient to label the Zeeman levels by fm_f, where f is the total angular momentum quantum number at $B=0$ with which the level adiabatically correlates. We will use such an explicit reference to the different Zeeman states in subsequent subsections. An alternative, brief notation (Stoof *et al.*, 1988; Mies *et al.*, 2000) indicated in Fig. 7 is to label the Zeeman components in order of increasing energy as $a,b,c,\ldots$; and it shall be used throughout this subsection.

2. Coupled channels scattering

The hyperfine splitting E_{hf} and the magnetic Zeeman energy are typically large compared to the kinetic energy for cold collisions. Consequently, the scattering properties of two atoms depend strongly on the Zeeman levels in which they are prepared. A scattering channel is defined by specifying the quantum numbers that describe each of the two initially separated atoms. In the following, it is convenient to perform a partial wave expansion of the stationary scattering wave function of the relative motion of an atom pair. Its components thus depend on the interatomic distance r in addition to the quantum numbers ℓ and m_ℓ associated with the angular momentum of the relative motion and its orientation with respect to the magnetic-field axis. Given this convention, a scattering channel is specified by the channel index $\alpha=\{f_1 m_{f_1} f_2 m_{f_2} \ell m_\ell\}$. Here the curly brackets signify that the wave function is (anti)symmetric with respect to exchange of identical Bose (Fermi) particles (Stoof *et al.*, 1988). Consequently, the order of atomic indices 1 and 2 is unimportant. Only those channels with even (odd) ℓ exist for two identical bosons (fermions) in the same Zeeman level. All ℓ values are possible for identical bosons or fermions in different Zeeman levels or for nonidentical species. The partial waves associated with $\ell=0$, 1, or 2 are designated s, p, or d waves. If the channel energy $E_\alpha=E_{f_1 m_{f_1}}+E_{f_2 m_{f_2}}$ is less than the total energy of the system E, channel α is said to be open. Conversely, if $E_\alpha>E$, channel α is referred to as closed. When E is lower than the lowest channel energy, all channels are closed and E can refer only to one of the discrete molecular levels. If E is higher than the lowest channel energy, then at least one channel is open, and E is associated with a stationary energy level in the scattering continuum.

In the case of the $^1S_0$ ^{4}He atom, the two-body interaction Hamiltonian is specified by a single-channel potential describing the helium dimer bound state as well as cold collisions. Such a treatment is not adequate for alkali atoms with nuclear spin because of intrinsic coupling among the various channels. It is therefore convenient to represent the wave functions for scattering or bound states as a coupled channels expansion into their components $\Psi_\alpha(r,E)$ in the separated atom spin basis labeled by α (Stoof *et al.*, 1988; Gao, 1996; Mies *et al.*, 1996). The associated radial wave function $F_\alpha(r,E)$ of the relative motion of an atom pair with the energy E is determined by

$$\Psi_\alpha(r,E)=F_\alpha(r,E)/r. \tag{9}$$

Substituting Eq. (9) into the stationary Schrödinger equation gives the following coupled channels equations, which in combination with the boundary conditions imposed on $F_\alpha(r,E)$ determine both the continuum and bound states:

$$\frac{\partial^2 F_\alpha(r,E)}{\partial r^2} + \frac{m}{\hbar^2}\sum_\beta [E\delta_{\alpha\beta} - V_{\alpha\beta}(r)]F_\beta(r,E) = 0. \quad (10)$$

We note that m should be identified in Eq. (10) with twice the reduced mass of an atom pair. The potential matrix $V(r)$ takes on the following form in the separated atom spin basis

$$V_{\alpha\beta}(r) = \left[E_{f_1 m_{f_1}} + E_{f_2 m_{f_2}} + \frac{\hbar^2 \ell\,(\ell+1)}{mr^2} \right]\delta_{\alpha\beta} + V^{\rm int}_{\alpha\beta}(r). \quad (11)$$

Here the atomic hyperfine and magnetic interaction terms are given by the experimentally known separated atom energies $E_{f_1 m_{f_1}}$ and $E_{f_2 m_{f_2}}$, and the kinetic energy of axis rotation is given by the centrifugal energy term proportional to $\ell(\ell+1)$. These terms are diagonal in the asymptotic basis. The complicated part of the scattering due to the electronic Born-Oppenheimer potentials and electron spin-dependent interactions is contained in the interaction matrix $V_{\rm int}(r)$ of Eq. (11), which is comprised of two parts:

$$V_{\rm int}(r) = V_{\rm el}(r) + V_{\rm ss}(r). \quad (12)$$

The contribution $V_{\rm el}(r)$ represents the strong electronic interaction. It is diagonal in ℓ but nondiagonal in the atomic channel quantum numbers $f_1 m_{f_1} f_2 m_{f_2}$. Its diagonal elements in $f_1 m_{f_1} f_2 m_{f_2}$ depend on weighted sums of the two Born-Oppenheimer potentials $V_{S=0}(r)$ and $V_{S=1}(r)$, whereas off-diagonal terms depend on the difference between $V_{S=0}(r)$ and $V_{S=1}(r)$. The strong electronic interaction $V_{\rm el}(r)$ is responsible for elastic scattering and inelastic spin-exchange collisions (Bender, 1963; Dalgarno and Rudge, 1965), and gives rise to the broadest scattering resonances.

The term $V_{\rm ss}(r)$ in Eq. (12) represents the weak relativistic spin-spin potential energy (Stoof *et al.*, 1988; Moerdijk *et al.*, 1995). It is due to the anisotropic dipolar interaction between two electron spins, and is nondiagonal in both $f_1 m_{f_1} f_2 m_{f_2}$ and ℓ, i.e., it couples different partial waves. In the limit of large interatomic distances, $V_{\rm ss}(r)$ is proportional to α^2/r^3, where $\alpha = 1/137.0426$ is the fine-structure constant. As $V_{\rm ss}(r)$ is a tensor operator of rank 2, only blocks that differ in ℓ by zero or two units have nonvanishing matrix elements, according to the Wigner-Eckart theorem (Wigner, 1927; Eckart, 1930). In addition, there are no s-wave diagonal potentials varying as $1/r^3$.

At short range the spin-dipole interaction can be modified by second-order spin-orbit contributions, which are important for a heavy atom such as Cs (Mies *et al.*, 1996; Kotochigova *et al.*, 2001). In general, the potential-energy contribution $V_{\rm ss}(r)$ is responsible for weak inelastic spin-dipolar relaxation and gives rise to narrow scattering resonances.

The low-energy collision physics of alkali atoms in specific hyperfine states is sensitive to the recoupling of electron spins between separated atoms and the short-range zone of strong chemical interactions. At small interatomic distances, the potential-energy scale is orders of magnitude larger than $E_{\rm hf}$. Whereas the electron spin is coupled to the nuclear spin on the same atom when atoms are separated, electron spins become uncoupled from the nuclear spin and couple strongly to one another at small r to make the $S=0$ and 1 states of the Born-Oppenheimer potentials. The distance where this recoupling occurs is near r_u of Fig. 6, where the difference in Born-Oppenheimer potentials $V_{S=1}(r_u) - V_{S=0}(r_u)$ due to the exchange potential is equal to the atomic hyperfine energy $E_{\rm hf}$. This occurs typically in the distance range of 20 to $25a_{\rm Bohr}$ for alkali atoms.

The coupled channels method (Stoof *et al.*, 1988; Mies *et al.*, 1996) of Eq. (10) properly accounts for dynamical changes in the couplings among the five angular momenta $\mathbf{s}_1$, $\mathbf{s}_2$, $\mathbf{i}_1$, $\mathbf{i}_2$, and ℓ as atoms move through the region near r_u. Basic symmetries of the coupling terms in $V_{\rm int}(r)$ of Eq. (12) allow us to separate the interaction matrix into blocks, within which the coupling is strong and between which the coupling is intrinsically weak. Such a separation gives rise to classifications of the various stationary energy states in terms of their predominant symmetry properties. Projected levels that are bound just within a particular block are, in general, associated with scattering resonances when their energy is above the scattering threshold. We note, however, that in contrast to the complete stationary states determined by Eq. (10), such Feshbach resonance levels depend on the separation of $V_{\rm int}(r)$ into blocks or, equivalently, on the choice of basis set.

In this context, the separated atom spin basis referred to in Eq. (11) is convenient at long range, but leads to off-diagonal elements at short range. One alternative, short-range basis would first couple $\mathbf{s}_1$ and $\mathbf{s}_2$ to a resultant $\mathbf{S}$ and $\mathbf{i}_1$ and $\mathbf{i}_2$ to a resultant $\mathbf{I}$. Then $\mathbf{S}$ and $\mathbf{I}$ can be coupled to a resultant $\mathbf{F}$, which in turn couples to ℓ to give the total angular momentum $\mathbf{F}_{\rm total}$ (Tiesinga *et al.*, 1993; Moerdijk *et al.*, 1995). Then we could set up a molecular basis set with quantum numbers $(SI)F\ell F_{\rm total}M$. Here M refers to the orientation quantum number associated with the projection of $\mathbf{F}_{\rm total}$ onto the magnetic-field axis. This short-range basis takes advantage of the fact that $V_{\rm el}(r)$ is diagonal in S. An alternative separated atom basis set could couple $\mathbf{f}_1$ and $\mathbf{f}_2$ to a resultant $\mathbf{F}$, and give the basis $(f_1 f_2)F\ell F_{\rm total}M$. This basis is useful at low B fields at which the Zeeman levels do not anticross, and where F may be viewed as a good quantum number. The unitary transformation between separated atom and molecular basis sets is called a frame transformation (Bender, 1963; Dalgarno and Rudge, 1965; Burke *et al.*, 1998; Gao *et al.*, 2005). Bound and metastable states of light elements such as Li and Na are best classified by the molecular basis (Moerdijk *et al.*, 1995; Simonucci *et al.*, 2005), whereas the separated atom basis is better for heavy elements such as Rb or Cs (Marte *et al.*, 2002; Chin *et al.*, 2004). Similarly, the long-range part of a scattering wave function is best described in the separated atom basis set, whereas the molecular basis is more appropriate for the short-range part.

3. Threshold collisions

The quantum numbers $f_1 m_{f_1}$ and $f_2 m_{f_2}$ associated with the Zeeman states of separated atoms in which a dilute gas is prepared determine the entrance channel of a two-body collision. In the context of cold collisions, it is usually sufficient to consider just the s-wave ($\ell=0$) component of an initial plane-wave momentum state of the relative motion of an atom pair. To avoid inelastic processes known as spin relaxation, most experimental applications of Feshbach resonances involve atom pairs in the lowest energetic Zeeman states for which s-wave scattering is allowed. In the following, we assume such a case and choose the zero of energy at the entrance-channel energy E_α. This convention implies that the total energy E of a colliding atom pair is identical to its positive kinetic energy $\hbar^2k^2/m$. Here k is referred to as the wave number and $p=\hbar k$ is the momentum of the relative motion. On the other hand, bound-state energies E_b are always negative.

The amplitudes associated with transitions between the initial and final states of a diatomic collision may be inferred from the asymptotic form of the scattering solutions to Eq. (10) in the limit of large distances $r\to\infty$. As the only open channel is assumed to be the entrance channel, the long-range boundary condition imposed on the associated component of the radial wave function reads (Taylor, 1972)

$$F_\alpha(r,\hbar^2k^2/m) \propto \sin[kr+\xi(\hbar k)]. \tag{13}$$

Here the absolute magnitude of $F_\alpha(r,\hbar^2k^2/m)$ is determined up to an overall energy-dependent prefactor whose value is a matter of convention. All information about a collision is contained in the scattering phase shift $\xi(\hbar k)$. According to effective range theory (Schwinger, 1947a, 1947b; Bethe, 1949), $\xi(\hbar k)$ determines the scattering length a via the following low-energy asymptotic expansion:

$$k\cot\xi(\hbar k) = -\frac{1}{a}+\frac{1}{2}k^2 r_{\rm eff}. \tag{14}$$

Here $r_{\rm eff}$ is known as the effective range. For most applications in this review, the scattering length alone is sufficient for the description of cold diatomic collisions.

In general, the scattering length is only weakly dependent on the magnetic-field strength B, unless B can be tuned in such a way that a closed-channel Feshbach resonance level crosses the entrance-channel scattering threshold. Such a scenario may occur due to a difference in magnetic moments $\partial E_\alpha/\partial B$ and $\partial E_\beta/\partial B$ associated with the entrance and closed channels, respectively. The metastability of the resonance state leads to a time delay during a collision when the energies of the scattered atoms and of the resonance level are nearly matched. This results in an enhancement of the scattering cross section whose width in energy depends on the strength of the coupling between the entrance and closed channels via the lifetime of the resonance state. As the zero-energy cross section is proportional to a^2, such a resonance enhancement of collisions may be used to widely tune the scattering length (Tiesinga *et al.*, 1993) as illustrated in Fig. 1. We note, however, that because of the interchannel coupling, the magnetic-field strength B_0 associated with the singularity of a differs from the crossing point between the resonance energy and the scattering threshold. The magnetic-field width and shift of such zero-energy resonances will be the subject of Sec. III.C.

Singularities of the s-wave scattering length are always accompanied by the degeneracy of a bound vibrational level with the scattering threshold (Taylor, 1972). In the context of magnetic Feshbach resonances, the properties of such a coupled channels stationary energy state, termed the Feshbach molecule, may be inferred from Eq. (10) in the zero bound-state energy limit $E_b\to 0$. Similarly to the studies of Sec. II, the derivation just relies upon the fact that the potential matrix $V_{\rm int}(r)$ of Eq. (11) vanishes at large separations $r\to\infty$. In such an asymptotic distance range the atoms cease to interact, and the solution of Eq. (10) associated with any s-wave ($\ell=0$) channel is given by

$$F_\alpha(r,E_b) \propto \exp[-\sqrt{-m(E_b-E_\alpha)}r/\hbar\,]. \tag{15}$$

Its prefactor depends on the overall normalization of the bound state and is thus determined by all components. In the limit $E_b\to 0$, however, only the entrance-channel radial wave function acquires a long range and, therefore, predominates all the others. The relation between the binding energy and scattering length in the vicinity of a zero-energy resonance will be the subject of Sec. III.D. This discussion will show, on the basis of general arguments, that E_b is determined by Eq. (1), while the Feshbach molecular wave function reduces to its entrance-channel component given by Eq. (2).

If the entrance channel is not the lowest in energy, the above scenario of zero-energy resonances and Feshbach molecules is only approximate. This implies that the scattering length is always finite even when a closed-channel Feshbach resonance level is magnetically tuned to cross the entrance-channel energy. The associated Feshbach molecule can decay into the lower energetic open channels via spin relaxation (Köhler *et al.*, 2005; Thompson *et al.*, 2005b). Such a rather general situation underlies, for instance, the experiments of Fig. 2 involving gases of ^{85}Rb, and serves as an example for the following explicit channel classification.

4. Example of channel classification

The most rigorous classification of scattering channels is by the total projection quantum number $M=m_{f_1}+m_{f_2}+m_\ell$. In the absence of external fields other than B, the symmetry with respect to rotation about the magnetic-field axis implies that M is strictly conserved during the course of a collision, i.e., states with different M cannot couple. The next useful classification is by the partial wave quantum number ℓ. Only weak coupling is normally possible between states of different ℓ, since it can only originate from the intrinsically small and anisotropic $V_{\rm ss}(r)$ matrix elements.

TABLE I. Separated atom quantum numbers for the s-wave ($\ell=0$) $M=-4$ block of the coupling matrix $V_{\rm el}(r)$ for ^{85}Rb, for which f assumes the values 2 and 3. The separated atom energies relative to $E_{ee}=0$ are shown for $B=0$ and 160 G (16.0 mT).

$(f_1 f_2)$	$m_{f_1}\, m_{f_2}$	α	E_α/h (GHz) for $B=0$	E_α/h (GHz) for $B=160$ G
(2 2)	−2 −2	ee	0	0
(2 3)	−1 −3	df	3.035 732	2.591 623
(2 3)	−2 −2	eg	3.035 732	2.756 754
(3 3)	−3 −1	fh	6.071 464	5.508 558
(3 3)	−2 −2	gg	6.071 464	5.513 508

Table I shows an example of the quantum numbers needed to describe the s-wave channels associated with the interaction of a pair of $f=2$, $m_f=-2$ ^{85}Rb atoms, which is the e state in the alphabetic notation. This state is one for which there is a broad Feshbach resonance close to the scattering threshold near 155 G. Both the binding energies of the associated Feshbach molecules and scattering length may be inferred from solutions of Eq. (10), using just the matrix elements of the potential $V_{\rm el}(r)$ between the channel states of Table I. Since the nuclear spin of a ^{85}Rb atom is $i=\frac{5}{2}$, the two ground-state f values are 2 and 3. The total projection quantum number for s waves is $M=-4$ for any B. There are only five possible separated atom spin channels. As the hyperfine splitting is $E_{\rm hf}/h=3.035$ GHz for this species, cold collisions associated with temperatures T on the order of 1 μK (where $k_BT/h=21$ kHz given the Boltzmann constant $k_B=1.380\,650\,5\times10^{-23}$ J/K) have only a single open s-wave channel, the ee channel. All other $\ell=0$ channels, df, eg, fh, and gg, are closed.

The anisotropic interaction $V_{\rm ss}(r)$ weakly couples the s-wave block to the d-wave block, the d-wave block to the g-wave block, etc. This has two consequences: extra spin-relaxation channels are possible, and projected energy states of d-wave character (or even higher partial wave character) can give rise to scattering resonances for s-wave collisions. In the ^{85}Rb case, there are a total of 23 $M=-4$ d-wave channels that couple to the s-wave block illustrated in Table I. Only the four listed in Table II are open with respect to the ee channel energy. These channels are all degenerate with the ee s-wave channel at $B=0$. Such a degeneracy at zero magnetic field implies a suppression of inelastic collisions due to the Wigner threshold law (Wigner, 1948) outlined in Sec. III.D. The d-wave channels of Table II become open, however, by a relatively large amount of energy on the cold μK temperature scale as B increases. The associated energy gap gives rise to inelastic decay by which a pair of e-state atoms can relax in a collision when B increases from zero (Roberts *et al.*, 2000b). These open d-wave channels are also responsible for the observed spontaneous dissociation of Feshbach molecules with binding energies near the ee scattering threshold

TABLE II. Separated atom quantum numbers for the open channel d-wave ($\ell=2$) $M=-4$ block of the coupling matrix $V_{\rm ss}(r)$ for ^{85}Rb. The separated atom energies relative to $E_{ee}=0$ are shown for $B=0$ and 160 G (16.0 mT). There are also 19 closed channels in the d-wave $M=-4$ block.

$(f_1 f_2)$	$m_{f_1}\, m_{f_2} m_\ell$	α	E_α/h (GHz) for $B=0$	E_α/h (GHz) for $B=160$ G
(2 2)	−1 −1 −2	dd	0	−0.161 496
(2 2)	0 −2 −2	ce	0	−0.157 321
(2 2)	−1 −2 −1	de	0	−0.080 748
(2 2)	−2 −2 0	ee	0	0

(Thompson *et al.*, 2005b). Associated lifetimes as a function of the magnetic-field strength will be discussed in Sec. III.E.

Table III illustrates the blocks of the matrix $V_{\rm int}(r)$ according to $\{f_1 f_2\}F\ell$ quantum numbers. The example refers to Bose atoms with a nuclear spin quantum number of $i=\frac{5}{2}$, such as ^{85}Rb. Basis states in the same vertical column of Table III, that is, with the same $F\ell$ quantum numbers, are coupled by the strong exchange interactions in $V_{\rm el}(r)$. Basis states from different vertical columns can only be coupled by weak interactions in $V_{\rm ss}(r)$. Classification using $F\ell$ blocks was used for Feshbach resonance states with $\ell>0$ observed for the comparatively heavy alkali-metal atoms ^{87}Rb (Marte *et al.*, 2002) and ^{133}Cs (Chin, Vuletic, *et al.*, 2004). In particular, the $^{133}Cs_2$ Feshbach molecules associated with the Stern-Gerlach separation experiments of Fig. 3 are mainly of g-wave character with $F=4$ and $\ell=4$. Such a separated atom classification shall be applied in the following to Feshbach resonance and molecular states of ^{85}Rb associated with the observations of Fig. 2.

5. Near-threshold bound states

The illustration of the relation between resonance and bound states, on the one hand, and singularities of the scattering length, on the other hand, relies on coupled channels calculations. Figure 8 shows the five separated atom channel energies $E_\alpha(B)$ for the s-wave block described in Table I. In accordance with the convention

TABLE III. Separated atom quantum numbers $(f_1 f_2)F\ell$ for the s- and d-wave part of $V_{\rm int}(r)$ for the bosonic isotope ^{85}Rb, for which f assumes the values 2 and 3. Odd values of F are missing when f_1 equals f_2 because of Bose symmetry. Spin-exchange interactions couple states in the same column, whereas states in different columns can only be coupled by spin-dipolar interactions.

$(f_1 f_2)$	$F\ell$												
(3 3)	0s		2s		4s		6s	0d		2d		4d		6d
(2 3)		1s	2s	3s	4s	5s			1d	2d	3d	4d	5d	
(2 2)	0s		2s		4s			0d		2d		4d		

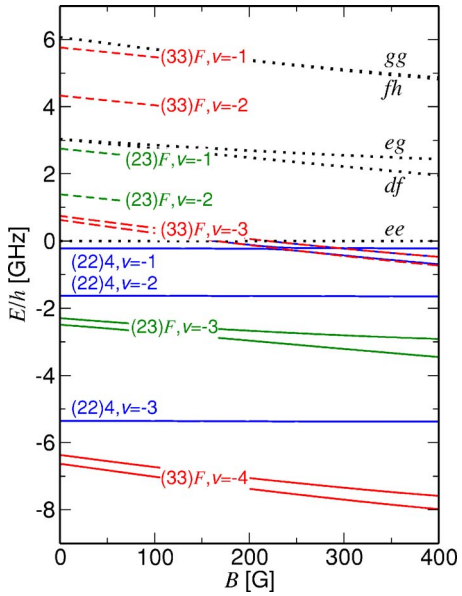

FIG. 8. (Color online) Magnetic-field-dependent $M=-4$ s-wave energy levels of the $^{85}Rb_2$ dimer. Dotted curves labeled by ee, df, eg, fh, and gg show the energies of the five separated atom channels of Table I. Solid curves indicate the calculated s-wave coupled-channel bound-state energies labeled by the vibrational quantum number v. Their symmetry labels refer to the set of quantum numbers $(f_1f_2)F$. The ee limit gives rise to a single vibrational progression with $F=4$; the df and eg limits give rise to two $(23)F$ series with $F=4$ and 5; and the fh and gg limits give rise to two $(33)F$ series with $F=4$ and 6. In all cases, the $F=4$ level has lower energy than the (f_1f_2) pairs. At $B=0$, the $v=-1$ and -2, $(23)F$ levels and the $v=-1$, -2, and -3, $(33)F$ levels represent metastable states with $E>0$ embedded in the (22)4 ee scattering continuum. These metastable levels are represented by dashed curves, which give approximate positions of scattering resonances in the ee channel. The metastable levels with $F=4$ are coupled to the ee s-wave scattering continuum through the exchange interaction. The $F=5$ and 6 metastable levels are not exchange coupled to the ee entrance channel at $B=0$, but become weakly coupled at higher fields where F is no longer a good quantum number.

used throughout, the scattering threshold associated with the ee entrance channel defines the zero of energy. As the five channel energies just reflect the sums of their associated atomic Zeeman energies, they cluster into three groups. The lowest energy group consists just of the ee entrance channel. The next group with energies on the order of $E_{\rm hf}$ includes the df and eg channels. Finally, the group with energies of about $2E_{\rm hf}$ refers to the fh and gg channels. Both channel energies associated with each one of the latter two groups are degenerate at $B=0$. At the low magnetic-field strengths shown in Fig. 8, the choice of $(f_1f_2)F$ quantum numbers well characterizes the two-body physics. The (22) entrance channel has $F=4$, the (23) group has $F=4$ and 5, and the (33) group has $F=4$ and 6. Only F values of 4 or more are possible because the projection quantum number is $M=-4$; the odd value $F=5$ is ruled out for identical bosons with $(f_1f_2)=(33)$.

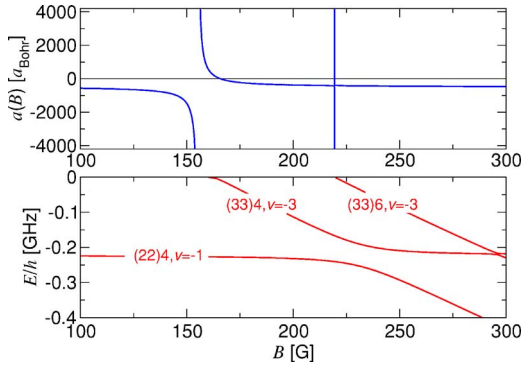

FIG. 9. (Color online) Scattering length (upper panel) and bound-state energy levels (lower panel) vs B for two ^{85}Rb atoms in the e state. The separated atom energy of two e-state atoms is taken to be zero. A singularity of the scattering length occurs where an energy level becomes degenerate with the scattering threshold at $E=0$. The resolution of the figure is not sufficient to show the variation of the bound-state energies with B just below threshold; this variation is discussed in Fig. 12. The broad resonance is due to the threshold crossing of the strongly coupled $(f_1f_2)F\ell=(33)4s$, $v=-3$ level, whereas the narrow resonance is due to the crossing of the weakly coupled $(f_1f_2)F\ell=(33)6s$, $v=-3$ level.

The solid curves in Fig. 8 show the s-wave bound states of the $^{85}Rb_2$ molecular dimer with negative energies $E_b<0$. The curves virtually parallel to the $E=0$ threshold refer to the $v=-1$, -2, and -3 states of the ee entrance channel, labeled by their vibrational quantum numbers v starting with $v=-1$ for the highest excited level. In addition to v, their low-field (22)4 quantum numbers are indicated in Fig. 8. These levels all have nearly the same magnetic moment as a pair of separated atoms in the entrance-channel Zeeman state configuration. Each one of the other four closed channels also has a vibrational series leading to each of the four closed-channel thresholds. The pair of $(23)F$, $v=-3$ levels with $F=4$ and 5 and the pair of $(33)F$, $v=-4$ levels with $F=4$ and 6 are both bound with respect to separated atoms. For both pairs, the lowest level has $F=4$. These levels have different magnetic moments from a pair of ee separated atoms. This implies that their bound-state energies $E_b(B)$ relative to $E=0$ vary significantly with the magnetic-field strength B.

While the $^{85}Rb_2$ molecular dimer states involve the complete strong electronic interaction $V_{\rm el}(r)$, the Feshbach resonance levels of Fig. 8 refer to blocks of the potential matrix associated with their symmetry labels. At zero magnetic field the (23), $v=-1$ and -2 levels and the (33), $v=-1$, -2, and -3 levels have positive energies so that they are metastable levels embedded in the ee scattering continuum. The two $(33)F$ levels are especially interesting, in that they cross the ee $E=0$ threshold and turn into bound states when B is sufficiently large. Figure 9 shows an expanded view of the bound-state energy levels in the near-threshold crossing region as well as the s-wave scattering length a of the ee entrance channel as a function of B. The scattering length has a

singularity at the magnetic-field value B_0 where a new bound state appears with $E_b(B_0)=0$. The $F=4$ (33) level is coupled by the exchange interaction to the $F=4$ *ee* entrance channel, and gives rise to a broad resonance with an associated singularity of a near 155 G. On the other hand, the $F=6$ (33) level is only weakly coupled to the $F=4$ *ee* entrance channel, and gives rise to a narrow zero-energy resonance near 220 G. In addition, the interaction between the (33)F levels and the highest excited entrance-channel bound state at $E_{-1}/h=-0.22$ GHz is evident in Fig. 9. It results, for instance, in the avoided crossing of the (22)4, $v=-1$ and (33)4, $v=-3$ levels between 200 and 250 G, which is due to the same coupling that leads to the broad singularity of the scattering length near 155 G.

B. Two-channel approach

Coupled-channels calculations based on realistic molecular potentials and known atomic properties are capable of accounting for a variety of experimental collisional and bound-state properties of alkali-metal species (Houbiers *et al.*, 1998; van Abeelen and Verhaar, 1998; Leo *et al.*, 2000; Loftus *et al.*, 2002; Marte *et al.*, 2002; Chin, Vuletic, *et al.*, 2004; Marcelis *et al.*, 2004; Bartenstein *et al.*, 2005). Their accuracy, including predictions of new resonances, is possible once the actual potentials have been calibrated in such a way that they recover the correct scattering lengths for the Born-Oppenheimer $^1\Sigma_g^+$ and $^3\Sigma_u^+$ potentials (Abraham *et al.*, 1997; van Kempen *et al.*, 2002) in addition to the van der Waals coefficient C_6. Coupled-channels approaches have the drawback, however, that they are not readily accessible. Consequently, it is desirable to find simpler approaches to Feshbach resonance and molecular levels close to the dissociation threshold energy. To this end, the physics of binary collisions as well as the properties of the highly excited molecular bound states can usually be well described in terms of just two scattering channels (Child, 1974; Moerdijk *et al.*, 1995; Timmermans *et al.*, 1999b; Mies *et al.*, 2000). In the following, we denote by the entrance-channel the Zeeman state configuration of a pair of asymptotically separated atoms in which a dilute gas is initially prepared. Under the conditions of resonance enhancement, this spin configuration is strongly coupled, in general, to several energetically closed scattering channels. In idealized treatments, however, this coupling is usually due to the near degeneracy of the energies of a single metastable vibrational state, the Feshbach resonance state $\phi_{\rm res}(r)$, and the colliding atoms. The spin configuration associated with the Feshbach resonance state is referred to, in the following, simply as the closed channel.

1. Two-channel Hamiltonian

The general Hamiltonian for the relative motion of an atom pair, i.e., the basis of all two-channel approaches (Child, 1974; Moerdijk *et al.*, 1995; Timmermans *et al.*, 1999b; Mies *et al.*, 2000) is given by the following matrix:

$$H_{\rm 2B}=\begin{pmatrix} H_{\rm bg} & W(r) \\ W(r) & H_{\rm cl}(B) \end{pmatrix}. \tag{16}$$

Its off-diagonal elements $W(r)$ are the energies associated with the spin exchange (or dipole) interaction and provide the interchannel coupling as a function of the distance r between atoms. The diagonal elements $H_{\rm bg}$ and $H_{\rm cl}(B)$ can be interpreted in terms of entrance- and closed-channel Hamiltonians in the hypothetical absence of coupling, respectively. These single-channel Hamiltonians consist of kinetic- and potential-energy contributions given by the following formulas:

$$H_{\rm bg}=-\frac{\hbar^2}{m}\nabla^2+V_{\rm bg}(r), \tag{17}$$

$$H_{\rm cl}(B)=-\frac{\hbar^2}{m}\nabla^2+V_{\rm cl}(B,r). \tag{18}$$

Here and in the following, we choose the zero of energy as the threshold for dissociation of the entrance channel. Consequently, the background scattering potential $V_{\rm bg}(r)$ of Eq. (17) vanishes in the limit of large interatomic separations, in accordance with the general asymptotic behavior of the van der Waals interaction described by Eq. (5). In this approach, the complete two-body Hamiltonian of Eq. (16) depends on the magnetic-field strength B simply via an overall shift of the closed-channel potential $V_{\rm cl}(B,r)$ with respect to the entrance-channel dissociation threshold. The amount of this shift is determined by the sum of the single-particle Zeeman energies associated with the closed-channel spin configuration of atom pairs. Typical diagonal potential-energy contributions to the two-body Hamiltonian are illustrated schematically in Fig. 10, whereas special requirements for them will be discussed in Sec. III.G.

2. Bare Feshbach resonance state

The closed-channel Hamiltonian supports the bare Feshbach resonance state in accordance with the following Schrödinger equation:

$$H_{\rm cl}(B)\phi_{\rm res}(r)=E_{\rm res}(B)\phi_{\rm res}(r). \tag{19}$$

The associated resonance energy $E_{\rm res}(B)$ can be tuned with respect to the entrance-channel dissociation threshold, i.e., the zero of energy in Fig. 10, by varying the magnetic-field strength. In the hypothetical absence of interchannel coupling, the Feshbach resonance level usually represents a comparatively tightly bound state of $H_{\rm cl}(B)$ with a classical radius $r_{\rm classical}$ smaller than the van der Waals length of Eq. (7). Under realistic conditions, however, $\phi_{\rm res}(r)$ is only a metastable state with a decay width depending on the strength of the interchannel coupling. Its precise form cannot always be unambiguously identified from full coupled-channels calculations because the two-channel picture is an idealization. The remarkable accuracy of such a simplifying approach is due to the fact that near resonance the physically relevant dressed stationary energy levels are largely insensitive to the detailed structure of the resonance state.

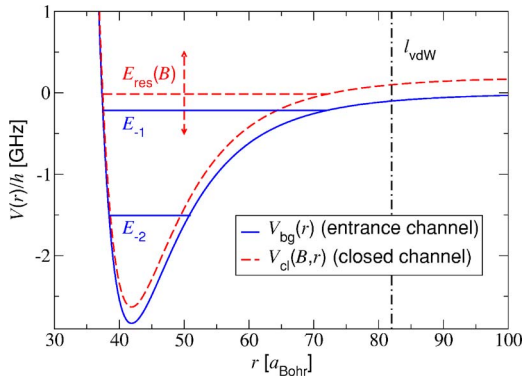

FIG. 10. (Color online) Scheme of the entrance- (solid curve) and closed-channel (dashed curve) potentials associated with a model representation of the 155 G zero-energy resonance of ^{85}Rb (Köhler, Gasenzer, Julienne, and Burnett, 2003). Horizontal dashed and vertical dot-dashed lines are the magnetic-field-dependent energy $E_{res}(B)$ of the Feshbach resonance level $\phi_{res}(r)$ and the van der Waals length of $l_{vdW}=82a_{Bohr}$, respectively. In this model, the outer classical turning point of the resonance level $\phi_{res}(r)$ associated with the energy $E_{res}(B)$ in the closed-channel potential is located at $r_{classical}=72a_{Bohr}$. Its vibrational quantum number $v=-1$ with respect to the dissociation threshold of $V_{cl}(B,r)$ is chosen arbitrarily. Horizontal solid lines indicate the energies E_{-1} and E_{-2} of bare vibrational bound states associated with the entrance-channel potential. This bare interaction is adjusted such that it mimics the highest excited $(f_1f_2)F=(22)4$, $v=-1$ and -2 levels of Fig. 8. In this model, the off-diagonal spin exchange coupling is $W(r)=\beta\exp(-r/\alpha)$, with $\alpha=5a_{Bohr}$ and $\beta/k_B=38.5$ mK used to match the measured Feshbach resonance parameters (Claussen *et al.*, 2003).

C. Dressed energy states

Dressed stationary energy states consist of two orthogonal components associated with the spin configurations $|bg\rangle$ and $|cl\rangle$ of the entrance and closed channels, respectively. Their wave functions are therefore of the following general form (Drummond *et al.*, 1998): $|bg\rangle\phi_{bg}(\mathbf{r})+|cl\rangle\phi_{cl}(\mathbf{r})$. The components $\phi_{bg}(\mathbf{r})$ and $\phi_{cl}(\mathbf{r})$ depend on the relative position $\mathbf{r}$ of the atoms. In accordance with Eq. (16), these components are determined by the following set of coupled stationary Schrödinger equations:

$$H_{bg}\phi_{bg}(\mathbf{r})+W(r)\phi_{cl}(\mathbf{r})=E\phi_{bg}(\mathbf{r}), \tag{20}$$

$$W(r)\phi_{bg}(\mathbf{r})+H_{cl}(B)\phi_{cl}(\mathbf{r})=E\phi_{cl}(\mathbf{r}). \tag{21}$$

In this review all applications will involve either symmetric or antisymmetric spin configurations of identical Bose and Fermi atom pairs, respectively. Their physical spatial wave functions will only consist of an s-wave component. The solutions of Eqs. (20) and (21) with a negative energy E below the entrance-channel dissociation threshold are associated with molecular bound states. Solutions with a positive energy belong to the continuum spectrum of the Hamiltonian and describe collisions of initially separated pairs of atoms.

1. Dressed continuum states

Dressed continuum states can be labeled by the relative momentum $\mathbf{p}$ of a pair of asymptotically separated atoms in the entrance-channel spin configuration and are associated with collision energies $E=p^2/m$. Due to the continuous range of angles of incidence between the atoms, any given collision energy is infinitely degenerate. In this context, it is convenient to postpone the introduction of any symmetry properties of the spatial wave functions associated with a possible identical nature of the atoms. Continuum states are usually chosen in such a way that their entrance-channel component $\phi_{\mathbf{p}}^{bg}(\mathbf{r})$ behaves at asymptotically large interatomic distances like a superposition of an incident plane wave and an outgoing spherical wave (Taylor, 1972). This choice of the wave function leads to the following boundary condition:

$$\phi_{\mathbf{p}}^{bg}(\mathbf{r})\underset{r\to\infty}{\sim}\frac{1}{(2\pi\hbar)^{3/2}}\left[e^{i\mathbf{p}\cdot\mathbf{r}/\hbar}+f(\vartheta,p)\frac{e^{ipr/\hbar}}{r}\right]. \tag{22}$$

The quantity $f(\vartheta,p)$ is known as the scattering amplitude and depends on the modulus p of the relative momentum of the atoms and on the scattering angle determined by the relation $\cos\vartheta=\mathbf{p}\cdot\mathbf{r}/(pr)$. Due to the off-diagonal coupling $W(r)$, the stationary continuum states also have a closed-channel component. The associated wave function $\phi_{\mathbf{p}}^{cl}(\mathbf{r})$ decays at asymptotically large interatomic distances because the cold collision energies of interest are below the closed-channel dissociation threshold. This property reflects physical intuition as closed-channel atom pairs are spatially confined by the potential $V_{cl}(r)$ of Fig. 10.

Due to their long range of Eq. (22), stationary continuum wave functions may be interpreted in terms of amplitudes for the density of particle flux rather than physical states (Taylor, 1972). In the present context, the entrance-channel component $\phi_{\mathbf{p}}^{bg}(\mathbf{r})$ determines observable low-energy scattering properties of colliding atom pairs, such as, for instance, the differential cross section of distinguishable atoms, $|f(\vartheta,p)|^2$. These properties can be represented in terms of bare energy states associated with the Hamiltonians H_{bg} and $H_{cl}(B)$. To this end, it is instructive to reformulate the coupled set of stationary Schrödinger equations (20) and (21), including the boundary condition of Eq. (22), in terms of the associated Green's functions in addition to the entrance-channel continuum states. The bare Green's functions depend on a complex variable z with the dimension of an energy in accordance with the following formulas:

$$G_{bg}(z)=(z-H_{bg})^{-1}, \tag{23}$$

$$G_{cl}(B,z)=[z-H_{cl}(B)]^{-1}. \tag{24}$$

The entrance-channel continuum wave functions $\phi_{\mathbf{p}}^{(+)}(\mathbf{r})$, also referred to as background scattering states, satisfy the stationary Schrödinger equation associated with the Hamiltonian H_{bg} of Eq. (17), i.e.,

$$H_{\rm bg}\phi_{\mathbf{p}}^{(+)}(\mathbf{r}) = \frac{p^2}{m}\phi_{\mathbf{p}}^{(+)}(\mathbf{r}). \tag{25}$$

Their long-range behavior is determined by boundary conditions analogous to Eq. (22) with $f(\vartheta,p)$ replaced by the bare amplitude $f_{\rm bg}(\vartheta,p)$ associated with the background scattering.

Expressed in terms of the bare Green's functions and continuum states, the Schrödinger equations (20) and (21) read

$$|\phi_{\mathbf{p}}^{\rm bg}\rangle = |\phi_{\mathbf{p}}^{(+)}\rangle + G_{\rm bg}(E+i0)W|\phi_{\mathbf{p}}^{\rm cl}\rangle, \tag{26}$$

$$|\phi_{\mathbf{p}}^{\rm cl}\rangle = G_{\rm cl}(B,E)W|\phi_{\mathbf{p}}^{\rm bg}\rangle. \tag{27}$$

The argument $z=E+i0$ of the entrance-channel Green's function in Eq. (26) indicates that the physical collision energy $E=p^2/m$ is approached from the upper half of the complex plane. This choice of the energy argument ensures that the scattering wave function $\phi_{\mathbf{p}}^{\rm bg}(\mathbf{r})$ is compatible with Eq. (22), in accordance with the following long-range asymptotic behavior of $G_{\rm bg}(z)$ in spatial coordinates:

$$G_{\rm bg}(z,\mathbf{r},\mathbf{r}') \underset{r\to\infty}{\sim} -\frac{m(2\pi\hbar)^{3/2}}{4\pi\hbar^2}\frac{e^{ipr/\hbar}}{r}[\phi_{\mathbf{p}}^{(-)}(\mathbf{r}')]^*. \tag{28}$$

Here $\phi_{\mathbf{p}}^{(-)}(\mathbf{r}')=[\phi_{-\mathbf{p}}^{(+)}(\mathbf{r}')]^*$ is the entrance-channel continuum energy state with incoming spherical wave boundary conditions (Taylor, 1972). Its label $\mathbf{p}=(mE)^{1/2}\mathbf{r}/r$ may be interpreted as the asymptotic momentum associated with the relative motion of scattered atoms. The closed-channel continuum wave function $\phi_{\mathbf{p}}^{\rm cl}(\mathbf{r})$ of Eq. (27) decays at asymptotically large interatomic distances because the bare Green's function on the right-hand side is evaluated at the collision energy $E=p^2/m$ below the dissociation threshold of $V_{\rm cl}(r)$.

Direct application of the two-channel Hamiltonian (16) to Eqs. (26) and (27) verifies their equivalence to the coupled Schrödinger equations (20) and (21). The associated set of integral equations for the spatial wave functions $\phi_{\mathbf{p}}^{\rm bg}(\mathbf{r})$ and $\phi_{\mathbf{p}}^{\rm cl}(\mathbf{r})$ may be used, for instance, to numerically determine the exact dressed energy states in the two-channel approach (Köhler, Gasenzer, Julienne, and Burnett, 2003). This formulation of the two-channel scattering problem is also particularly useful for an approximate treatment based on the singularities of the closed-channel Green's function. The single resonance approach, underlying this treatment, provides analytic formulas for the dressed continuum wave functions as well as their associated collision parameters in terms of bare energy states.

2. Single resonance approach

In accordance with Eqs. (19) and (24), the closed-channel Green's function has a singularity at the resonance energy $E_{\rm res}(B)$. Provided that the Feshbach resonance state $\phi_{\rm res}(r)$ is unit normalized, i.e., $\langle\phi_{\rm res}|\phi_{\rm res}\rangle=1$, the singular diagonal matrix element of $G_{\rm cl}(B,E)$ is given by

$$\langle\phi_{\rm res}|G_{\rm cl}(B,E)|\phi_{\rm res}\rangle = [E-E_{\rm res}(B)]^{-1}. \tag{29}$$

Based on Eq. (29), the single resonance approach takes advantage of the near degeneracy of the resonance energy with the entrance channel dissociation threshold illustrated in Fig. 10: At typical cold collision energies $E=p^2/m$, the resonance detuning $\Delta E(B)=E-E_{\rm res}(B)$ in Eq. (29) is negligible compared to the spacings between the discrete energy levels of $H_{\rm cl}(B)$. Consequently, the closed-channel Green's function in Eq. (27) is dominated by its virtually singular diagonal contribution associated with the Feshbach resonance level. These estimates thus lead to the following approximation (Child, 1974; Góral *et al.*, 2004):

$$G_{\rm cl}(B,E) \approx |\phi_{\rm res}\rangle\frac{1}{\Delta E(B)}\langle\phi_{\rm res}|. \tag{30}$$

The single resonance approach consists in replacing the bare Green's function in Eq. (27) with the right-hand side of Eq. (30). This replacement implies that the functional form of the closed-channel component of the dressed continuum wave function $\phi_{\mathbf{p}}^{\rm cl}(\mathbf{r})$ is given by the Feshbach resonance state $\phi_{\rm res}(r)$. The associated overlap factor $\langle\phi_{\rm res}|\phi_{\mathbf{p}}^{\rm cl}\rangle$ is determined by the energy and magnetic-field-dependent amplitude,

$$A(B,E) = \langle\phi_{\rm res}|W|\phi_{\mathbf{p}}^{\rm bg}\rangle/\Delta E(B). \tag{31}$$

The dressed-state component $|\phi_{\mathbf{p}}^{\rm cl}\rangle$ on the right-hand side of Eq. (26) can then be eliminated in favor of the product of $|\phi_{\rm res}\rangle$ and $A(B,E)$. These replacements in Eqs. (26) and (27) give the following explicit formulas for the dressed continuum states in terms of the bare Feshbach resonance and background scattering states:

$$|\phi_{\mathbf{p}}^{\rm bg}\rangle = |\phi_{\mathbf{p}}^{(+)}\rangle + G_{\rm bg}(E+i0)W|\phi_{\rm res}\rangle A(B,E), \tag{32}$$

$$|\phi_{\mathbf{p}}^{\rm cl}\rangle = |\phi_{\rm res}\rangle A(B,E). \tag{33}$$

The amplitude $A(B,E)$ of Eq. (31) may be expressed in terms of the same bare states by inserting Eq. (32) into Eq. (31). This yields

$$A(B,E) = \frac{\langle\phi_{\rm res}|W|\phi_{\mathbf{p}}^{(+)}\rangle}{\Delta E(B) - \langle\phi_{\rm res}|WG_{\rm bg}(E+i0)W|\phi_{\rm res}\rangle}. \tag{34}$$

We note that the dressed continuum wave functions of Eqs. (32) and (33) depend on the magnetic-field strength only through the detuning $\Delta E(B)$ of the resonance energy $E_{\rm res}(B)$ in the denominator of Eq. (34). Within the typical range of experimental magnetic-field strengths $E_{\rm res}(B)$ is a linear function of B to a good approximation. This linear dependence may be represented in terms of an expansion of $E_{\rm res}(B)$ about the resonant field $B_{\rm res}$ at which the Feshbach resonance level crosses the dissociation threshold of the entrance channel. In accordance with the choice of the zero of energy in Fig. 10, $B_{\rm res}$ is determined by $E_{\rm res}(B_{\rm res})=0$. This implies the simple formula (Moerdijk *et al.*, 1995)

$$E_{\rm res}(B) = \mu_{\rm res}(B - B_{\rm res}). \tag{35}$$

Here the slope of the linear curve $\mu_{\rm res}$ is the difference between the magnetic moments of the Feshbach resonance state and a pair of asymptotically separated noninteracting atoms.

The single resonance approach of Eqs. (32)–(34) gives an exact representation of the dressed continuum states provided that the spatial configuration of a closed-channel atom pair is restricted to the Feshbach resonance state $\phi_{\rm res}(r)$. Such an assumption is associated with the following replacement of the closed-channel Hamiltonian:

$$H_{\rm cl}(B) \to |\phi_{\rm res}\rangle E_{\rm res}(B)\langle\phi_{\rm res}|. \tag{36}$$

This simplification of the complete two-channel Hamiltonian of Eq. (16) yields low-energy scattering amplitudes $f(\vartheta,p)$ sufficiently accurate to determine the magnetic-field dependence of the s-wave scattering length $a(B)$.

3. Width and shift of a zero-energy resonance

The s-wave scattering length is determined by the long-range asymptotic behavior associated with the dressed continuum states in terms of the scattering amplitude in the zero momentum limit. This limit is well represented by the following partial wave analysis (Taylor, 1972):

$$f(\vartheta,p) = \sum_{\ell=0}^{\infty} (2\ell+1) f_\ell(p) P_\ell(\cos\vartheta) \underset{p\to 0}{\sim} -a. \tag{37}$$

Here ℓ labels the quantum number associated with the orbital angular momentum and $P_\ell(\cos\vartheta)$ is a Legendre polynomial. The s-wave scattering amplitude is related to the phase shift of Eq. (13) through $f_0(p) = \hbar\exp[i\xi(p)]\sin\xi(p)/p$. We note that the limit $p\to 0$ implies rotational symmetry of the entire wave function $\phi_{\mathbf{p}}^{\rm bg}(\mathbf{r})$, i.e., independence of the scattering angle ϑ, because the incident plane wave in Eq. (22) is isotropic at zero momentum. The higher angular momentum components $f_\ell(p)$ of the scattering amplitude, besides the s wave associated with $\ell=0$, are usually negligible in applications to binary collisions in cold gases due to their proportionality to $p^{2\ell}$.

The behavior of $\phi_{\mathbf{p}}^{\rm bg}(\mathbf{r})$ at asymptotically large interatomic distances r can be inferred from Eq. (28) and from the bare amplitude $f_{\rm bg}(\vartheta,p)$ associated with the background scattering wave function $\phi_{\mathbf{p}}^{(+)}(\mathbf{r})$. In accordance with the explicit representation of the dressed continuum wave function given by Eq. (32), the scattering amplitude is thus given by

$$f(\vartheta,p) = f_{\rm bg}(\vartheta,p) - \frac{m(2\pi\hbar)^3\langle\phi_{\mathbf{p}}^{(-)}|W|\phi_{\rm res}\rangle}{4\pi\hbar^2} A(B,E). \tag{38}$$

In the zero momentum limit, this expression recovers the resonance enhanced s-wave scattering length in terms of the following formula (Moerdijk *et al.*, 1995):

$$a(B) = a_{\rm bg}\left(1 - \frac{\Delta B}{B - B_0}\right). \tag{39}$$

Its parameters are the background scattering length $a_{\rm bg}$, the width ΔB, and the position of the zero-energy resonance B_0. The background scattering length is associated with the bare scattering amplitude $f_{\rm bg}(\vartheta,p)$ via a relation analogous to Eq. (37). The zero momentum limit of Eq. (38) determines the width of the resonance to be

$$\Delta B = \frac{m(2\pi\hbar)^3}{4\pi\hbar^2 a_{\rm bg}\mu_{\rm res}} |\langle\phi_{\rm res}|W|\phi_0^{(+)}\rangle|^2. \tag{40}$$

We note that Eq. (39) predicts the scattering length $a(B)$ to assume all values from $-\infty$ to $+\infty$ due to its singularity at B_0, the measurable magnetic-field strength at which the zero-energy resonance occurs. The width ΔB characterizes the distance in magnetic fields between the position of the singularity B_0 and the zero of the scattering length. The denominator of the amplitude $A(B,E=0)$ given by Eq. (34) determines the physical resonance position B_0 relative to the zero-energy crossing point of the bare Feshbach resonance level $B_{\rm res}$ to be

$$B_0 = B_{\rm res} - \langle\phi_{\rm res}|WG_{\rm bg}(0)W|\phi_{\rm res}\rangle/\mu_{\rm res}. \tag{41}$$

The absolute magnitude of B_0 enters the two-channel approach as an adjustable parameter because the magnetic-field strength $B_{\rm res}$ is not directly measurable. The resonance shift $B_0 - B_{\rm res}$, however, determines characteristic properties of the highest excited dressed vibrational bound state, such as, e.g., the admixture of the closed-channel spin configuration to its wave function.

4. Dressed molecular bound states

In analogy to Eqs. (26) and (27), the two-channel dressed molecular bound states are determined in terms of the bare Green's functions by coupled matrix equations of the following form:

$$|\phi_b^{\rm bg}\rangle = G_{\rm bg}(E_b)W|\phi_b^{\rm cl}\rangle, \tag{42}$$

$$|\phi_b^{\rm cl}\rangle = G_{\rm cl}(B,E_b)W|\phi_b^{\rm bg}\rangle. \tag{43}$$

The discrete bound-state energies E_b are negative, i.e., below the dissociation threshold of the entrance channel. Both channels are therefore closed and, consequently, atom pairs are confined by the potential wells of $V_{\rm bg}(r)$ and $V_{\rm cl}(r)$ in Fig. 10. Their associated wave functions $\phi_b^{\rm bg}(\mathbf{r})$ and $\phi_b^{\rm cl}(\mathbf{r})$ vanish accordingly in the limit of large interatomic distances, similarly to the long-range asymptotic behavior of diatomic halo molecules of Eq. (2). The components of the dressed two-channel bound states can therefore be interpreted in terms of probability amplitudes, subject to the normalization condition

$$\langle\phi_b^{\rm bg}|\phi_b^{\rm bg}\rangle + \langle\phi_b^{\rm cl}|\phi_b^{\rm cl}\rangle = 1. \tag{44}$$

Figure 11 illustrates the magnetic-field dependence of the highest excited dressed vibrational bound state, re-

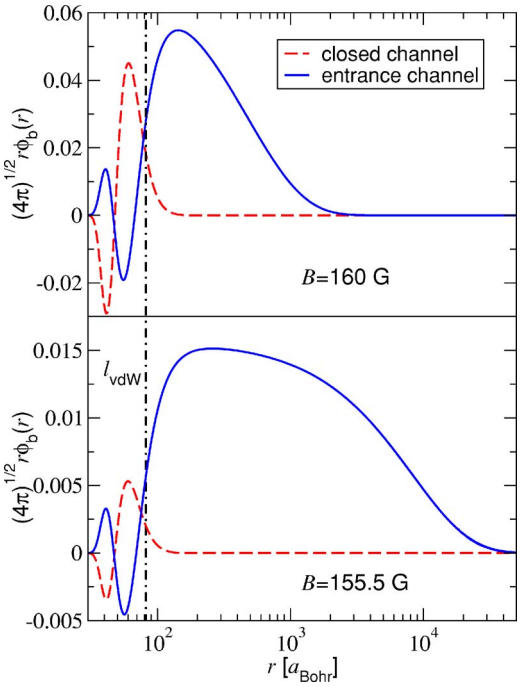

FIG. 11. (Color online) Entrance- and closed-channel components of the highest excited vibrational bound state associated with the 155 G zero-energy resonance of ^{85}Rb vs the interatomic distance r (Köhler, Gasenzer, Julienne, and Burnett, 2003). The wave functions were determined using the model in Fig. 10 for magnetic-field strengths of 160 G (upper panel) and 155.5 G (lower panel), respectively. Nodes of the wave functions at short distances are associated with the vibrational states supported by the bare potentials. The long-range behavior of the entrance-channel wave functions, beyond the van der Waals length of $82a_{\mathrm{Bohr}}$ (dot-dashed line), is largely determined just by the binding energy of the Feshbach molecule (Köhler, Gasenzer, and Burnett, 2003). Note that the interatomic distance is given on a logarithmic scale.

ferred to in the following as the Feshbach molecule, for the example of the 155 G zero-energy resonance of ^{85}Rb. The wave functions $\phi_b^{\mathrm{bg}}(\mathbf{r})$ and $\phi_b^{\mathrm{cl}}(\mathbf{r})$ represent exact solutions of Eqs. (42) and (43) associated with the model potentials of Fig. 10 using $\mu_{\mathrm{res}}/h=-3.46$ MHz/G. The entrance-channel components $\phi_b^{\mathrm{bg}}(\mathbf{r})$ of Fig. 11 are extended over a wide range of interatomic distances. This range increases beyond all limits as the magnetic-field strength B approaches the zero-energy resonance position of $B_0\approx 155$ G. The bond length of the Feshbach molecules in Fig. 11, i.e., their mean interatomic distance, is given, for instance, by $\langle r\rangle=521a_{\mathrm{Bohr}}$ at 160 G and $4255a_{\mathrm{Bohr}}$ at 155.5 G. Figure 11 also suggests that the functional form of the closed-channel component $\phi_b^{\mathrm{cl}}(\mathbf{r})$ is virtually independent of B. Numerical studies (Köhler, Gasenzer, Julienne, and Burnett, 2003) reveal that $\phi_b^{\mathrm{cl}}(\mathbf{r})$ is proportional to the bare resonance wave function $\phi_{\mathrm{res}}(r)$ which indicates the applicability of Eq. (36). The probability of detecting an atom pair in the closed-channel spin configuration, i.e., $\langle\phi_b^{\mathrm{cl}}|\phi_b^{\mathrm{cl}}\rangle=\int d\mathbf{r}|\phi_b^{\mathrm{cl}}(\mathbf{r})|^2$, decreases from about 4.7% at $B=160$ G to only 0.1% at $B=155.5$ G. Given that $\phi_b^{\mathrm{cl}}(\mathbf{r})$ is spatially confined in the same manner as the resonance state, the suppression of the closed-channel component is a consequence of the increasing range of $\phi_b^{\mathrm{bg}}(\mathbf{r})$ and the normalization condition of Eq. (44). These trends reflect general properties of Feshbach molecules that can be readily explained using the single resonance approach.

In analogy to the treatment of the dressed continuum levels, the single resonance approach to the two-channel bound states is equivalent to the pole approximation to the closed-channel Green's function of Eq. (30). This approximation renders Eq. (43) into a practical form. Its analytic solution may be inserted into Eq. (42), which yields the following unit-normalized dressed molecular two-component state:

$$\begin{pmatrix}|\phi_b^{\mathrm{bg}}\rangle\\ |\phi_b^{\mathrm{cl}}\rangle\end{pmatrix}=\frac{1}{\mathcal{N}_b}\begin{pmatrix}G_{\mathrm{bg}}(E_b)W|\phi_{\mathrm{res}}\rangle\\ |\phi_{\mathrm{res}}\rangle\end{pmatrix}. \tag{45}$$

Here $\mathcal{N}_b$ is the associated normalization constant whose explicit expression reads

$$\mathcal{N}_b=\sqrt{1+\langle\phi_{\mathrm{res}}|WG_{\mathrm{bg}}^2(E_b)W|\phi_{\mathrm{res}}\rangle}. \tag{46}$$

In the single resonance approach, all bound-state energies E_b are determined by a constraint on Eq. (45) which can be derived by multiplying Eq. (42) by $\langle\phi_{\mathrm{res}}|W$ from the left. This leads to the following formula:

$$E_b=\mu_{\mathrm{res}}(B-B_{\mathrm{res}})+\langle\phi_{\mathrm{res}}|WG_{\mathrm{bg}}(E_b)W|\phi_{\mathrm{res}}\rangle. \tag{47}$$

We note that Eq. (47) recovers Eq. (41) in the limits $E_b\to 0$ and $B\to B_0$, provided that the magnetic-field strength approaches B_0 from the side of positive scattering lengths. This confirms that the binding energy of the Feshbach molecule vanishes at the measurable resonance position B_0. Such a weak bond implies that the properties of the near-resonant highest excited dressed vibrational state are determined solely by the scattering length a in analogy to the general findings with respect to halo dimers in Sec. II. The range of magnetic-field strengths in which the Feshbach molecular state as well as its energy depend just on a is usually referred to as the universal regime.

D. Universal properties of Feshbach molecules

In accordance with the results of Sec. II, the properties of halo dimers, such as, e.g., the large spatial extent of their wave functions in Fig. 11, can all be inferred from Eq. (1), the universal formula for their binding energy.

1. Universal binding energy

The formal derivation of Eq. (1) for Feshbach molecules (Góral *et al.*, 2004) relies upon an explicit determination of the matrix element involving $G_{\mathrm{bg}}(E_b)$ on the right-hand side of Eq. (47). This may be performed on the basis of the following resolvent identity:

$$G_{\rm bg}(E_b) = G_{\rm bg}(0) - E_b G_{\rm bg}(0) G_{\rm bg}(E_b). \quad (48)$$

Multiplication of Eq. (48) by $G_{\rm bg}^{-1}(0) = -H_{\rm bg}$ from the left and by $G_{\rm bg}^{-1}(E_b) = E_b - H_{\rm bg}$ from the right readily verifies this identity. The contribution to Eq. (47) from the first term $G_{\rm bg}(0)$ on the right-hand side of Eq. (48) yields the energy shift $\mu_{\rm res}(B_{\rm res} - B_0)$ due to Eq. (41). To evaluate the contribution from the second term $-E_b G_{\rm bg}(0) G_{\rm bg}(E_b)$ it is instructive to employ the spectral decomposition of the bare entrance-channel Green's function,

$$G_{\rm bg}(z) = \int d\mathbf{p} \frac{|\phi_{\mathbf{p}}^{(+)}\rangle\langle\phi_{\mathbf{p}}^{(+)}|}{z - p^2/m} + G_{\rm bg}^b(z). \quad (49)$$

Here the energy argument z is either zero or E_b. The quantity $G_{\rm bg}^b(z)$ includes all contributions to $G_{\rm bg}(z)$ from the bare bound states whose energies, depicted in Fig. 10, are usually far detuned from typical energies of Feshbach molecules in the universal regime. Thus neglecting $G_{\rm bg}^b(z)$ in the product $-E_b G_{\rm bg}(0) G_{\rm bg}(E_b)$ determines the zero bound-state energy limit of Eq. (47) to be

$$\mu_{\rm res}(B - B_0) - m^2 E_b \int d\mathbf{p} \frac{|\langle\phi_{\rm res}|W|\phi_{\mathbf{p}}^{(+)}\rangle|^2}{p^2(p^2 + m|E_b|)} \underset{E_b \to 0}{\sim} 0. \quad (50)$$

The corrections neglected on the left-hand side of Eq. (50) are all linear in E_b, while the leading contribution involving the momentum integral is proportional to $\sqrt{|E_b|}$ in the limit $E_b \to 0$. In particular, the asymptotic behavior of the integral can be determined explicitly via a change of variable in spherical coordinates from the modulus of the momentum p to the dimensionless quantity $p/\sqrt{m|E_b|}$. This yields

$$\int d\mathbf{p} \frac{|\langle\phi_{\rm res}|W|\phi_{\mathbf{p}}^{(+)}\rangle|^2}{p^2(p^2 + m|E_b|)} \underset{E_b \to 0}{\sim} \frac{2\pi^2 |\langle\phi_{\rm res}|W|\phi_0^{(+)}\rangle|^2}{(m|E_b|)^{1/2}}. \quad (51)$$

Equation (40) may be used to eliminate the matrix element involving the coupling $W(r)$ on the right-hand side of Eq. (51) in favor of the product $a_{\rm bg}\Delta B \mu_{\rm res}$. The solution of Eq. (50) with respect to the bound-state energy thus reads

$$E_b = -\frac{\hbar^2}{m[-a_{\rm bg}\Delta B/(B - B_0)]^2}. \quad (52)$$

As anticipated (Donley *et al.*, 2002) for the general reasons outlined in Sec. II, this formula exactly recovers Eq. (1) in the limit $B \to B_0$ as the singular contribution to $a(B)$ on the right-hand side of Eq. (39) exceeds $|a_{\rm bg}|$.

2. Wigner threshold law

The preceding derivation of the low binding-energy behavior on the right-hand side of Eq. (47) may be extended also to positive continuum energies $E = \hbar^2 k^2/m$ which determines the width of the Feshbach resonance level (Moerdijk *et al.*, 1995; Mies *et al.*, 2000). This width in energy is related to the decay rate of the bare resonance state into a given continuum level associated with the wave number k via Fermi's golden rule (Mukaiyama *et al.*, 2003; Dürr, Volz, and Rempe, 2004; Góral *et al.*, 2004; Haque and Stoof, 2005). The approach underlying these derivations is based on the spectral decomposition of $G_{\rm bg}(z)$ in Eq. (49), in addition to the following formula:

$$\frac{1}{z - p^2/m} = -i\pi\delta(E - p^2/m) + \mathcal{P}\frac{1}{E - p^2/m}. \quad (53)$$

Here $z = E + i0$ is the complex argument of $G_{\rm bg}(z)$ introduced in Eq. (26), and $\mathcal{P}$ indicates the principal value of the momentum integral in Eq. (49). In accordance with Fermi's golden rule, the width of the resonance level is given by the modulus of the imaginary part of the following matrix element of the bare entrance-channel Green's function:

$$\langle\phi_{\rm res}|W G_{\rm bg}(z) W|\phi_{\rm res}\rangle \underset{k \to 0}{\sim} \mu_{\rm res}(B_{\rm res} - B_0 - ika_{\rm bg}\Delta B). \quad (54)$$

We note, however, that Eq. (53) is not suitable for determining the left-hand side of Eq. (54) in the case of negative bound-state energies $z = E_b$ as the δ-function contribution vanishes identically. The derivation of Eq. (52) therefore relies upon Eq. (48).

As the imaginary part of Eq. (54) is associated with the decay of the bare resonance state, the product $a_{\rm bg}\mu_{\rm res}\Delta B$ is always positive and characterizes the strength of the interchannel coupling. Equation (54) also determines the low-energy dressed continuum wave functions of Eqs. (32) and (33) via Eq. (34). In particular, the s-wave scattering amplitude of Eqs. (37) and (38) is given by its well-known general expansion about zero momentum (Taylor, 1972),

$$f_0(\hbar k) \underset{k \to 0}{\sim} -a(1 - ika), \quad (55)$$

which is applicable provided that the condition $ka \ll 1$ is fulfilled. The proportionality to $k = \sqrt{mE}/\hbar$ of the imaginary parts on the right-hand sides of Eqs. (54) and (55) reflects a general prediction known as the Wigner threshold law (Wigner, 1948). In the context of an analytic continuation to imaginary wave numbers $k = i\sqrt{m|E_b|}/\hbar$, Eq. (54) also yields the universal bound-state energy of Eq. (52) using Eq. (47) (Duine and Stoof, 2004). The universal regime may therefore be considered as the range of magnetic-field strengths in which the Wigner threshold law applies to the energy of the Feshbach molecule in Eq. (47). Its extension about B_0 depends on the interplay between the spin exchange (or dipolar) and entrance-channel interactions as well as on the properties of the Feshbach resonance state (Mies *et al.*, 2000; Köhler, Gasenzer, Julienne, and Burnett, 2003; Marcelis *et al.*, 2004; Nygaard *et al.*, 2006).

Figure 12, for instance, illustrates several theoretical approaches to the bound-state energy of the $^{85}Rb_2$ Feshbach molecule in the vicinity of the 155 G zero-energy resonance. Although the universal formula of Eq. (1) determines the asymptotic behavior of E_b in the limit $B \to B_0$, it provides a reasonable approximation only in a

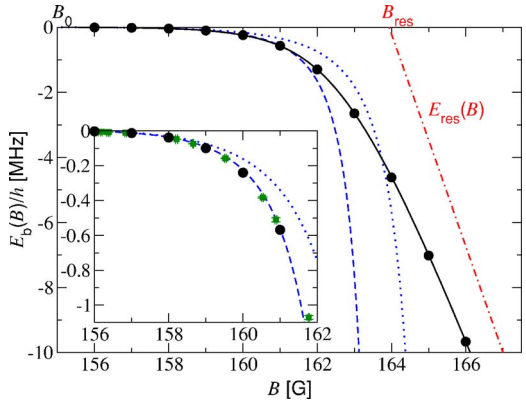

FIG. 12. (Color online) Bound-state energy of the $^{85}Rb_2$ Feshbach molecule as a function of the magnetic field strength in the vicinity of the 155 G zero-energy resonance. Circles indicate a full coupled-channels calculation (Kokkelmans, 2002). The solid curve results from a two-channel approach (Góral *et al.*, 2005). For comparison, the dotted curve represents the universal estimate of E_b, while the dashed curve includes the leading correction to Eq. (1) due to the van der Waals tail of the background scattering potential (Gribakin and Flambaum, 1993; Köhler, Gasenzer, and Burnett, 2003) given by Eq. (66). We note the pronounced shift of about 9 G between the measurable resonance position B_0 and the magnetic-field strength B_{res} at which the resonance energy (dot-dashed line) crosses the dissociation threshold of the entrance channel. Inset: Theoretical approaches compared with measurements (Claussen *et al.*, 2003) indicated by squares.

small region between $B_0 \approx 155$ and about 158 G. Both the full coupled channels calculation (circles) and two-channel predictions (solid curve) depend on specific properties of the particular ^{85}Rb zero-energy resonance besides the scattering length. These approaches fully recover the measured Feshbach molecular energies (see the inset of Fig. 12) over the entire experimental range of magnetic-field strengths from about 156 to 162 G (Claussen *et al.*, 2003). The slope of the linear magnetic-field dependence E_b in the limit of high fields in Fig. 12 is determined by the bare resonance energy $E_{res}(B)$ (dot-dashed line). This indicates an increasing admixture of the closed-channel spin configuration to the dressed bound state.

3. Closed-channel admixture

In accordance with Eq. (45) and the unit normalization of the bare Feshbach resonance state, the closed-channel admixture to the Feshbach molecule is determined by the wave-function normalization constant $\mathcal{N}_b$ of Eq. (46) to be

$$\langle \phi_b^{cl} | \phi_b^{cl} \rangle = \mathcal{N}_b^{-2} 4\pi \int_0^\infty r^2 dr |\phi_{res}(r)|^2 = \mathcal{N}_b^{-2}. \tag{56}$$

In the context of field-theoretic approaches to the many-body physics of cold gases, the inverse square of the normalization constant $\mathcal{N}_b^{-2}$ is sometimes referred to as the wave-function renormalization constant $Z(B)$ (Braaten *et al.*, 2003; Duine and Stoof, 2003a; Bruun and Pethick, 2004; Góral *et al.*, 2004). The quantity $Z(B)$ can be expressed in terms of the difference in magnetic moments of the Feshbach molecular state and a pair of separated atoms in the entrance-channel spin configuration, i.e., $\partial E_b / \partial B$, via

$$Z(B) = \mathcal{N}_b^{-2} = \mu_{res}^{-1} \frac{\partial E_b}{\partial B}. \tag{57}$$

This exact result follows directly from Eqs. (46) and (47) using the general relation

$$G_{bg}^2(E_b) = -\frac{\partial}{\partial E_b} G_{bg}(E_b). \tag{58}$$

Within the universal regime of magnetic-field strengths, the closed-channel admixture to the Feshbach molecule can therefore be inferred from the derivative of Eq. (1) with respect to B. This yields

$$Z(B) \underset{B \to B_0}{\sim} \frac{2a\hbar^2/ma^2}{\mu_{res} \Delta B a_{bg}}. \tag{59}$$

Here the limit $B \to B_0$ is performed on the side of positive scattering lengths of the zero-energy resonance.

In accordance with Eq. (59), the wave-function normalization constant $\mathcal{N}_b$ diverges as the magnetic-field strength approaches B_0, i.e., in the limit $a \to \infty$, due to the proportionality of its leading contribution to $\sqrt{a}$. This implies that the closed-channel admixture to the Feshbach molecule of Eq. (56) is negligible in the universal regime and vanishes at the measurable zero-energy resonance position. Within this limited range of magnetic-field strengths about B_0, the Feshbach molecule can therefore be described in terms of just its entrance-channel component, in analogy to Sec. II. In particular, the wave function $\phi_b^{bg}(\mathbf{r})$ is determined by Eq. (2) at interatomic distances large compared to the van der Waals length of Fig. 11. In accordance with Eq. (3), the mean distance between the atomic constituents of universal Feshbach molecules is well estimated by its asymptotic value of one-half of the scattering length in the limit $a \to \infty$ (Köhler, Gasenzer, Julienne, and Burnett, 2003). In the universal regime of magnetic-field strengths, Feshbach molecules are therefore proper diatomic halo states with the general properties described in Sec. II.

E. Experimental signatures of universality

The suppression of the closed-channel admixture to the Feshbach molecular state has been directly observed for near-resonant $^6Li_2$ dimers (Partridge *et al.*, 2005). Figure 13 shows a comparison of these measurements with the universal estimate of Eq. (59) as well as with Eq. (68) of Sec. III.F. The estimate of Eq. (68) is based on Eq. (57) using the approximation for E_b of Eq. (66), which is illustrated in the inset of Fig. 12. The underlying approach (Gribakin and Flambaum, 1993) accounts for the corrections to the universal bound-state energy of Eq. (1) due to the van der Waals interaction of the back-

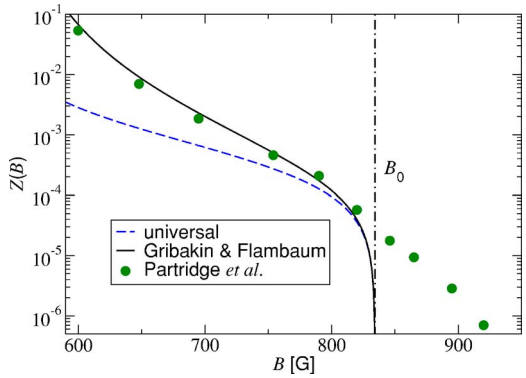

FIG. 13. (Color online) Occupation of the closed-channel resonance level relative to the number of atom pairs in a balanced mixture of two spin components of ^{6}Li vs magnetic-field strength in the vicinity of the 834 G zero-energy resonance (Partridge *et al.*, 2005). On the low-field side of the resonance position B_0 (dot-dashed line), the gas was prepared as a Bose-Einstein condensate of $^6Li_2$ Feshbach molecules. Experimental data (circles) indicate the suppression of the closed-channel admixture to the dressed molecular state, i.e., $Z(B)=\mathcal{N}_b^{-2}$, over three orders of magnitude in agreement with Eq. (68) (solid curve). The dashed curve shows the universal estimate of Eq. (59) for comparison. Note that the bond length of the Feshbach molecules given by Eq. (3) reaches the order of magnitude of the average interatomic spacing of the gas $10^4 a_{\mathrm{Bohr}}$ at a magnetic-field strength of about 800 G. In this strongly interacting regime, the purely two-body theories are bound to break down. On the high-field side of B_0, the remnant small resonance state population indicates pairing phenomena in a cold, strongly correlated two-spin-component Fermi gas with a negative scattering length (Partridge *et al.*, 2005).

ground scattering potential in addition to the scattering length $a(B)$. Its predictions agree well with exact coupled channels calculations of the closed-channel admixture to the Feshbach molecular state (Partridge *et al.*, 2005). Several experiments to date have also directly confirmed the universal limit of the binding energy, in analogy to the inset of Fig. 12 (Donley *et al.*, 2002; Claussen *et al.*, 2003) for a variety of alkali atomic species (Regal *et al.*, 2003a; Bartenstein *et al.*, 2005; Moritz *et al.*, 2005).

1. Collisional relaxation

Besides these demonstrations of universality, the long-range nature of highly excited Feshbach molecules is manifest in their lifetimes with respect to deeply inelastic collisions. Such molecular loss may occur due to relaxation into tightly bound diatomic states upon collisions with surrounding atoms or dimers (Cubizolles *et al.*, 2003; Mukaiyama *et al.*, 2003; Regal *et al.*, 2004a). The associated loss mechanism was discussed first, in the context of cold gases, for collisions between H_2 dimers and hydrogen atoms (Balakrishnan *et al.*, 1997). In these thresholdless reactions, the energy lost through deexcitation is transferred to the relative motion of the products in accordance with momentum conservation. The associated relative velocities are sufficiently high for scattered particles to leave an atom trap. The density n_d of dimer molecules in a homogeneous gas is therefore depleted in accordance with the following rate equation:

$$\dot{n}_d/n_d = -K_{\mathrm{ad}} n_a - K_{\mathrm{dd}} n_d. \tag{60}$$

Here n_a is the density of atoms and K_{ad} and K_{dd} denote the inelastic loss rate constants associated with atom-dimer and dimer-dimer collisions, respectively.

Several theoretical studies of collisional relaxation of alkali-metal systems have been performed in the limit of low vibrational excitation of the initial dimer states (Cvitas *et al.*, 2002, 2005a, 2005b) as well as for Feshbach molecules (Petrov *et al.*, 2004, 2005b). In the case of collisions between alkali-metal atoms and their dimers in excited states, whose bond lengths are smaller than l_{vdW}, *ab initio* calculations suggest the inelastic rate constants K_{ad} to be on the order of 10^{-10} cm^3/s (Cvitas *et al.*, 2002, 2005a, 2005b). For such species, the collisional relaxation rates in cold gases would be too large for the observation of any phenomena relying upon the equilibration of the molecular component. The expected short lifetimes of alkali dimers have been confirmed, for instance, via photoassociation of ^{87}Rb atoms in a Bose-Einstein condensate (Wynar *et al.*, 2000).

2. Lifetime of Feshbach molecules in Fermi gases

Therefore it came as a surprise that cold Feshbach molecules produced from incoherent mixtures of two spin components of fermionic atoms could be stabilized for up to several seconds at densities of about 10^{13} atoms/cm^3 (Cubizolles *et al.*, 2003; Jochim *et al.*, 2003a; Strecker *et al.*, 2003; Regal *et al.*, 2004a). Under such conditions, the ratio of elastic to inelastic collisions is sufficiently large to allow for an efficient evaporative cooling of dimers. As a consequence of their stability, even the Bose-Einstein condensation of Feshbach molecules has been observed in the vicinity of broad zero-energy resonances of ^{6}Li and ^{40}K at about 830 and 202 G, respectively (Greiner *et al.*, 2003; Jochim *et al.*, 2003b; Zwierlein *et al.*, 2003). The associated resonance widths ΔB are on the order of 300 G for ^{6}Li (Bartenstein *et al.*, 2005) and about 8 G for ^{40}K (Greiner *et al.*, 2003). Such a broadness provides the opportunity for performing measurements in the universal regime of magnetic-field strengths.

Both species of dimers in these experiments consist of pairs of unlike fermionic atoms in the lowest energetic Zeeman states. For ^{40}K, the associated atomic spin components are determined by the quantum numbers $(f=9/2, m_f=-9/2)$ and $(f=9/2, m_f=-7/2)$. Here f labels the angular momentum quantum number of the hyperfine level with which the Zeeman state correlates adiabatically at zero magnetic field, and m_f indicates its spin orientation with respect to the field axis. Similarly, the pair of atomic Zeeman states associated with the 830 G zero-energy resonance of ^{6}Li is described by the quantum numbers $(f=1/2, m_f=1/2)$ and $(f=1/2, m_f=-1/2)$.

We note that the Pauli exclusion principle allows such atom pairs to interact via *s* waves given that their spin wave functions are antisymmetric. Consequently, the results of Sec. II on isotropic halo dimers apply to these Feshbach molecules consisting of unlike fermions. Experiments on molecular Bose-Einstein condensation have been performed at near-resonant magnetic-field strengths for which the associated dimer bond lengths can be as large as 100 nm (Zwierlein *et al.*, 2003).

The stability of such Feshbach molecules with respect to collisional relaxation relies upon the Pauli exclusion principle in addition to the separation of length scales associated with the initial and final states (Petrov *et al.*, 2004, 2005b). In accordance with Eq. (3), the spatial extent of the initial halo wave function is determined by the scattering length a. The bond length of the final, deeply bound target level may be estimated by the van der Waals length l_{vdW}, which is much smaller than a. Both dimer-dimer and atom-dimer relaxation, therefore, require at least three fermions to come together at short distances on the order of l_{vdW}. One pair among these atoms necessarily shares the same spin state and can interact at most via p waves. As the momentum scale associated with the initial Feshbach molecular state is determined by the wave number $k \sim 1/a$, the inelastic loss rate constants are suppressed by powers of $kl_{\mathrm{vdW}} \ll 1$.

Based on the halo wave function of Eq. (2), the precise a dependences of the suppression factors for atom-dimer and dimer-dimer relaxation have been predicted to be $a^{-3.33}$ and $a^{-2.55}$, respectively (Petrov *et al.*, 2004, 2005b). While these predictions strictly apply just to the universal regime of magnetic-field strengths, Fig. 14 illustrates that their general trends agree with measurements on cold gases of ^{40}K with a component of Feshbach molecules (Regal *et al.*, 2004a). These observations are consistent with the reduction of a predominant dimer-dimer relaxation in the limit of large scattering lengths, where the lifetimes reach about 100 ms. Conversely, as the magnetic-field strength is tuned away from the zero-energy resonance, the molecular lifetimes approach those small values of less than a millisecond, typical for short-ranged alkali dimers in cold gases.

Besides their scaling properties with respect to the scattering length, the inelastic loss rate constants of Feshbach molecules depend sensitively on interatomic interactions at short distances below l_{vdW}. The experimental trends regarding collisional relaxation of alkali dimers confined to such length scales are inconclusive. Remarkably long lifetimes on the order of seconds were reported, for instance, even in the case of short-ranged, closed-channel dominated Feshbach molecules produced in a fermionic ^{6}Li gas in the vicinity of the narrow 543 G zero-energy resonance (Strecker *et al.*, 2003). Such alkali dimers, however, are not described by the halo wave function of Eq. (2). Their observed stability, therefore, suggests a mechanism for the suppression of collisional relaxation beyond the scaling of the associated loss rate constants with powers of the inverse scattering length.

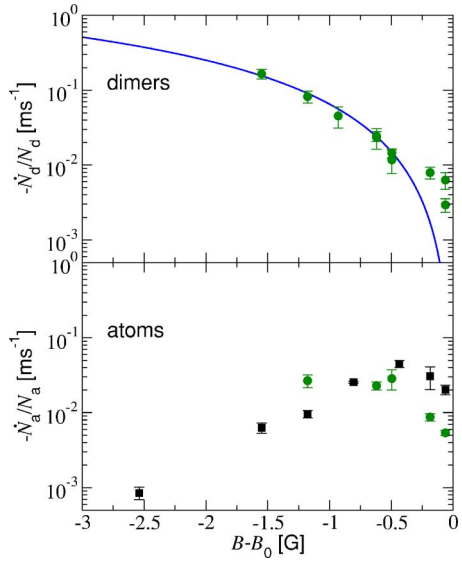

FIG. 14. (Color online) Loss rates of diatomic Feshbach molecules (upper panel) and remnant atoms (lower panel) vs magnetic-field detuning $B-B_0$ in the vicinity of the 202 G zero-energy resonance in a cold gas of ^{40}K with a peak density of about 1.5×10^{13} atoms/cm^3 (Regal *et al.*, 2004a). Dimers were produced by adiabatic sweeps of the magnetic-field strength described in Sec. IV. Their number is denoted by N_d, while N_a refers to the number of remnant unbound atoms. Circles in the upper panel indicate the measured dimer loss, whose general trend is well fit by an $a^{-2.3\pm0.4}$ power law as a function of the scattering length (solid curve). Significant deviations from this scattering length dependence occur in a small region of magnetic-field strengths where the bond length of the dimers given by Eq. (3) is comparable to the average distance of the atoms in the gas. The lower panel shows the loss rate of remnant unbound atoms in gases with (circles) or without (squares) deliberate production of Feshbach molecules. The associated trends suggest that the atomic loss is largely unaffected by the presence of a dimer component in the gas (Regal *et al.*, 2004a).

3. Lifetime of Feshbach molecules in Bose gases

Feshbach molecules consisting of identical Bose atoms generally tend to be less stable than their fermionic counterparts. Large collisional relaxation rate constants on the order of 10^{-10} cm^3/s have been reported for those dimers associated in cold gases in the vicinity of comparatively narrow zero-energy resonances of ^{87}Rb, ^{133}Cs, and ^{23}Na (Yurovsky *et al.*, 1999b, 2000; Herbig *et al.*, 2003; Mukaiyama *et al.*, 2003; Dürr, Volz, Mate, and Rempe, 2004). With a width of about 11 G (Claussen *et al.*, 2003) the 155 G zero-energy resonance of ^{85}Rb is by far the broadest among the bosonic species from which Feshbach molecules were produced. The atomic constituents of these dimers are prepared in the excited Zeeman state determined by the quantum numbers $(f=2, m_f=-2)$, which, in contrast to the electronic ground state, can be magnetically trapped. Pairs of such atoms

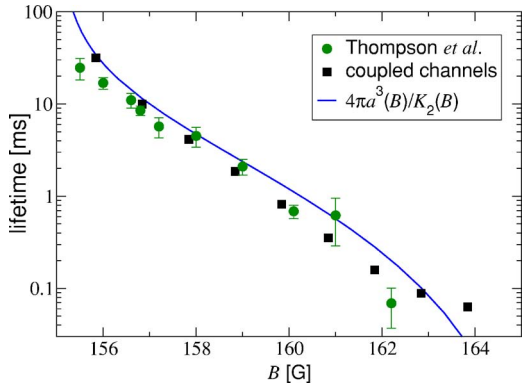

FIG. 15. (Color online) Lifetime of $^{85}Rb_2$ dimers vs magnetic-field strength in the vicinity of the 155 G zero-energy resonance. Circles indicate measurements in a cold thermal gas with a peak density of 6.6×10^{11} atoms/cm^3 (Thompson *et al.*, 2005b), while squares refer to exact coupled-channels calculations for spontaneous dissociation of Feshbach molecules due to spin relaxation (Köhler *et al.*, 2005). The solid curve represents an asymptotic estimate of the lifetime based on the universal halo wave function given by Eq. (2) and the spin relaxation loss rate constant $K_2(B)$ associated with a nondegenerate Bose gas in the limit of zero collision energy. The two-body theory only fails close to resonance when the molecular bond length becomes comparable to the average interatomic distance of the gas.

are subject to inelastic spin relaxation collisions involving the thresholdless transition of the atomic energy level to a deeper Zeeman state (Roberts *et al.*, 2000b). The associated d-wave exit channels are illustrated in Table II. It is the spontaneous dissociation via spin relaxation, rather than collisional relaxation of the molecular vibrational state, that predominantly limits the observed lifetimes of Feshbach molecules produced in dilute gases of ^{85}Rb. This decay mechanism has been unequivocally identified through comparisons with quantitative predictions (Köhler *et al.*, 2005; Thompson *et al.*, 2005b).

Figure 15 shows the monotonic increase of the measured lifetimes over three orders of magnitude as the magnetic-field strength approaches the resonance position B_0. The lifetime of these Feshbach molecules is density independent and reaches several tens of milliseconds. The molecular decay behavior can be explained in terms of a probabilistic estimate based on the average volume $\mathcal{V}=4\pi\langle r^3\rangle/3$ occupied by an atom pair in the universal halo state of Eq. (2). In analogy with Eq. (3), this volume is determined in terms of the scattering length a by $\mathcal{V}=\pi a^3$. The event rate γ associated with the spin relaxation of such a bound atom pair may be expressed in terms of the loss rate constant K_2 for spin relaxation in a nondegenerate Bose gas (Roberts *et al.*, 2000b). This yields $\gamma=K_2/4\mathcal{V}$ (Stoof *et al.*, 1989). The lifetime $\tau=1/\gamma$ is therefore proportional to the ratio of the magnetic-field-dependent quantities $a^3(B)$ and $K_2(B)$, i.e., $\tau=4\pi a^3(B)/K_2(B)$, where near resonance $K_2(B)$ can be evaluated at zero collision energy. The same formula for the molecular lifetime also follows rigorously from Fermi's golden rule (Köhler *et al.*, 2005) and exactly recovers the results of the full coupled channels calculations of Fig. 15 in the limit $B\to B_0$. The magnetic-field dependence of $K_2(B)$ can be inferred from general properties of inelastic collisions (Bohn and Julienne, 1997, 1999). Consequently, the stability of Feshbach molecules in both two-spin-component Fermi gases of ^{40}K and dilute vapors of ^{85}Rb directly probes the halo nature of these dimers near resonance, despite their different decay mechanisms.

F. Classification of zero-energy resonances

The singular behavior of the scattering length as well as the existence of a universal regime of magnetic-field strengths are common to all Feshbach resonance phenomena in cold gases. Two-body universality implies, in particular, that the long-range properties of the dressed diatomic bound states are well described in terms of an effective entrance-channel interaction. The range of validity of such single-channel approaches provides classification schemes for zero-energy resonances.

1. Size of the universal regime

The halo wave function of Eq. (2) may be interpreted as the only bound state supported by a contact pseudopotential $g\delta(\mathbf{r})$ describing the low-energy spectrum of an atom pair with a positive scattering length. Due to their simplicity, contact interactions are widely used in theoretical descriptions of cold gases (Randeria, 1995; Dalfovo *et al.*, 1999; Dalibard, 1999). In these approaches the properties of interatomic collisions enter the many-body Hamiltonian in terms of a coupling constant $g=4\pi\hbar^2a/m$ depending on the microscopic potential just through the scattering length a. The associated binary s-wave scattering amplitude is given by

$$f_0(\hbar k)=-a/(1+ika). \tag{61}$$

We note that Eq. (61) also recovers the general low wave-number expansion of Eq. (55) in the Wigner threshold law regime. Consequently, the contact interaction approach provides a minimal implementation of the universal low-energy two-body physics, applicable to both positive and negative scattering lengths. In the latter case the contact pseudopotential does not support any bound state.

Assuming universality of the Feshbach molecular state implies the closed-channel admixture of Eq. (56) to be negligible. For magnetic-field strengths B far inside the width of the zero-energy resonance, i.e., $|B-B_0|\ll\Delta B$, Eqs. (39) and (59) therefore yield the following condition necessary for the applicability of the contact interaction approach:

$$\left|\frac{B-B_0}{\Delta B}\right|\ll\frac{|\mu_{\rm res}\Delta B|}{2\hbar^2/ma_{\rm bg}^2}. \tag{62}$$

The energy ratio on the right-hand side of Eq. (62) provides an upper estimate for the extent of the universal

regime relative to the width of the zero-energy resonance. A ratio small compared to unity indicates weak coupling between the closed and entrance channels. Conversely, broad zero-energy resonances with a large product $|\mu_{\rm res}\Delta B|$ tend to favor negligible admixtures of the bare resonance level to the dressed Feshbach molecular state over a substantial fraction of their width. This trend may be enhanced by a small energy $\hbar^2/ma_{\rm bg}^2$, which indicates the presence of bound vibrational ($a_{\rm bg}>0$) or virtual ($a_{\rm bg}<0$) near-resonant energy levels of the bare background scattering potential.

A small closed-channel admixture to the Feshbach molecular state, however, is not necessarily identical to the universality of the binding energy. While for the example of the comparatively weakly coupled 1007 G zero-energy resonance of ^{87}Rb (Dürr, Volz, and Rempe, 2004) the right-hand side of Eq. (62) gives 0.1, it is as large as 81 for the 155 G zero-energy resonance of ^{85}Rb. The estimate of Eq. (62) for ^{85}Rb, however, is inaccurate with respect to the extension of the universal regime in units of the width ΔB given the results of Fig. 12. The inset of Fig. 12 reveals that this inaccuracy originates predominantly from corrections to the universal binding energy due to the van der Waals tail of the bare ^{85}Rb background scattering potential (Gribakin and Flambaum, 1993). In the case of such entrance-channel-dominated zero-energy resonances, even the lowest-order corrections to universality may be described just by a single-channel approach (Köhler, Gasenzer, and Burnett, 2003). The minimal requirements on the associated effective potential $V(B,r)$, besides its long-range asymptotic behavior of Eq. (5), are closely related to general properties of alkali dimer energy wave functions.

2. Entrance-channel-dominated resonances

In accordance with Fig. 11, the vibrational bound-state wave functions of $^{85}Rb_2$ Feshbach molecules consist of short- and long-range contributions. The characteristic scale for such a spatial separation is the van der Waals length of Eq. (7). Due to the deep wells of realistic background scattering potentials, the entrance-channel wave functions of alkali dimers are well described by the semiclassical Wentzel-Kramers-Brillouin (WKB) approximation at short interatomic distances $r\ll l_{\rm vdW}$. Their behavior at large separations $r\gg l_{\rm vdW}$ is determined mainly by the van der Waals interaction of Eq. (5) in addition to the energy of the state. In both spatial regions, the functional forms of the associated asymptotic solutions to the radial Schrödinger equation are known analytically (Gribakin and Flambaum, 1993; Gao, 1998a, 1998b). As interactions between alkali atom pairs are dominated by large van der Waals coefficients C_6, on the order of thousands of atomic units (the atomic unit of C_6 is 9.5734×10^{-26} J nm^6), the asymptotic wave functions can be matched. Such a matching procedure provides the basis of accurate semiclassical treatments of bound as well as continuum entrance-channel wave functions (Gribakin and Flambaum, 1993; Flambaum *et al.*, 1999).

Provided that the interaction of alkali atom pairs is well described by an effective entrance-channel potential $V(B,r)$, the semiclassical approach to the zero-energy wave function gives the following scattering length (Gribakin and Flambaum, 1993):

$$a=\bar{a}[1-\tan(\varphi_{\rm WKB}-\pi/8)]. \tag{63}$$

Here $\bar{a}$ is the mean scattering length and $\varphi_{\rm WKB}$ is the semiclassical phase shift. In accordance with the WKB approach, $\varphi_{\rm WKB}$ consists of the following integral between the zero-energy classical turning point r_0 associated with the effective potential $V(B,r)$ and infinite distances:

$$\varphi_{\rm WKB}=\frac{1}{\hbar}\int_{r_0}^{\infty}dr\sqrt{-mV(B,r)}. \tag{64}$$

While $\varphi_{\rm WKB}$ is sensitive to the entire well of the interaction, from $V(B,r_0)=0$ to its long-range tail of Eq. (5), the coefficient $\bar{a}$ of Eq. (63) only depends on the van der Waals length $l_{\rm vdW}$. Its explicit expression in terms of $l_{\rm vdW}$ and Euler's Γ function reads

$$\bar{a}=\frac{l_{\rm vdW}}{\sqrt{2}}\frac{\Gamma(3/4)}{\Gamma(5/4)}\approx 0.955\ 98 l_{\rm vdW}. \tag{65}$$

In accordance with Eq. (63), the parameter $\bar{a}$ determines the characteristic scale of the scattering length. This average potential range is modulated by the poles of the tangent function provided that its argument $\varphi_{\rm WKB}-\pi/8$ is close to an odd integer multiple of $\pi/2$. As $\varphi_{\rm WKB}$ increases, each singularity of a indicates the emergence of an additional vibrational bound state in the potential well.

The functional form of Eq. (63) using a realistic interaction is analogous to the formula for the scattering length of the simplified square well plus hard-core model of an interatomic potential (Gribakin and Flambaum, 1993). Using this exactly solvable model, the mean scattering length $\bar{a}$ recovers the finite outer radius of the well. The analogy between these realistic and simplified interactions implies that in the limit $a\gg\bar{a}$, the energy of the highest excited vibrational state is well approximated by the following asymptotic formula:

$$E_b\approx-\hbar^2/m(a-\bar{a})^2. \tag{66}$$

An independent analysis based on effective range theory for realistic interatomic interactions (Gao, 1998a; Flambaum *et al.*, 1999) confirms the magnitude of the range parameter $\bar{a}$ of Eq. (66) up to a constant factor on the order of unity (Gao, 2004). The remnant uncertainties associated with Eq. (66) may be related to the divergence of the effective range expansion for any potential with a long-range van der Waals tail (Taylor, 1972). Figure 12 illustrates the accuracy of Eq. (66) within the experimentally relevant range of binding energies of near-resonant $^{85}Rb_2$ Feshbach molecules.

According to the semiclassical approach, at magnetic-field strengths in the vicinity of entrance-channel-dominated zero-energy resonances diatomic bound and continuum spectra are determined by $a(B)$ and $\bar{a}$. In such a case, any potential $V(B,r)$, which at each magnetic-field strength B accounts for the scattering length as well as the van der Waals tail of Eq. (5), provides a suitable description of the near-resonant binary physics. This conclusion is rather intuitive because cold collisions are characterized by de Broglie wavelengths too large to resolve details of the effective entrance-channel interaction besides its long-range behavior. The adjustment of $V(B,r)$ to recover the exact magnetic-field dependence of the scattering length of Eq. (39) may be achieved, for instance, by varying the radius of its hard core. In the context of quantum defect theory, such a description of alkali dimer spectra in terms of just the parameters a and C_6 has been rigorously derived for a range of energies much wider than the cold regime (Gao, 1998a).

Since $\bar{a}$ is positive, the semiclassical estimate of the bound-state energy of Eq. (66) is always below the universal prediction of Eq. (1) and becomes singular in the limit $a(B)\rightarrow\bar{a}$, outside the range of validity of Eq. (66). This unphysical behavior is counterbalanced in Eq. (47) by an increasing closed-channel admixture to the Feshbach molecule, in accordance with Eq. (59), which tends to impose a linear slope on $E_b(B)$. The principal question of applying single-channel approaches outside the universal regime of magnetic-field strengths is determined by which one of these trends prevails near resonance (Köhler *et al.*, 2004). Consequently, the bound-state energy $E_b(B)$ in the vicinity of an entrance-channel-dominated zero-energy resonance is subject to the following inequality:

$$\left|E_b(B)+\frac{\hbar^2}{m[a(B)-\bar{a}]^2}\right|<\left|E_b(B)+\frac{\hbar^2}{ma^2(B)}\right|. \quad (67)$$

Within the range of validity of Eq. (66), the admixture of the closed-channel resonance state to the Feshbach molecule is small compared to unity and can be determined from the binding energy via Eq. (57). This yields

$$Z(B)=\frac{2a\hbar^2/ma^2}{\mu_{\rm res}\Delta B a_{\rm bg}}\frac{(1-a_{\rm bg}/a)^2}{(1-\bar{a}/a)^3}. \quad (68)$$

The accuracy of Eq. (68) in applications to $^6Li_2$ Feshbach molecules in the vicinity of the entrance-channel-dominated 834 G zero-energy resonance is illustrated in Fig. 13.

Based on Eq. (67), a more practical criterion can be derived from a low-energy expansion of the right-hand side in Eq. (47) using a specific implementation of the general two-channel approach (Góral *et al.*, 2004). This yields a dimensionless parameter η whose smallness indicates the validity of Eq. (66) beyond the universal regime of magnetic-field strengths (Stoll and Köhler, 2005). Consequently, an entrance-channel-dominated zero-energy resonance fulfills the condition

$$\eta=\frac{\bar{a}}{a_{\rm bg}}\frac{\hbar^2/m\bar{a}^2}{\mu_{\rm res}\Delta B}\ll 1. \quad (69)$$

Such a criterion also results from an adiabatic description of Feshbach resonances (Petrov, 2004).

In the opposite limit $\eta\gg 1$ a zero-energy resonance is referred to as closed-channel-dominated. Closed-channel-dominated zero-energy resonances are typically narrow and their universal regime of magnetic-field strengths is experimentally largely inaccessible. The description of their physical properties, therefore, crucially depends on an explicit treatment of at least two scattering channels.

G. Characteristic parameters of zero-energy resonances

For any two-channel approach to be sensible its implementation should describe the two-body energy spectrum beyond the Wigner threshold law domain. Otherwise, the same physics could be captured simply by using the contact pseudo-interaction of Sec. III.F. The approach should therefore recover both the scattering length of Eq. (39) and the binding energy of the Feshbach molecule beyond the universal regime. Even within such a comparatively wide range of energies, a variety of interatomic potentials are capable of describing the same two-body physics. It is the objective here to provide a minimal set of physical parameters that every two-channel approach should account for, and to illustrate a practical implementation for a typical experimental situation. The adjustment of the Hamiltonian given by Eq. (16) in the single resonance approach of Eq. (36) will be performed on the basis of its energy spectrum derived in Sec. III.C. According to these derivations, the dressed two-channel energy states depend on the bare states associated with the background scattering via $G_{\rm bg}(z)$, on the resonance energy $E_{\rm res}(B)$, and on the product $W|\phi_{\rm res}\rangle$ characterizing the interchannel coupling. Just these quantities need to be adjusted. The specific form of the resonance wave function $\phi_{\rm res}(r)$ does not affect the two-body spectrum in the single resonance approach.

1. Background scattering potential

In accordance with Sec. III.F, all implementations of $V_{\rm bg}(r)$ which recover $a_{\rm bg}$ in addition to Eq. (5) yield equivalent energy spectra beyond the cold regime (Gao, 1998a), provided that their number of levels is large compared to unity. A hard sphere in addition to the van der Waals tail of Eq. (5), for instance, provides a background scattering potential with a minimal number of parameters. Its explicit expression reads

$$V_{\rm bg}(r)=\begin{cases}+\infty, & r<r_0\\ -C_6/r^6, & r>r_0.\end{cases} \quad (70)$$

The associated background scattering length is given by the following exact formula (Gribakin and Flambaum, 1993):

TABLE IV. Parameters characterizing the background scattering potential associated with experimentally relevant zero-energy resonances. Those values of a_{bg} and E_{-1} that are unreferenced refer to calculations performed for this review. The energy E_{-1} associated with the highest excited vibrational state of the background scattering potential is given only for isolated resonances. The atomic unit of the van der Waals dispersion coefficient C_6 is 9.5734×10^{-26} J nm^6, $a_{Bohr}=0.052\,917$ nm is the Bohr radius, and 1 G$=10^{-4}$ T.

Species	B_0 (G)	a_{bg} (a_{Bohr})	C_6 (a.u.)	$\lvert E_{-1}\rvert/h$ (MHz)
^{6}Li	543.25(5) (Strecker *et al.*, 2003)	59	1393.39 (Yan *et al.*, 1996)	
	834.149 (Bartenstein *et al.*, 2005)	−1405 (Bartenstein *et al.*, 2005)	1393.39 (Yan *et al.*, 1996)	
^{23}Na	853 (Stenger *et al.*, 1999)	63.9 (Mies *et al.*, 2000)	1561 (Kharchenko *et al.*, 1997)	208
	907 (Stenger *et al.*, 1999)	62.8 (Mies *et al.*, 2000)	1561 (Kharchenko *et al.*, 1997)	218
^{40}K	202.10(7) (Regal *et al.*, 2004c)	174(7) (Loftus *et al.*, 2002)	3897 (Derevianko *et al.*, 1999)	8.6
	224.21(5) (Regal and Jin, 2003)	174(7) (Loftus *et al.*, 2002)	3897 (Derevianko *et al.*, 1999)	8.6
^{85}Rb	155.0 (Thompson *et al.*, 2005a)	−443(3) (Claussen *et al.*, 2003)	4703 (van Kempen *et al.*, 2002)	218
^{87}Rb	1007.40(4) (Volz *et al.*, 2003)	100.5 (Volz *et al.*, 2003)	4703 (van Kempen *et al.*, 2002)	24.0
^{133}Cs	19.90(3) (Chin, Vuletic, *et al.*, 2004)	163 (Julienne *et al.*, 2004)	6890(35) (Leo *et al.*, 2000)	
	47.97(3) (Chin, Vuletic, *et al.*, 2004)	905 (Julienne *et al.*, 2004)	6890(35) (Leo *et al.*, 2000)	0.045

$$a_{bg}=\bar{a}[1-\tan(\varphi_{WKB}-3\pi/8)]. \quad (71)$$

Here $\bar{a}$ is the mean scattering length of Eq. (65) and $\varphi_{WKB}=2l_{vdW}^2/r_0^2$ is the semiclassical phase shift of Eq. (64). The difference of $\pi/4$ between the arguments of the tangent functions in Eqs. (63) and (71) is due to the discontinuity of Eq. (70) at the core radius r_0. Equation (71) may be used to determine r_0 such that $V_{bg}(r)$ of Eq. (70) exactly recovers the background scattering length. Similar procedures have been performed using two-channel approaches with continuous implementations of $V_{bg}(r)$ (Mies *et al.*, 2000; Köhler, Gasenzer, Julienne, and Burnett, 2003; Marcelis *et al.*, 2004; Nygaard *et al.*, 2006). An example of such an effective interaction is illustrated in Fig. 10 in addition to its energy levels. Table IV provides the parameters a_{bg} and C_6 characterizing the background scattering potential for experimentally relevant zero-energy resonances.

Equation (70), as well as those equivalent implementations of $V_{bg}(r)$ that explicitly include the long-range asymptotic van der Waals interaction of Eq. (5) are, in principle, suited to describe several bare energy levels. The number of bound states supported by Eq. (70), for instance, can be arbitrarily increased by decreasing the core radius r_0 under the constraint of a fixed background scattering length. The description of such wide energy ranges, however, is usually beyond the scope of two-channel approaches. In addition, the explicit treatment of the van der Waals tail of the background scattering potential is largely impractical in applications to the many-body physics of dilute gases. Several implementations of two-channel approaches, therefore, use effective low-energy interactions to recover different aspects of the cold collision physics under the conditions of resonance enhancement (Kokkelmans *et al.*, 2002; Bruun and Pethick, 2004; Drummond and Kheruntsyan, 2004; Duine and Stoof, 2004; Góral *et al.*, 2004; Chin, 2005).

Figure 16 shows a typical range of energies relevant to the Stern-Gerlach separation of Feshbach molecules

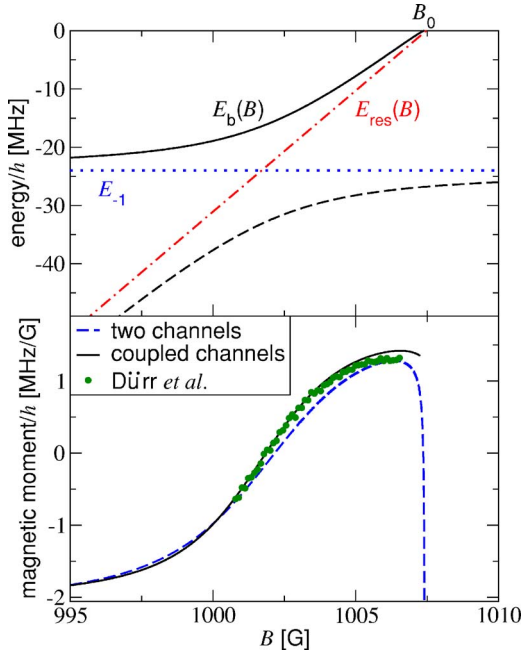

FIG. 16. (Color online) Avoided crossing of the highest excited vibrational levels of $^{87}Rb_2$ (upper panel) and the magnetic moment of the Feshbach molecule (lower panel) vs the magnetic-field strength in the vicinity of the 1007 G zero-energy resonance. The solid curve in the upper panel indicates the bound-state energy $E_b(B)$ of the Feshbach molecule, while the dashed curve refers to the next more tightly bound dressed vibrational level. Dotted and dot-dashed lines are associated with the energies $E_{-1}/h=-24$ MHz of the bare highest excited vibrational level of $V_{bg}(r)$ and $E_{res}(B)$ of the closed-channel resonance state, respectively. The crossing between the bare levels at 1001.7 G leads to the measured variation in the magnetic moment of the Feshbach molecule indicated by circles in the lower panel (Dürr, Volz, Marte, and Rempe, 2004). For comparison, the solid and dashed curves refer to exact coupled-channels calculations (van Kempen and Verhaar, 2004) and a two-channel approach (Góral *et al.*, 2004), respectively.

from a ^{87}Rb Bose-Einstein condensate (Dürr, Volz, Marte, and Rempe, 2004). This experimental technique based on exposing a mixture of atoms and dimers to an inhomogeneous magnetic field (Herbig *et al.*, 2003; Dürr, Volz, Marte, and Rempe, 2004; Chin *et al.*, 2005) is illustrated in Fig. 3 for the example of $^{133}Cs_2$. The relative force between the two components of the gas is proportional to the field gradient as well as to the difference in magnetic moments of a Feshbach molecule and a pair of separated atoms, i.e., $\partial E_b/\partial B$. In the rubidium case, the magnetic-field dependence of $E_b(B)$ in Fig. 16 is sensitive to the avoided crossing of $^{87}Rb_2$ dressed energy levels due to the highest excited bare vibrational level of $V_{bg}(r)$. In accordance with the size of the positive background scattering length of about $100a_{Bohr}$ (Volz *et al.*, 2003), this level is sufficiently close to the dissociation threshold that its energy E_{-1} is directly probed by experiment (Dürr, Volz, Marte, and Rempe, 2004).

An effective entrance-channel interaction suitable for a description of this experiment needs to recover both the precise value of a_{bg} and the bare vibrational level with the energy E_{-1}, beyond the Wigner threshold law regime. The associated minimal bare Green's function $G_{bg}(z)$ is therefore required to reproduce the bound-state pole at the energy argument $z=E_{-1}$. Similarly to Eq. (30), this requirement leads to the following separable representation (Góral *et al.*, 2004):

$$G_{bg}(z) = G_0(z) + G_0(z)|\chi_{bg}\rangle\tau_{bg}(z)\langle\chi_{bg}|G_0(z). \tag{72}$$

Here the form factor $|\chi_{bg}\rangle$ needs to recover, via the relation $G_0(E_{-1})|\chi_{bg}\rangle \propto |\phi_{-1}\rangle$, the bare vibrational state satisfying the Schrödinger equation $H_{bg}|\phi_{-1}\rangle = E_{-1}|\phi_{-1}\rangle$. The resonance term $\tau_{bg}(z)$ may be represented by the following ratio:

$$\tau_{bg}(z) = \frac{\xi_{bg}}{1 - \xi_{bg}\langle\chi_{bg}|G_0(z)|\chi_{bg}\rangle}. \tag{73}$$

Since $\tau_{bg}(z)$ is required to reproduce the singularity of the bare Green's function in the limit $z \to E_{-1}$, the amplitude ξ_{bg} is given by $1/\langle\chi_{bg}|G_0(E_{-1})|\chi_{bg}\rangle$.

The separable representation of $G_{bg}(z)$ given by Eq. (72) provides the exact Green's function associated with an effective potential,

$$V_{bg}^{eff} = |\chi_{bg}\rangle\xi_{bg}\langle\chi_{bg}|, \tag{74}$$

determined by the amplitude ξ_{bg} and the form factor $|\chi_{bg}\rangle$. This follows directly from the resolvent identity (Taylor, 1972), i.e.,

$$G_{bg}(z) = G_0(z) + G_0(z)V_{bg}^{eff}G_{bg}(z), \tag{75}$$

which is verified upon multiplication by $G_{bg}^{-1}(z) = z - H_{bg}$ from the right and by $G_0^{-1}(z) = z + \hbar^2\nabla^2/m$ from the left. Iterating Eq. (75) yields the Born series, which reduces to a geometric series for the separable potential of Eq. (74). Its exact sum is given by Eq. (72) with the resonance term of Eq. (73).

Such effective interactions are commonly employed for few-particle systems (Yamaguchi, 1954; Mitra, 1962; Lovelace, 1964) as well as in condensed-matter physics (Schrieffer, 1964). For cold gases, the form factor is unresolved because it is sensitive only to the physics on distances on the order of the van der Waals length. Its associated functional form is therefore arbitrary and may be chosen, for instance, to be Gaussian (Góral *et al.*, 2004). In the momentum space representation, this yields

$$\langle\mathbf{p}|\chi_{bg}\rangle = \chi_{bg}(p) = \frac{\exp(-p^2\sigma_{bg}^2/2\hbar^2)}{(2\pi\hbar)^{3/2}}. \tag{76}$$

Here σ_{bg} accounts for the range of the interaction, and $\langle\mathbf{r}|\mathbf{p}\rangle = \exp(i\mathbf{p}\cdot\mathbf{r}/\hbar)/(2\pi\hbar)^{3/2}$ denotes the plane wave with relative momentum $\mathbf{p}$. Given this choice of form factor, the parameters σ_{bg} and ξ_{bg} are determined by the requirement that the bare Green's function of Eq. (72) exactly recovers a_{bg} and E_{-1}. The zero-energy limit of the scattering amplitude associated with Eq. (72), i.e., $f_{bg}(0) = -m\tau_{bg}(0)/4\pi\hbar^2$, yields the condition

$$a_{bg} = \sigma_{bg}\frac{x}{1 + x/\sqrt{\pi}}, \tag{77}$$

where $x = m\xi_{bg}/4\pi\hbar^2\sigma_{bg}$ is a dimensionless variable. In addition, the bare energy level determined by the pole of the resonance term of Eq. (73) gives

$$1 - \frac{x}{\sqrt{\pi}}[\sqrt{\pi}ye^{y^2}\mathrm{erfc}(y) - 1] = 0. \tag{78}$$

Here $\mathrm{erfc}(y) = \frac{2}{\sqrt{\pi}}\int_y^\infty e^{-u^2}du$ is the complementary error function with the argument $y = \sqrt{m|E_{-1}|}\sigma_{bg}/\hbar$.

For the 1007 G zero-energy resonance of ^{87}Rb, the energy E_{-1} can be determined using the potential of Eq. (70). To this end, its parameter r_0 should be chosen such that the number of vibrational levels is large compared to unity and that the known quantities a_{bg} and C_6 of Table IV are recovered. This yields $E_{-1}/h = -24$ MHz in agreement with coupled channels calculations (van Kempen and Verhaar, 2004). Based on the precise values of E_{-1} and a_{bg}, Eqs. (77) and (78) in turn determine the range parameter and amplitude of the separable potential to be $\sigma_{bg} = 44a_{Bohr}$ and $m\xi_{bg}/(4\pi\hbar^2) = -339a_{Bohr}$, respectively.

We note that the above adjustment of the effective entrance-channel interaction is restricted to zero-energy resonances with a positive background scattering length, i.e., $a_{bg} > 0$. In the opposite case $a_{bg} < 0$ separable interactions do not support any bound state, similarly to the universal contact pseudopotential of Sec. III.F. Among the experimentally relevant examples of Table IV, only the broad, entrance-channel-dominated zero-energy resonances of ^{6}Li and ^{85}Rb have a negative background scattering length. Associated two-channel approaches describing the dressed energy levels beyond the Wigner threshold law regime exist, at least, in applications to the broad resonance of ^{85}Rb (Kokkelmans and Holland, 2002; Köhler *et al.*, 2004; Góral *et al.*, 2005). For ^{6}Li a

double resonance approach suitable for describing many-body systems has been suggested (Kokkelmans *et al.*, 2002).

Figures 12 and 13 reveal, however, that in both cases ^{85}Rb and ^{6}Li, the Feshbach molecule is well described by an effective single channel interaction, over a wide range of magnetic-field strengths, in accordance with Sec. III.F. An appropriate magnetic-field-dependent single-channel separable potential, suitable for applications to few-body bound states (Stoll and Köhler, 2005) as well as the dynamics of cold gases (Köhler, Gasenzer, and Burnett, 2003), may be constructed on the basis of Eqs. (74) and (76). The associated constant range parameter of the form factor is given by $\sigma_{\rm bg}\approx\sqrt{\pi}\bar{a}/2$. The adjustment of $\xi_{\rm bg}$ via Eq. (77) to the magnetic-field-dependent scattering length $a(B)$ of Eq. (39) instead of just $a_{\rm bg}$ ensures that the near-resonant energy $E_{\rm b}(B)$ of the Feshbach molecule recovers Eq. (66).

2. Resonance energy

In accordance with the single resonance approach of Eq. (36), the difference in energies of the resonance level and the entrance-channel dissociation threshold $E_{\rm res}(B)$ characterizes the closed-channel part of the Hamiltonian. The associated relative magnetic moment $\mu_{\rm res}=\partial E_{\rm res}/\partial B$ may be inferred from a Stern-Gerlach separation experiment, relying upon the force experienced by an atom due to the inhomogeneous magnetic field **B**. Given any definite Zeeman state, this force is of the general form $\mathbf{F}_a=-\boldsymbol{\nabla}E_a$, where E_a is the Zeeman energy. The magnitude of $\mathbf{F}_a=-(\partial E_a/\partial B)\boldsymbol{\nabla}|\mathbf{B}|$ depends on the orientation quantum number m_f of the total angular momentum with respect to the field direction. This dependence is well described by the Breit-Rabi formula (Breit and Rabi, 1931),

$$\mathbf{F}_a=\pm\frac{2m_f/(2i+1)+x}{2[1+x4m_f/(2i+1)+x^2]^{1/2}}g_j\mu_{\rm Bohr}\boldsymbol{\nabla}|\mathbf{B}|. \quad (79)$$

Here i is the quantum number associated with the nuclear spin, $\mu_{\rm Bohr}=9.274\,009\,49\times10^{-24}$ J/T denotes the Bohr magneton, and the Landé factor $g_j\approx2$ refers to the electronic magnetic moment. The dimensionless variable $x=g_j\mu_{\rm Bohr}|\mathbf{B}|/E_{\rm hf}$ depends on the field strength $|\mathbf{B}|$ in addition to the hyperfine energy splitting in the absence of magnetic fields $E_{\rm hf}$ (Arimondo *et al.*, 1977). For any given orientation quantum number m_f and atomic species, the sign of the force given by Eq. (79) is determined by the Zeeman multiplet.

For the example illustrated in Fig. 17, the nuclear spin quantum number $i=3/2$ of ^{87}Rb (Arimondo *et al.*, 1977) in addition to the electronic spin give rise to two Zeeman multiplets. These states adiabatically correlate with the hyperfine levels of total angular momentum quantum numbers $f=1$ and 2 in the limit of zero magnetic field. The *s*-wave entrance-channel spin configuration of any pair of identical Bose atoms in Fig. 16 is characterized by the quantum numbers $(f_1=1,m_{f_1}=+1;f_2=1,m_{f_2}=+1)$, referring to their electronic ground states. In accordance with Eq. (79) and the zero-field hyperfine structure splitting of $E_{\rm hf}/h=6834$ MHz (Arimondo *et al.*, 1977), the total magnetic moment associated with these ground-state atoms at $B_0=1007.4$ G is determined by $2\partial E_{\rm a}/\partial B=-h\times2$ MHz/G. This derivative varies by less than 1% over the range of magnetic-field strengths displayed in Fig. 16.

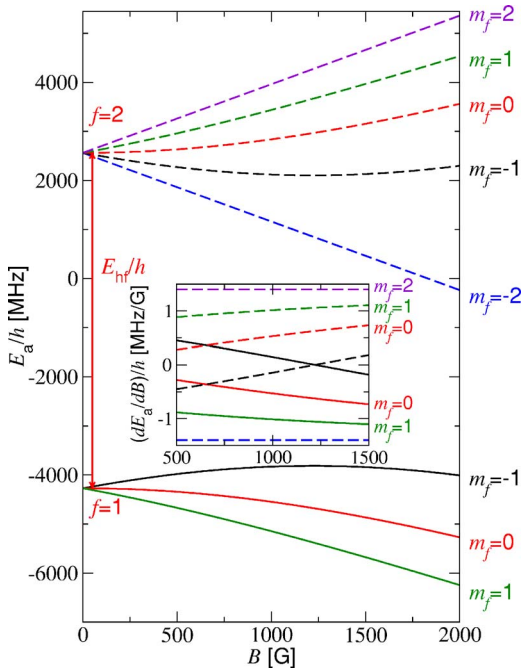

FIG. 17. (Color online) The Zeeman multiplets of ^{87}Rb associated with the total angular momentum quantum numbers $f=1$ (solid curves) and $f=2$ (dashed curves). Inset: The magnetic moments $\partial E_a/\partial B$ determined by Eq. (79) and the orientation quantum numbers m_f of those Zeeman states that are relevant to Fig. 16.

The predominant spin exchange interaction couples pairs of ^{87}Rb ground-state atoms to four *s*-wave scattering channels characterized by pairs of Zeeman levels, $(f_1,m_{f_1};f_2,m_{f_2})$, whose total angular momentum orientation quantum number is conserved, i.e., $m_{f_1}+m_{f_2}=+2$. These closed channels are therefore described by (1,1;2,1), (1,0;2,2), (2,0;2,2), and (2,1;2,1). In accordance with the inset of Fig. 17, their associated total magnetic moments at resonance amount to 0, $h\times0.9$ MHz/G, $h\times1.9$ MHz/G, and $h\times2$ MHz/G, respectively. The magnetic moment of the ^{87}Rb$_2$ Feshbach molecule in the lower panel of Fig. 16 consists, in principle, of contributions from all five channels weighted by their admixtures. Both the experimental data (Dürr *et al.*, 2004) and coupled channels predictions (van Kempen and Verhaar, 2004), however, are consistent with a Feshbach resonance state predominantly consisting of Zeeman states from the $f=2$ multiplet. The Breit-Rabi formula, therefore, yields an estimated difference in the magnetic moments of the resonance state and entrance-channel spin configuration of about $\mu_{\rm res}=h\times4$ MHz/G near the zero-energy resonance position. In a similar manner, the size of the parameter $\mu_{\rm res}$ may be

TABLE V. Parameters characterizing the interchannel coupling associated with experimentally relevant zero-energy resonances. Those values of ΔB and μ_{res} that are unreferenced refer to calculations performed for this review. In accordance with Eq. (69), the size of the parameter η indicates whether a zero-energy resonance is closed- or entrance-channel-dominated.

Species	B_0 (G)	ΔB (G)	μ_{res}/h (MHz/G)	η
^{6}Li	543.25(5) (Strecker *et al.*, 2003)	0.1	2.8	1215
	834.149 (Bartenstein *et al.*, 2005)	−300 (Bartenstein *et al.*, 2005)	2.8	0.02
^{23}Na	853 (Stenger *et al.*, 1999)	0.01 (Mies *et al.*, 2000)	5.24 (Mies *et al.*, 2000)	1090
	907 (Stenger *et al.*, 1999)	1.0 (Mies *et al.*, 2000)	5.24 (Mies *et al.*, 2000)	11
^{40}K	202.10(7) (Regal *et al.*, 2004c)	7.8(6) (Greiner *et al.*, 2003)	2.35 (Nygaard *et al.*, 2006)	0.46
	224.21(5) (Regal and Jin, 2003)	9.7(6) (Regal and Jin, 2003)	2.35 (Nygaard *et al.*, 2006)	0.37
^{85}Rb	155.0 (Thompson *et al.*, 2005a)	10.71(2) (Claussen *et al.*, 2003)	−3.26 (Kokkelmans, 2002)	0.04
^{87}Rb	1007.40(4) (Volz *et al.*, 2003)	0.21 (Dürr, Volz, and Rempe, 2004)	4.2 (Dürr, Volz, Marte, and Rempe, 2004)	5.9
^{133}Cs	19.90(3) (Chin, Vuletic, *et al.*, 2004)	0.005 (Julienne *et al.*, 2004)	0.798 (Julienne *et al.*, 2004)	437
	47.97(3) (Chin, Vuletic, *et al.*, 2004)	0.15 (Julienne *et al.*, 2004)	2.09 (Julienne *et al.*, 2004)	0.99

inferred from Eq. (79) for a variety of species. This procedure is particularly useful for genuinely two-channel problems, such as, for instance, the spin configurations relevant to the 202 G zero-energy resonance of ^{40}K (Bruun and Pethick, 2004). The recommended values of μ_{res} of Table V are based on coupled channels predictions.

3. Interchannel coupling

Interchannel coupling leads to the decay width and energy shift of the bare resonance level due to its interaction with the background scattering continuum and entrance-channel bare vibrational states. In accordance with Eq. (54), both quantities are determined by the parameters ΔB of Eq. (40) and $B_0 - B_{res}$ of Eq. (41) in the Wigner threshold law domain. While the width in the magnetic-field strength ΔB is measured routinely, the associated shift is not directly observable. Its magnitude, however, may be inferred using multichannel quantum defect theory (Julienne and Mies, 1989; Mies and Raoult, 2000, 2004). This yields the following approximate formula:

$$B_0 - B_{res} = \Delta B \frac{a_{bg}}{\bar{a}} \left[\frac{1 - a_{bg}/\bar{a}}{1 + (1 - a_{bg}/\bar{a})^2} \right]. \tag{80}$$

Here $\bar{a}$ is the mean scattering length of Eq. (65). Consequently, the size of the resonance shift depends just on the quantities a_{bg}, ΔB, and C_6, which are all accessible to experimental studies. Entrance-channel-dominated zero-energy resonances, such as ^{85}Rb illustrated in Fig. 12, tend to have large shifts comparable to the size of ΔB. The predicted magnitude of $B_0 - B_{res} = 9$ G in Fig. 12 is consistent with the coupled channels binding energies (Kokkelmans, 2002). For the closed-channel-dominated 1007 G zero-energy resonance of ^{87}Rb in the upper panel of Fig. 16, the value of $B_0 - B_{res} = 0.07$ G of Eq. (65) is significantly smaller than the width. For the examples given in Tables IV and V, the corrections to Eq. (80) are negligible.

The quantity $W|\phi_{res}\rangle$, characterizing the interchannel coupling in the single resonance approach, should be adjusted such that the matrix element of the bare Green's function in Eq. (54) recovers both ΔB and $B_0 - B_{res}$. Such an adjustment ensures, in particular, that the bound-state energy of Eq. (47) properly interpolates between the universal and asymptotic regimes of magnetic-field strengths. An explicit minimal implementation of the two-channel Hamiltonian given by Eq. (16) may therefore be based on the separable background scattering potential of Eq. (74) in addition to the following general expression:

$$W|\phi_{res}\rangle = |\chi\rangle\zeta. \tag{81}$$

Here the amplitude ζ determines the interchannel coupling and $|\chi\rangle$ its functional form. Since the off-diagonal potential $W(r)$ is unresolved by the large de Broglie wavelengths associated with cold collisions, the form factor $|\chi\rangle$ may be chosen as a Gaussian function in momentum space, similarly to Eq. (76). This yields (Góral *et al.*, 2004)

$$\langle \mathbf{p}|\chi\rangle = \chi(p) = \frac{\exp(-p^2\sigma^2/2\hbar^2)}{(2\pi\hbar)^{3/2}}. \tag{82}$$

The associated range parameter σ and amplitude ζ are determined by requiring the imaginary and real parts of Eq. (54) to recover the physical quantities ΔB and $B_0 - B_{res}$, respectively. For the purpose of this adjustment, it is convenient to introduce the average range parameter $\bar{\sigma} = (\sigma^2 + \sigma_{bg}^2)^{1/2}/\sqrt{2}$. The imaginary part of the bare Green's function on the left-hand side of Eq. (54) yields the first condition

$$\Delta B = \frac{m|\zeta|^2}{4\pi\hbar^2 a_{bg}\mu_{res}} \left(1 - \frac{a_{bg}}{\sqrt{\pi}\bar{\sigma}}\right)^2. \tag{83}$$

The associated widths of experimentally relevant zero-energy resonances are summarized in Table V. Given the bare Green's function of Eq. (72) and Gaussian form factors, the real part of Eq. (54) can be evaluated analytically. This leads to the second condition,

$$B_0 - B_{\rm res} = \Delta B \frac{a_{\rm bg}}{\sqrt{\pi}\sigma} \frac{1-(a_{\rm bg}/\sqrt{\pi}\sigma)(\sigma/\bar{\sigma})^2}{[1-(a_{\rm bg}/\sqrt{\pi}\sigma)\sigma/\bar{\sigma}]^2}, \tag{84}$$

whose value for the resonance shift on the left-hand side is given by Eq. (80). Equations (83) and (84), in turn, simultaneously determine the parameters σ and ζ characterizing the interchannel coupling. We note that the overall phase of the amplitude ζ is irrelevant to the physics described by the associated Hamiltonian.

For the 1007 G zero-energy resonance of ^{87}Rb, such an adjustment yields $\sigma=22a_{\rm Bohr}$ and $m|\zeta|^2/4\pi\hbar^2\sigma=h\times 10$ MHz. Given the effective background scattering potential of Eq. (74) and $\mu_{\rm res}$ of Table V, this procedure provides a complete implementation of the two-channel single-resonance approach. Its predictions with respect to dressed binding energies are illustrated in the upper panel of Fig. 16 as well as in Fig. 12. The lower panel of Fig. 16 shows the magnetic moment of ^{87}Rb Feshbach molecules determined from the product $\mu_{\rm res}Z(B)$ via Eqs. (46) and (57) using the two-channel single resonance approach. The overall data offset of about −2 MHz refers to the magnetic moment associated with the entrance-channel spin configuration. Comparisons with measurements (Dürr, Volz, Marte, and Rempe, 2004) and results of coupled channels calculations (van Kempen and Verhaar, 2004) indicate that the effective two-channel approach can fully recover the microscopic physics within the experimental energy range.

IV. ASSOCIATION OF FESHBACH MOLECULES

The different experimental techniques for molecular association in cold gases all depend in one way or another on the properties of the diatomic energy spectra. Several approaches to the production of cold Feshbach molecules are based on the relaxation of an atomic gas into dimers near resonance (Jochim *et al.*, 2003a; Zwierlein *et al.*, 2003) or on dynamical sweeps of the magnetic-field strength across B_0 (Cubizolles *et al.*, 2003; Herbig *et al.*, 2003; Regal *et al.*, 2003a; Strecker *et al.*, 2003; Xu *et al.*, 2003; Dürr, Volz, Marte, and Rempe, 2004). Both techniques take advantage of the degeneracy of the Feshbach molecular energy $E_{\rm b}$ and the threshold for dissociation into free atoms in the limit $B\to B_0$. Relaxation of an atomic gas into dimer molecules requires collisions of at least three atoms to balance the energies and is commonly employed, to date, just in two-spin-component mixtures of ^{6}Li Fermi gases. The conceptually simpler molecular association via magnetic-field sweeps seems more generally applicable to both Bose and Fermi gases and will therefore be the main subject of this section. Figure 16 illustrates its principle which relies, for the 1007 G zero-energy resonance of ^{87}Rb, upon the adiabatic transition from the diatomic zero-energy continuum level to the bound-state energy $E_b(B)$ with decreasing B. Conversely, Fig. 12 suggests that for the 155 G zero-energy resonance of ^{85}Rb, free atom pairs may be associated to Feshbach molecules by increasing B across B_0. The difference in energy of colliding atoms and diatomic molecules is absorbed by the time-dependent magnetic field. As the field is, in general, spatially homogeneous the association process does not affect the center-of-mass momentum of atom pairs. From this viewpoint, Feshbach molecules produced by magnetic-field sweeps or other related dynamical techniques (Donley *et al.*, 2002; Thompson *et al.*, 2005a) are as cold as the atomic gas they originate from.

A. Linear sweeps of the magnetic-field strength

In an idealized treatment of molecular association, the magnetic-field strength may be assumed to vary linearly in time. This implies that

$$B(t) = B_{\rm res} + \dot{B}(t - t_{\rm res}), \tag{85}$$

where $\dot{B}$ is usually referred to as the ramp speed and $t_{\rm res}$ is the time at which the bare resonance energy $E_{\rm res}$ crosses the dissociation threshold of the entrance channel. The field strength $B_{\rm res}$ associated with $t_{\rm res}$ is indicated in Fig. 12. In accordance with Eq. (35), the resonance energy is also a linear function of time,

$$E_{\rm res}(t) = \dot{E}_{\rm res}(t - t_{\rm res}), \tag{86}$$

with a constant derivative $\dot{E}_{\rm res}=\mu_{\rm res}\dot{B}$. Equation (86) presupposes that the magnetic-field sweep is sufficiently slow for the electronic degrees of freedom to adiabatically adjust to magnetic-field strength changes. To achieve molecular association of an atom pair, $\dot{E}_{\rm res}$ needs to be negative (Mies *et al.*, 2000). Consequently, the Feshbach resonance level is swept downward in time. This requirement determines $\dot{B}$ through the sign of $\mu_{\rm res}$. Conversely, upward sweeps of the Feshbach resonance level across B_0 lead to heating of the atomic cloud. This general principle may be readily verified on the basis of the magnetic-field dependence of the discrete spectrum of dressed energy levels of a trapped atom pair.

1. Adiabatic association of Feshbach molecules

Tight traps containing just a single pair of atoms may be realized, for instance, by individual sites of an optical lattice (Tiesinga *et al.*, 2000; Jaksch *et al.*, 2002) or by microfabricated materials (Weinstein and Libbrecht, 1995; Müller *et al.*, 1999; Thywissen *et al.*, 1999; Hinds *et al.*, 2001; Folman *et al.*, 2002; Long *et al.*, 2003). The two-body energy spectra associated with periodic potentials of optical lattices have been studied theoretically in the Wigner threshold law domain (Orso *et al.*, 2005; Wouters and Orso, 2006) as well as observed experimentally (Moritz *et al.*, 2005). While in the limit of high excitations the tunneling of atoms is significant, the deepest localized diatomic levels of tight lattice sites are well described by the harmonic oscillator approximation. As a consequence, the center of mass and relative motions

of an atom pair confined to a single site can be treated separately, similarly to the two-body problem in free space.

A spherically symmetric harmonic confinement modifies the bare entrance-channel Hamiltonian associated with the resonance enhanced interaction as follows:

$$H_{\rm bg} = -\frac{\hbar^2}{m}\nabla^2 + V_{\rm bg}(r) + V_{\rm trap}(r). \tag{87}$$

Here $V_{\rm trap}(r)$ denotes the potential energy of the isotropic harmonic oscillator in the barycentric frame, which is given in terms of the reduced mass $m/2$ and the angular frequency $\omega_{\rm ho}$ to be

$$V_{\rm trap}(r) = \frac{1}{2}\frac{m}{2}\omega_{\rm ho}^2 r^2. \tag{88}$$

Similarly to Eq. (25), the associated bare vibrational energy levels are determined by the stationary Schrödinger equation,

$$H_{\rm bg}\phi_v(r) = E_v\phi_v(r). \tag{89}$$

Here the index $v=\ldots,-2,-1,0,1,2,\ldots$ labels the vibrational excitation in such a way that $v=0$ correlates adiabatically, in the limit $\omega_{\rm ho}\to 0$, with the dissociation threshold of the entrance channel. According to this counting scheme, negative indices $v<0$ are associated with the bare vibrational levels E_{-1}, E_{-2}, etc., indicated in Fig. 10. In the limit of low vibrational excitation $v \gtrsim 0$, the spatial extents of the bare states, including $\phi_0(r)$, are characterized by the trap length $a_{\rm ho} = \sqrt{\hbar/m\omega_{\rm ho}}$. This length scale usually greatly exceeds the modulus of the background scattering length $|a_{\rm bg}|$. To first order in $a_{\rm bg}/a_{\rm ho}$, the energies of the excited levels are well approximated by the following formula (Busch *et al.*, 1998):

$$E_v \approx \left[\frac{3}{2} + 2v + \sqrt{\frac{2}{\pi}}\binom{v+1/2}{v}\frac{a_{\rm bg}}{a_{\rm ho}}\right]\hbar\,\omega_{\rm ho}. \tag{90}$$

Here $\binom{v+1/2}{v}$ is a combinatorial. Dressed energy levels may be determined via the two-channel Hamiltonian of Eq. (16) using the single resonance approach of Eq. (36) (Mies *et al.*, 2000), or via a single-channel energy-dependent contact interaction (Blume and Greene, 2002; Bolda *et al.*, 2002). Both methods yield spectra consistent with full coupled channels calculations (Tiesinga *et al.*, 2000).

Figure 18 shows the magnetic-field dependence of dressed two-body energy levels of ground-state ^{87}Rb atoms predicted by the two-channel approach for a tight trap with a frequency of $\nu_{\rm ho}=\omega_{\rm ho}/2\pi=39$ kHz (Thalhammer *et al.*, 2006). An atom pair from a rubidium Bose-Einstein condensate prepared on the high-field side of the 1007 G zero-energy resonance and loaded adiabatically into an optical lattice site is well described by the $v=0$ state. According to Fig. 18, this level adiabatically correlates with the Feshbach molecule on the low-field side of B_0. Consequently, a magnetic downward sweep across B_0 associates the separated rubidium atoms to molecules with certainty in the limit of zero ramp speed, i.e., $\dot{B}\to 0$. An excited trap level with vibrational quantum number v is transferred to $v-1$. Conversely, an adiabatic upward magnetic-field sweep across B_0 dissociates ^{87}Rb$_2$ Feshbach molecules and leads to heating transitions from v to $v+1$ in excited trap levels. In general, the ramp direction for such cooling or heating transitions is determined by the sign of $\mu_{\rm res}$ or, equivalently, by the time variation of the resonance energy $\dot{E}_{\rm res}$.

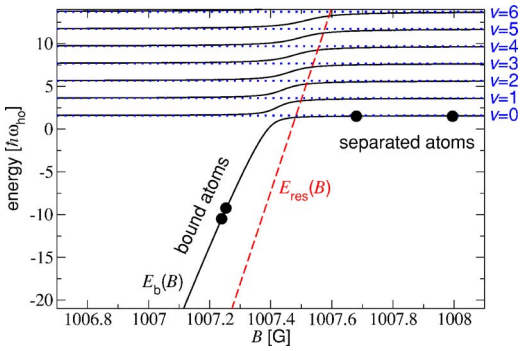

FIG. 18. (Color online) Schematic illustration of molecular association of ground-state ^{87}Rb atoms via a downward magnetic-field sweep in a spherical harmonic atom trap with an oscillator frequency $\nu_{\rm ho}=39$ kHz (Thalhammer *et al.*, 2006). The bare vibrational levels ($v=0,\ldots,6$) associated with the background scattering quasicontinuum and the Feshbach resonance energy $E_{\rm res}(B)$ are indicated by dotted and dashed lines, respectively. Solid curves refer to the magnetic-field dependence of dressed energy levels in the vicinity of the zero-energy resonance position $B_0=1007.4$ G.

2. Exact time evolution of a single atom pair

While the dressed energy levels of Fig. 18 reveal the mechanism of Feshbach molecular association in the limit of zero ramp speed, the dynamics of the diatomic wave function is described by the Schrödinger equation

$$i\hbar\frac{\partial}{\partial t}|\Psi(t)\rangle = H_{\rm 2B}(t)|\Psi(t)\rangle. \tag{91}$$

Here $H_{\rm 2B}$ is the two-channel Hamiltonian of Eq. (16) in the single resonance approach of Eq. (36). Its time dependence is determined by the linear variation of the resonance energy given by Eq. (86). The diatomic state $|\Psi(t)\rangle$ has components in the entrance and closed channels, whose wave functions may be expanded into bare states, in accordance with

$$\Psi_{\rm bg}(r,t) = \sum_v \phi_v(r)C_v(t), \tag{92}$$

$$\Psi_{\rm cl}(r,t) = \phi_{\rm res}(r)C_{\rm res}(t). \tag{93}$$

Such a basis-set expansion of Eq. (91) leads to the following dynamical equations for the associated time-dependent coefficients:

$$i\hbar\,\dot{C}_v(t) = E_v C_v(t) + \langle \phi_v | W | \phi_{\rm res}\rangle C_{\rm res}(t), \tag{94}$$

$$i\hbar\,\dot{C}_{\rm res}(t) = E_{\rm res}(t) C_{\rm res}(t) + \sum_v \langle \phi_{\rm res} | W | \phi_v\rangle C_v(t). \tag{95}$$

This configuration interaction approach is particularly useful for numerical treatments of Feshbach molecular association using any form of time-dependent magnetic-field variation (Mies *et al.*, 2000). The special case of linear sweeps belongs to those quantum-mechanical problems whose exact dynamics can be treated analytically (Demkov and Osherov, 1968; Macek and Cavagnero, 1998).

To this end, it is useful to split $H_{\rm 2B}(t)$ into stationary and time-dependent contributions,

$$H_{\rm 2B}(t) = H_{\rm stat} + H_{\rm cl}(t). \tag{96}$$

Here the stationary Hamiltonian $H_{\rm stat}=H_{\rm 2B}(t_{\rm res})$ is associated with the magnetic-field strength $B_{\rm res}$. In the single resonance approach, the dynamical contribution $H_{\rm cl}(t)$ is given by

$$H_{\rm cl}(t) = |\phi_{\rm res},{\rm cl}\rangle E_{\rm res}(t) \langle \phi_{\rm res},{\rm cl}|. \tag{97}$$

Similarly to the effective potential of Eq. (74), the time-dependent interaction $H_{\rm cl}(t)$ involves only a single state associated with the closed channel, the product $|\phi_{\rm res},{\rm cl}\rangle = |\phi_{\rm res}\rangle|{\rm cl}\rangle$. The following derivations will show that it is the separable form of Eq. (97) in addition to the linear dependence of the resonance energy $E_{\rm res}$ on t that allow for the analytic treatment of the time evolution.

The complete dynamics of an atom pair exposed to a linear magnetic-field sweep may be inferred from the time evolution operator determined by the Schrödinger equation,

$$i\hbar\,\frac{\partial}{\partial t} U_{\rm 2B}(t,t') = H_{\rm 2B}(t) U_{\rm 2B}(t,t'), \tag{98}$$

in addition to the boundary condition $U_{\rm 2B}(t,t)=1$. The diatomic state at time t is thus given in terms of $U_{\rm 2B}(t,t')$ and the state at time t' by

$$|\Psi(t)\rangle = U_{\rm 2B}(t,t')|\Psi(t')\rangle. \tag{99}$$

Similarly, the dynamics in the absence of the interaction of Eq. (97) is described by $\exp[-iH_{\rm stat}(t-t')/\hbar]$. Associated with these free and complete time evolution operators are the retarded Green's functions,

$$G^{(+)}_{\rm stat}(t-t') = \frac{1}{i\hbar}\theta(t-t')\exp[-iH_{\rm stat}(t-t')/\hbar], \tag{100}$$

$$G^{(+)}_{\rm 2B}(t,t') = \frac{1}{i\hbar}\theta(t-t')U_{\rm 2B}(t,t'), \tag{101}$$

where $\theta(t-t')$ is the step function that yields unity if $t>t'$ and zero elsewhere. The Schrödinger equation (98) may be represented in terms of Eqs. (100) and (101) via

$$G^{(+)}_{\rm 2B}(t,t') = G^{(+)}_{\rm stat}(t-t') + \int d\tau G^{(+)}_{\rm stat}(t-\tau) H_{\rm cl}(\tau) G^{(+)}_{\rm 2B}(\tau,t'). \tag{102}$$

Differentiation with respect to the variable t readily verifies this relation by recovering the time derivative of the complete retarded Green's function of Eq. (101), which is directly determined by Eq. (98). The integral representation of Eq. (98) chosen in Eq. (102) is usually referred to as the postform of the dynamical equation. The associated preform reads

$$G^{(+)}_{\rm 2B}(t,t') = G^{(+)}_{\rm stat}(t-t') + \int d\tau G^{(+)}_{\rm 2B}(t,\tau) H_{\rm cl}(\tau) G^{(+)}_{\rm stat}(\tau-t'), \tag{103}$$

and can be verified similarly to the derivation of Eq. (102).

While, in general, the operator equation (102) requires a complete basis-set expansion for its numerical solution, the separable form of Eq. (97) reduces this problem to the calculation of just the pair of matrix elements,

$$g^{(+)}_{\rm stat}(t-t') = \langle \phi_{\rm res},{\rm cl}|G^{(+)}_{\rm stat}(t-t')|\phi_{\rm res},{\rm cl}\rangle, \tag{104}$$

$$g^{(+)}_{\rm 2B}(t,t') = \langle \phi_{\rm res},{\rm cl}|G^{(+)}_{\rm 2B}(t,t')|\phi_{\rm res},{\rm cl}\rangle. \tag{105}$$

This follows from Eq. (97) via multiplying Eq. (102) by $\langle\phi_{\rm res},{\rm cl}|$ from the left and by $|\phi_{\rm res},{\rm cl}\rangle$ from the right which, in turn, determines Eq. (105) through the following integral equation:

$$g^{(+)}_{\rm 2B}(t,t') = g^{(+)}_{\rm stat}(t-t') + \int d\tau\, g^{(+)}_{\rm stat}(t-\tau) E_{\rm res}(\tau) \times g^{(+)}_{\rm 2B}(\tau,t'). \tag{106}$$

Given the free retarded Green's function of Eq. (100), the complete time evolution operator can be inferred from the solution of Eq. (106) by inserting Eq. (103) into Eq. (102) and performing the time integrations.

Using the convolution theorem, a Fourier transform turns the integral on the right-hand side of Eq. (106) into a product of functions. In the case of a linear magnetic field sweep, such a procedure allows Eq. (106) to be solved analytically. To this end, it is instructive to introduce the energy-dependent matrix elements,

$$g_{\rm stat}(z) = \int dt\, e^{iz(t-t')/\hbar} g^{(+)}_{\rm stat}(t-t'), \tag{107}$$

$$g_{\rm 2B}(z,t') = \int dt\, e^{iz(t-t')/\hbar} g^{(+)}_{\rm 2B}(t,t'), \tag{108}$$

associated with the free and complete retarded Green's functions. Here the regularized argument $z=E+i0$ ensures the convergence of the time integrals in the limit $t\to+\infty$ by approaching the real energy E from the upper half of the complex plane. Given the resonance energy of Eq. (86), a Fourier transform renders Eq. (106) into

the following inhomogeneous first-order linear differential equation:

$$i\hbar\frac{\partial g_{2B}(z,t')}{\partial E} = \hbar\,\varphi'(z,t')g_{2B}(z,t') + 1/\dot{E}_{\rm res}. \tag{109}$$

Its dependence on the interatomic interaction is incorporated in the energy derivative $\varphi'(z,t')=\partial\varphi(z,t')/\partial E$ of the complex phase

$$\varphi(z,t') = -\frac{1}{\hbar\dot{E}_{\rm res}}\int_0^E \frac{dE'}{g_{\rm stat}(z')} + E(t'-t_{\rm res})/\hbar\,, \tag{110}$$

where $z'=E'+i0$ denotes a regularized integration variable with the same imaginary part as z.

The imaginary part of $\varphi(z,t')$ can be inferred from the Hamiltonian $H_{\rm stat}$ using a spectral decomposition of $g_{\rm stat}(z)$ analogous to Eq. (49). In particular, Eq. (53) determines the sign of Im $\varphi(z,t')$ to be

$$\mathrm{sgn}[\mathrm{Im}\,\varphi(z,t')] = -\,\mathrm{sgn}(\dot{E}_{\rm res})\mathrm{sgn}(\mathrm{Im}\,z). \tag{111}$$

Consequently, in the case of a downward ramp of the Feshbach resonance level, i.e., $\dot{E}_{\rm res}<0$, the damped retarded solution to Eq. (109) is given by

$$g_{2B}(z,t') = -\int_E^\infty dE'\frac{e^{-i[\varphi(z,t')-\varphi(z',t')]}}{i\hbar\,\dot{E}_{\rm res}}. \tag{112}$$

Equation (112) may be verified from Eq. (109) by differentiation with respect to E. The matrix element of the complete retarded Green's function of Eq. (105) is the inverse Fourier transform of Eq. (112), which yields

$$g_{2B}^{(+)}(t,t') = -\int\frac{dE}{2\pi\hbar}\int_E^\infty dE'\frac{e^{-i[\varphi(z,t)-\varphi(z',t')]}}{i\hbar\,\dot{E}_{\rm res}}. \tag{113}$$

The exact time evolution operator determined by Eq. (113) is applicable to the association of Feshbach molecules in free space as well as to the case of a trapped atom pair illustrated in Fig. 18.

3. Landau-Zener approach

In 1932, Landau and Zener had independently derived a simple estimate of the probability for molecule production in linear magnetic-field sweeps (Landau, 1932; Zener, 1932). Their generic approaches may be interpreted in terms of a coupled system of two channels, each of which containing just a single state. In applications to Feshbach molecular association, such a treatment is equivalent to the single resonance approach of Eq. (36) in addition to the following replacement of the entrance-channel Hamiltonian:

$$H_{\rm bg}\to|\phi_0\rangle E_0\langle\phi_0|. \tag{114}$$

Here $|\phi_0\rangle$ may be interpreted, for instance, in terms of the zeroth vibrational state of the relative motion of a trapped atom pair with the energy E_0. This reduction of the two-channel continuum to a two-level system gives rise to analytic solutions of the coupled set of stationary Schrödinger equations (20) and (21). Given the simple form of the entrance-channel Green's function in the Landau-Zener approach, i.e.,

$$G_{\rm bg}(z) = |\phi_0\rangle\frac{1}{z-E_0}\langle\phi_0|, \tag{115}$$

Eq. (47) determines the two-level dressed energies to be

$$E_\pm = \frac{E_0+E_{\rm res}}{2} \pm \frac{|E_0-E_{\rm res}|}{2}\sqrt{1+4\frac{|\langle\phi_{\rm res}|W|\phi_0\rangle|^2}{(E_0-E_{\rm res})^2}}. \tag{116}$$

The magnetic-field-dependent slopes of the levels E_+ and E_- indicate, quite generally, a crossing of the discrete bare entrance- and closed-channel energies E_0 and $E_{\rm res}$, respectively. Analytic representations of the associated dressed two-component stationary states $|\phi_+\rangle$ and $|\phi_-\rangle$ can be inferred from Eq. (45).

In accordance with Eq. (116), a downward sweep of $E_{\rm res}$ across E_0 transfers a pair of atoms in the initial state $|\phi_0,\mathrm{bg}\rangle$ into the final state $|\phi_{\rm res},\mathrm{cl}\rangle$ in the limit of zero ramp speed. Their energies adiabatically follow the E_- curve. Given the linear variation of $E_{\rm res}$ of Eq. (86), such a simplified scenario presupposes the sweep to start and end asymptotically far from the crossing point of the bare levels. This, in turn, implies the formal limits $t_i\to-\infty$ and $t_f\to\infty$ of the initial and final times, respectively. The adiabatic energy variation of the Landau-Zener two-level approach is similar to the harmonic trap case illustrated in Fig. 18, except that the quasicontinuum of excited levels with indices $v>0$ is neglected.

Finite ramp speeds allow an atom pair to end up in a superposition of the entrance- and closed-channel bare states $|\phi_0,\mathrm{bg}\rangle$ and $|\phi_{\rm res},\mathrm{cl}\rangle$, respectively. In accordance with Eq. (105) and the assumption of a two-level system, the probability for an asymptotic transition between the bare levels is given by

$$p_{0,\rm res} = |\langle\phi_{\rm res},\mathrm{cl}|U_{2B}(t_f,t_i)|\phi_0,\mathrm{bg}\rangle|^2 = 1-|i\hbar\,g_{2B}(t_f,t_i)|^2, \tag{117}$$

in the limits $t_i\to-\infty$ and $t_f\to\infty$. These time limits can be determined analytically using the stationary phase condition for the energy integrals over the oscillatory functions on the right-hand side of Eq. (113). This exact approach relies upon the observation that asymptotically only those regions close to zeros of the derivatives of the phases $\varphi'(z,t_i)$ and $\varphi'(z,t_f)$ contribute to the integrals. All the remaining energy ranges in which the complex exponentials are rapidly oscillating yield negligible averages.

The positions of the stationary phases can be readily found for a two-level system. An explicit determination of the stationary Green's function $G_{\rm stat}(z)=(z-H_{\rm stat})^{-1}$ associated with the Hamiltonian $H_{\rm stat}$ of Eq. (96) yields

$$1/g_{\rm stat}(z) = z-\langle\phi_{\rm res}|WG_{\rm bg}(z)W|\phi_{\rm res}\rangle. \tag{118}$$

Equations (110) and (118) give the derivative of the phase to be

$$\varphi'(z,t) = -\frac{E - E_{\rm res}(t) - \langle \phi_{\rm res}|WG_{\rm bg}(z)W|\phi_{\rm res}\rangle}{\hbar \dot{E}_{\rm res}}. \quad (119)$$

Consequently, $\varphi'(z,t)$ vanishes at the dressed energies $E_\pm$ associated with the magnetic-field strength at time t, in accordance with Eq. (47).

As only those regions of parameters E and E' in the close proximity of $E_\pm$ significantly contribute to Eq. (113), the phases may be expanded to second order about their stationary points. This yields

$$\varphi(z,t) \approx \varphi(z_\pm,t) + \tfrac{1}{2}\varphi''(E_\pm,t)(E - E_\pm)^2. \quad (120)$$

Here $z_\pm = E_\pm + i0$ denotes the regularized energy parameter associated with $E_\pm$ at time t. The second derivative,

$$\varphi''(E_\pm,t) = -\frac{1}{\hbar \dot{E}_{\rm res}}[1 + \langle \phi_{\rm res}|WG_{\rm bg}^2(E_\pm)W|\phi_{\rm res}\rangle], \quad (121)$$

is always positive in the case of a downward ramp of $E_{\rm res}(t)$ and its inverse plays the role of a variance in the complex Gaussian integrals over E and E'. Performing the Gaussian integration associated with t_i on the right-hand side of Eq. (113) gives

$$\int_E^\infty dE' e^{i\varphi(z',t_i)} \approx \sqrt{2\pi}\sum_{n=\pm} \frac{e^{i[\varphi(z_n^i,t_i)+\pi/4]}}{\sqrt{\varphi''(E_n^i,t_i)}}\theta(E_n^i - E). \quad (122)$$

Here $z_\pm^i$ and $E_\pm^i$ refer to the dressed energies at the initial magnetic-field strength. Their asymptotic values in the case of a downward sweep of $E_{\rm res}$ are given by $E_+^i \to \infty$ and $E_-^i \to E_0$ in the limit $t_i \to -\infty$. This implies $\varphi''(E_+^i,t_i) \to -1/\hbar\dot{E}_{\rm res}$ and $\varphi''(E_-^i,t_i) \to \infty$. Consequently, only the term associated with E_+^i significantly contributes to the sum of Eq. (122). The integral over the parameter E on the right-hand side of Eq. (113) can be evaluated similarly to Eq. (122). This yields

$$i\hbar\, g_{\rm 2B}^{(+)}(t_f,t_i) = e^{-i[\varphi(E_-^f,t_f)-\varphi(E_+^i,t_i)]} \quad (123)$$

in the limits $t_i \to -\infty$ and $t_f \to \infty$. Here E_-^f refers to the dressed energy with asymptotic behavior $E_- \to -\infty$ at the final time of the magnetic-field sweep. The imaginary parts of the phases $\varphi(E_-^f,t_f)$ and $\varphi(E_+^i,t_i)$ relevant to the transition probability of Eq. (117) may be obtained from Eqs. (110) and (53). This leads to the Landau-Zener formulas

$$p_{0,\rm res} = 1 - e^{-2\pi\delta_{\rm LZ}}, \quad (124)$$

$$p_{0,0} = e^{-2\pi\delta_{\rm LZ}}. \quad (125)$$

Here $p_{0,0}$ denotes the probability for detecting the atom pair in the bare state $|\phi_0,{\rm bg}\rangle$ at the end of the magnetic-field sweep, and

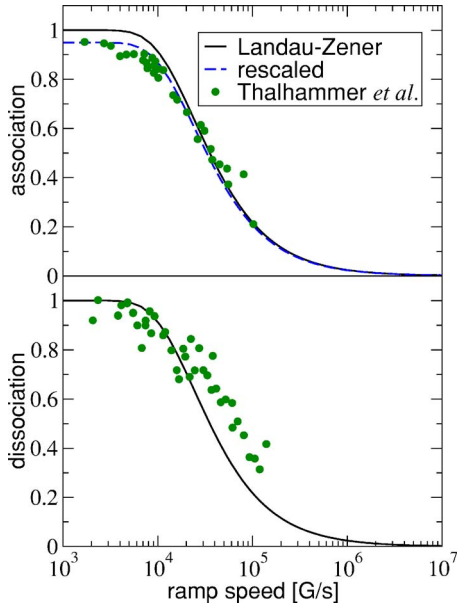

FIG. 19. (Color online) Efficiency of Feshbach molecular association (upper panel) and dissociation into the lowest energy band of an optical lattice (lower panel) via linear magnetic-field sweeps across the 1007 G zero-energy resonance of ^{87}Rb vs the ramp speed (Thalhammer *et al.*, 2006). Solid curves refer to the Landau-Zener formula given by Eq. (124) and the coefficient for a harmonic oscillator given by Eq. (128) using the measured frequency $\nu_{\rm ho}$=39 kHz. The dashed curve indicates the same Landau-Zener prediction scaled by a factor of 0.95, which accounts for possible deficits in the ideal diatomic filling, for instance, due to tunneling between lattice sites (Thalhammer *et al.*, 2006).

$$\delta_{\rm LZ} = \frac{|\langle \phi_{\rm res}|W|\phi_0\rangle|^2}{\hbar|\dot{E}_{\rm res}|} \quad (126)$$

is the Landau-Zener parameter.

For a pair of atoms in an isotropic harmonic trap, the matrix element involving the interchannel coupling W can be inferred from Eq. (40) via the general approximate relation

$$|\langle \phi_{\rm res}|W|\phi_\nu\rangle|^2 \approx 2\pi m\sqrt{mE_\nu}|\langle \phi_{\rm res}|W|\phi_0^{(+)}\rangle|^2 \frac{\partial E_\nu}{\partial \nu}. \quad (127)$$

Here E_ν is the energy of the bare oscillator level of Eq. (90) in the limit of low excitations in the Wigner threshold law regime. Assuming that the single-particle trap length greatly exceeds the background scattering length, i.e., $|a_{\rm bg}|/a_{\rm ho} \ll 1$, the density of states is given by $\partial E_\nu/\partial\nu = 2\hbar\omega_{\rm ho}$. Consequently, Eqs. (40) and (127) determine the Landau-Zener parameter associated with a trapped atom pair to be (Julienne *et al.*, 2004)

$$\delta_{\rm LZ}^{\rm ho} = \frac{\sqrt{6}\hbar}{\pi m a_{\rm ho}^3}\left|\frac{a_{\rm bg}\Delta B}{\dot{B}}\right|. \quad (128)$$

Figure 19 illustrates the validity of the Landau-Zener approach to Feshbach molecular association and disso-

ciation in an optical lattice where the sites are filled with two atoms (Thalhammer *et al.*, 2006).

On the basis of Eq. (113), the preceding determination of the asymptotic behavior of transition amplitudes may be extended to an arbitrary number of energy states of the entrance-channel interaction (Demkov and Osherov, 1968; Macek and Cavagnero, 1998; Yurovsky and Ben-Reuven, 1998; Yurovsky *et al.*, 1999a). This shows that despite the fact that the Landau-Zener approach neglects the bare excited and molecular levels, it gives the exact probability for the loss of atom pairs from the $v=0$ mode of a harmonic trap. At the end of an asymptotic linear downward sweep of E_{res}, the entire population either remains in the initial $v=0$ state or is transferred into energetically lower levels $v<0$ or into the resonance state. A similar statement applies to asymptotic upward sweeps, which are also exactly described by Eqs. (124), (125), and (128). Consequently, in the limits $t_i\rightarrow-\infty$ and $t_f\rightarrow\infty$ transitions between states occur only in the intuitive direction of the sweep. The intermediate dynamics, however, involves all levels, i.e., the amplitudes associated with unintuitive transitions interfere away only at asymptotically large times.

B. Magnetic-field sweeps in Bose-Einstein condensates

Several pioneering studies on the properties of zero-energy resonances of alkali atom pairs (Inouye *et al.*, 1998; Stenger *et al.*, 1999; Cornish *et al.*, 2000) have been performed in dilute Bose-Einstein condensates (Anderson *et al.*, 1995; Davis *et al.*, 1995; Bradley *et al.*, 1995, 1997). Condensation of Bose atoms (Bose, 1924; Einstein, 1924, 1925) occurs when the occupation number N_c of a particular single-particle state becomes comparable to the total number of atoms N such that N_c/N remains finite in the thermodynamic limit. Signatures of this phenomenon in dilute alkali gases have been identified, for instance, through a specific, narrow momentum distribution of the atoms or a characteristic spectrum of collective excitations (Dalfovo *et al.*, 1999). While low collision momenta facilitate the theoretical description of the two-body physics of molecular association, the complex many-particle nature of Bose-Einstein condensates subject to dynamically resonance enhanced interactions becomes particularly significant on long time scales. In addition, Feshbach molecules of some alkali species associated with closed-channel-dominated resonances proved to be unstable in the gas environment (Herbig *et al.*, 2003; Xu *et al.*, 2003; Dürr, Volz, Marte, and Rempe, 2004). For this reason, such experiments were performed in part under conditions of free expansion (Dürr, Volz, Marte, and Rempe, 2004; Yurovsky and Ben-Reuven, 2004; 2005; Mark *et al.*, 2005). Comparisons between predicted and measured molecule production via magnetic-field sweeps in Bose-Einstein condensates are, therefore, less conclusive than in the case of a single atom pair confined to an optical lattice site.

1. Limit of high ramp speeds

In the limit of high ramp speeds the transfer of condensed atoms into Feshbach molecules may be estimated using the two-body Landau-Zener approach (Mies *et al.*, 2000; Góral *et al.*, 2004). To this end, it is instructive to divide the dilute gas into regions of virtually constant density. Their volumes $\mathcal{V}$ can be chosen sufficiently large for the thermodynamic limit to be applicable. The state of an arbitrary atom pair of a uniform Bose-Einstein condensate in each of these periodic boxes is well described by the lowest quasicontinuum energy level. Accordingly, the associated Landau-Zener parameter can be inferred from Eq. (126) using the following replacement of the initial wave function:

$$|\phi_0\rangle\rightarrow|\phi_0^{(+)}\rangle\sqrt{(2\pi\hbar)^3/\mathcal{V}}. \tag{129}$$

Given that the size of a dilute gas is on the order of several μm, the volume $\mathcal{V}$ is sufficiently large for the transition probability of Eq. (124) to reduce to its first-order approximation $p_{0,\mathrm{res}}\approx 2\pi\delta_{\mathrm{LZ}}$. A typical order of magnitude of $p_{0,\mathrm{res}}$ is 10^{-6} (Mies *et al.*, 2000).

While the association of a particular pair of condensed atoms is a rare event, the fact that each atom has all the others to interact with grossly enhances the efficiency of molecule formation. Just in the limit of high ramp speeds the Bose-Einstein condensate may be treated as a reservoir whose total atom number is barely affected by an asymptotic magnetic-field sweep across B_0. This assumption implies that the small fraction of lost atoms is well described in terms of the pairwise average of microscopic transition probabilities. The number of pairs in a box with N atoms is $N(N-1)/2$, which in the limit $|\dot{B}|\rightarrow\infty$ yields the following estimate for the condensate depletion (Góral *et al.*, 2004):

$$N_{\mathrm{loss}}=2\pi(N-1)(N/\mathcal{V})\frac{4\pi\hbar}{m}\left|\frac{a_{\mathrm{bg}}\Delta B}{\dot{B}}\right|. \tag{130}$$

Here $N/\mathcal{V}$ is the uniform density of the gas in the volume $\mathcal{V}$. In accordance with the local-density approximation, the total number of atoms lost from a Bose-Einstein condensate is given by the spatial average of Eq. (130) over the densities of all boxes.

We note that the Landau-Zener estimate of Eq. (130) is applicable to both sweep directions of the Feshbach resonance level. In the case of downward sweeps, the condensed atoms are partly transferred into diatomic Feshbach molecules whose final number N_d^f, equals one-half of the atom loss of Eq. (130), i.e.,

$$N_d^f=N_{\mathrm{loss}}/2. \tag{131}$$

Upward sweeps lead to the production of correlated pairs with a comparatively high relative velocity depending on the ramp speed. In some experiments using nonlinear field variations (Donley *et al.*, 2001, 2002), such atom pairs were detected as a trapped dilute cloud with an average spatial extent much larger than the size of the remnant Bose-Einstein condensate.

2. Two-level mean-field approach

A description of atom loss from a Bose-Einstein condensate consistent with both Eq. (130) and the dynamical depletion of pairs during a magnetic-field sweep across B_0 may be based on Eqs. (94) and (95). Such an extended two-level configuration interaction approach to the probability amplitudes $C_0(t)$ and $C_{\rm res}(t)$ associated with the zero-energy mode of an atom pair and its depletion, respectively, is given by (Góral *et al.*, 2004; Julienne *et al.*, 2004)

$$i\hbar\,\dot{C}_0(t) = E_0 C_0(t) + (N/\mathcal{V})^{1/2} g_{\rm res}^* C_0^*(t) C_{\rm res}(t), \tag{132}$$

$$i\hbar\,\dot{C}_{\rm res}(t) = E_{\rm res}(t) C_{\rm res}(t) + (N/\mathcal{V})^{1/2} g_{\rm res} C_0^2(t). \tag{133}$$

Here N is the total number of atoms of the homogeneous gas in the volume $\mathcal{V}$. The interchannel coupling is determined by the matrix element

$$g_{\rm res} = (2\pi\hbar)^{3/2} \langle \phi_{\rm res} | W | \phi_0^{(+)} \rangle, \tag{134}$$

in accordance with Eqs. (94), (95), and (129). Similarly to the two-body configuration interaction approach, Eqs. (132) and (133) lead to a constant of motion $|C_0(t)|^2 + |C_{\rm res}(t)|^2 = 1$. This implies an interpretation of the quantities $N|C_0(t)|^2$ and $N|C_{\rm res}(t)|^2$ in terms of the number of atoms associated with the remnant Bose-Einstein condensate and correlated pairs, respectively. The nonlinear nature of Eqs. (132) and (133) in terms of the Bose enhancement factor $(N/\mathcal{V})^{1/2} C_0(t)$ ensures consistency with Eq. (130) and, therefore, accounts for the surrounding gas.

The long-time asymptotic populations may be estimated analytically based on a linearized version of Eqs. (132) and (133) using a static Bose enhancement factor $(N/\mathcal{V})^{1/2}$ (Mies *et al.*, 2000). This treatment of the interchannel coupling neglects the time dependence of the depletion of condensed atoms and leads to dynamical equations formally equivalent to those of the two-body Landau-Zener approach. In accordance with Eq. (130), the associated Landau-Zener coefficient is given by

$$\delta_{\rm LZ}^{\rm BEC} = (N/\mathcal{V}) \frac{4\pi\hbar}{m} \left| \frac{a_{\rm bg}\Delta B}{\dot{B}} \right| = N\delta_{\rm LZ}. \tag{135}$$

The asymptotic condensate depletion and its remnant uniform density can be inferred from Eqs. (124) and (125), respectively, using $\delta_{\rm LZ}^{\rm BEC}$ instead of $\delta_{\rm LZ}$.

An approach similar to Eqs. (132) and (133) but applicable to trapped gases beyond a local-density treatment was derived on the basis of a mean-field approximation (Drummond *et al.*, 1998; Tommasini *et al.*, 1998; Timmermans *et al.*, 1998, 1999a). The associated many-body model Hamiltonian was originally introduced in the context of superconductivity (Ranninger and Robaszkiewicz, 1985; Friedberg and Lee, 1989). This procedure leads to the following dynamical equations:

$$i\hbar\,\dot{\Psi}(\mathbf{x},t) = H_{\rm GP}\Psi(\mathbf{x},t) + g_{\rm res}^* \Psi^*(\mathbf{x},t)\Psi_{\rm res}(\mathbf{x},t), \tag{136}$$

$$i\hbar\,\dot{\Psi}_{\rm res}(\mathbf{R},t) = H_{\rm res}(t)\Psi_{\rm res}(\mathbf{R},t) + g_{\rm res}\Psi^2(\mathbf{R},t). \tag{137}$$

Here the background scattering is included in terms of the usual Gross-Pitaevskii mean-field Hamiltonian $H_{\rm GP}$ in the contact pseudo-interaction approximation (Gross, 1961; Pitaevskii, 1961). Given a spherically symmetric harmonic atom trap, $H_{\rm GP}$ therefore consists of the following contributions:

$$H_{\rm GP} = -\frac{\hbar^2\nabla^2}{2m} + \frac{m}{2}\omega_{\rm ho}^2|\mathbf{x}|^2 + \frac{4\pi\hbar^2}{m} a_{\rm bg}|\Psi(\mathbf{x},t)|^2. \tag{138}$$

Typical frequencies $\nu_{\rm ho} = \omega_{\rm ho}/2\pi$ associated with such comparatively weakly confining traps are on the order of 100 Hz. The generalized resonance energy $H_{\rm res}(t)$ contains the center-of-mass kinetic energy of correlated pairs as well as a magnetic-field shift from $B_{\rm res}$ to the measurable position of the singularity of the scattering length. Its explicit expression reads

$$H_{\rm res}(t) = -\frac{\hbar^2\nabla^2}{4m} + m\omega_{\rm ho}^2|\mathbf{R}|^2 + \mu_{\rm res}[B(t) - B_0]. \tag{139}$$

The mean fields $\Psi(\mathbf{x},t)$ and $\Psi_{\rm res}(\mathbf{R},t)$ refer to the amplitudes of the densities of atoms in the condensate at the position $\mathbf{x}$ and of correlated pairs with the center of mass $\mathbf{R}$, respectively. Similarly to the configuration interaction approach, Eqs. (136) and (137) give rise to a constant of motion consistent with the conservation of the total number of atoms,

$$\int d\mathbf{x}|\Psi(\mathbf{x},t)|^2 + \int d\mathbf{R}|\Psi_{\rm res}(\mathbf{R},t)|^2 = N. \tag{140}$$

Since its first applications in the context of Feshbach resonances in the physics of cold gases, this two-level mean-field approach has been continually extended to a variety of physical situations (van Abeelen and Verhaar, 1999; Góral *et al.*, 2001; Holland *et al.*, 2001; Duine and Stoof, 2003b; Yurovsky and Ben-Reuven, 2003b).

Figure 20 shows that Eqs. (136) and (137) give reasonable agreement with the loss of condensed atoms observed in experiments involving zero-energy resonances of ^{23}Na (Stenger *et al.*, 1999). These measurements refer to asymptotic upward sweeps of the Feshbach resonance level across B_0 leading to the production of unbound correlated pairs of atoms (van Abeelen and Verhaar, 1999). We note that Eqs. (136) and (137) account well for the onset of atom loss over ranges of ramp speeds, which differ by three orders of magnitude between the upper and lower panels of Fig. 20. A similarly fair agreement has been reported for predictions of several different approaches (Mackie *et al.*, 2002; Yurovsky and Ben-Reuven, 2003a; Köhler *et al.*, 2004) on the observed atom loss of a Bose-Einstein condensate exposed to magnetic-field sweeps across the 155 G zero-energy resonance of ^{85}Rb (Cornish *et al.*, 2000). The dashed curves in Fig. 20 indicate the asymptotic Landau-Zener predictions based on the coefficient of Eq. (135) and the local-density approximation. Both theoretical approaches recover the asymptotic behavior of the loss of condensed atoms in the case of fast sweeps given by Eq.

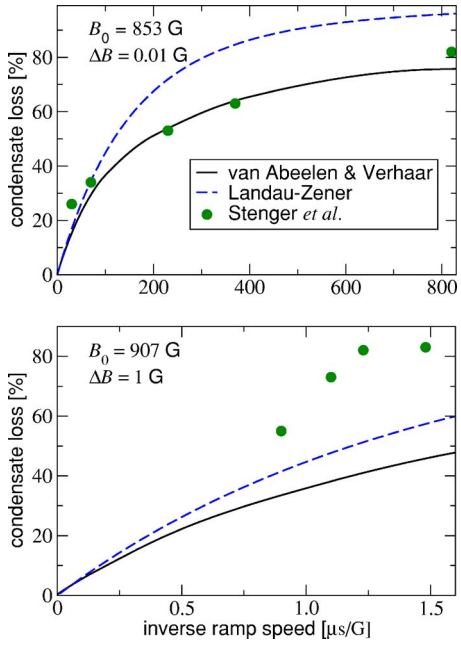

FIG. 20. (Color online) Loss of condensate atoms in upward sweeps of the Feshbach resonance level across the 853 and 907 G zero-energy resonances of ^{23}Na vs the inverse ramp speed $1/|\dot{B}|$ (Stenger *et al.*, 1999). Experimental data are compared to theoretical predictions using the Landau-Zener (Mies *et al.*, 2000; Góral *et al.*, 2004) and two-level mean-field (van Abeelen and Verhaar, 1999) approaches. The theoretical Feshbach resonance parameters employed refer to the values of a_{bg} and ΔB given in Tables IV and V. Note the differences in ramp speeds of three orders of magnitude between the upper and lower panels, which reflect the different widths of the 853 and 907 G zero-energy resonances.

(130). Their functional forms differ in the opposite, adiabatic limit of low ramp speeds (Góral *et al.*, 2004; Ishkhanyan *et al.*, 2004), i.e., when the parameter $1/|\dot{B}|$ in Fig. 20 increases. We note that both the two-level mean-field approach and its associated Landau-Zener estimate of asymptotic populations do not distinguish between sweep directions. Consequently, the molecule production in a downward sweep of the Feshbach resonance level is treated symmetrically to the heating of the gas in an upward sweep.

While Eqs. (132) and (133) refer to a genuinely two-level system, the two-level mean-field approach accounts for the background scattering continuum, in principle, through the parameter a_{bg} of the mean-field Hamiltonian of Eq. (138). Such a contact pseudo-interaction treatment presupposes a separation between the typical time scales associated with the evolution of the Bose-Einstein condensate and the diatomic collisional duration (Proukakis *et al.*, 1998; Köhler and Burnett, 2002). Accordingly, the two-level mean-field approach can be derived in terms of the Markov limit of microscopic many-body theories of dilute gases (Góral *et al.*, 2004) outlined in Sec. V.C. The assumption of a separation of time scales between two- and many-body evolutions is violated during a magnetic-field sweep across a singularity of the scattering length. This implies that Eqs. (136) and (137) can describe the dynamics, at most, in the asymptotic regime where the dilute gas parameter $[N|a(B)|^3/\mathcal{V}]^{1/2}$ is small compared to unity. Similarly to the limitations of the two-body Landau-Zener model, the intermediate evolution of a Bose-Einstein condensate is influenced by phenomena beyond the range of validity of the mean-field approximation (Holland *et al.*, 2001; Góral *et al.*, 2004; Köhler *et al.*, 2004). While most theoretical approaches agree in their predictions on the condensate loss in the fast sweep limit of Eq. (130), the saturation of molecule production is a matter of ongoing research (Naidon and Masnou-Seeuws, 2003, 2006).

C. Molecule production in cold Bose and Fermi gases

Cold Bose and two-spin-component Fermi gases are subject to a considerable momentum spread, which generally tends to reduce the efficiency of molecule production via linear magnetic-field sweeps across a zero-energy resonance. Its significance is particularly obvious in the case of slow asymptotic sweeps, given the spectrum of dressed energies of an atom pair illustrated in Fig. 18. Only the $\nu=0$ mode adiabatically correlates with the Feshbach molecular level when the resonance energy is decreased, while all excited states undergo cooling transitions. From this too simplistic viewpoint, for instance, two spin components of a dilute vapor of Fermi atoms distributed according to the Pauli exclusion principle would produce just a single molecule in the adiabatic limit of the ramp speed. Contrary to the case of Bose-Einstein condensates, binary physics alone is therefore not even sufficient to qualitatively explain the observed substantial molecule production in such gases (Regal *et al.*, 2003a; Strecker *et al.*, 2003).

1. Transitions from continuum to bound states

A quantitative analysis of the problems associated with the theoretical description of molecule production in the presence of momentum spread may be based on the exact treatment of linear magnetic-field sweeps of Sec. IV.A. Accordingly, the probability for transitions from an initial dressed continuum level of a pair of distinguishable atoms in a periodic box of volume $\mathcal{V}$ to the Feshbach molecular state at the final magnetic-field strength is given by

$$p_{\mathrm{ass}}(\mathbf{k}) = \frac{(2\pi\hbar)^3}{\mathcal{V}} |\langle \phi_b^f | U_{2\mathrm{B}}(t_f,t_i) | \phi_{\hbar\mathbf{k}}^i \rangle|^2. \tag{141}$$

Here the arguments of the two-body time evolution operator t_i and t_f refer to the initial and final times of the sweep, respectively, and $\hbar\mathbf{k}$ denotes the initial relative momentum of the atoms. Similarly to the derivation of Eq. (123), the asymptotic transition probability including the background scattering continuum can be determined analytically using the stationary phase approach in Eq. (141) in the limits $t_i \to -\infty$ and $t_f \to \infty$. This yields

$$p_{\rm ass}(\mathbf{k}) = \frac{(2\pi\hbar)^3}{\mathcal{V}} \frac{2\pi}{\hbar|\dot{E}_{\rm res}|} |\langle \phi_{\rm res}|W|\phi^{(+)}_{\hbar\mathbf{k}}\rangle|^2 e^{-2\ {\rm Im}\ \varphi(z_i,t_i)}. \tag{142}$$

Here $z_i=\hbar^2k^2/m+i0$ denotes the regularized energy argument of the initial phase. In accordance with Eqs. (110), (118), and (53), the exponent of Eq. (142) is determined by the formula

$${\rm Im}\ \varphi(z_i,t_i) = \frac{\pi\hbar^2}{|\dot{E}_{\rm res}|} \int d\mathbf{k}'\, \theta(k-k') |\langle \phi_{\rm res}|W|\phi^{(+)}_{\hbar\mathbf{k}'}\rangle|^2. \tag{143}$$

Here the step function of wave numbers $\theta(k-k')$ indicates that transitions occur just in the intuitive, downward direction of an asymptotic sweep across B_0 (Demkov and Osherov, 1968). According to Eq. (143), the exponential damping of Eq. (142) increases in the limit $|\dot{E}_{\rm res}|\to 0$. This confirms the intuitive picture suggested by Fig. 18 that adiabatic sweeps in a diatomic system with a continuum of modes eventually lead to negligible molecule production. While the momentum dependence of the exponent in Eq. (143) recovers experimental dissociation spectra (Mukaiyama *et al.*, 2003), in the context of molecular association in cold gases Eq. (142) gives rise to exact predictions just in the fast sweep limit.

2. Fast sweep limit of molecule production

The onset of molecule production in asymptotic magnetic-field sweeps across zero-energy resonances is sensitive to the statistics associated with identical atoms. Section V.B provides a strict approach to the determination of dimer populations on the basis of the two-particle correlation function of the gas. Similarly to the prediction of the loss of condensed atoms of Eq. (130), however, low depletions can be inferred intuitively from the fast sweep limit of Eq. (142), treating the gas as a reservoir of atom pairs. In the limit $|\dot{B}|\to\infty$, the damping term of Eq. (143) describing cooling transitions into continuum levels below the initial energy $\hbar^2k^2/m$ vanishes. In the context of cold collisions within the Wigner threshold law regime, the matrix element involving the interchannel coupling in Eq. (142) may be evaluated at $\mathbf{k}=\mathbf{0}$. Consequently, the transition probability of Eq. (142) becomes momentum independent and recovers the result of the Landau-Zener approach $p_{\rm ass}=2\pi\delta_{\rm LZ}$.

For the purpose of studies involving s-wave collisions, Fermi gases are usually prepared as incoherent mixtures of two different Zeeman states with occupation numbers N_1 and N_2. Accordingly, $N=N_1+N_2$ is the total number of atoms. Each of the N_1 atoms of the first component has N_2 atoms of the second component to interact with via s-wave collisions. Classical probability theory and the incoherent nature of the initial state, therefore, lead to the following estimate for the number of diatomic Feshbach molecules produced in the fast sweep limit (Chwedeńczuk *et al.*, 2004):

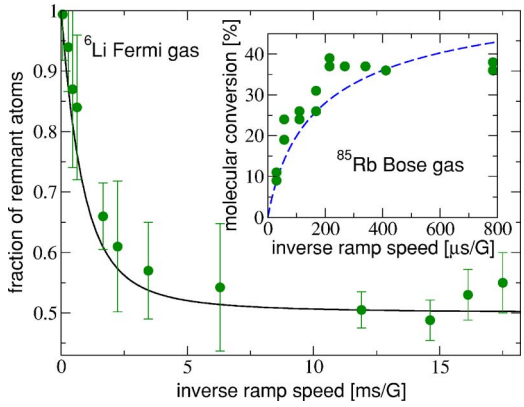

FIG. 21. (Color online) Fraction of remnant atoms $1-2N_d^f/N$ at the end of asymptotic magnetic-field sweeps across the closed-channel-dominated 543 G zero-energy resonance of ^{6}Li vs the inverse ramp speed (Strecker *et al.*, 2003). The solid curve refers to a Landau-Zener estimate for the onset of molecule production in the fast sweep limit (Chwedeńczuk *et al.*, 2004) using the local-density approximation. Inset: The molecular conversion $2N_d^f/N$ observed in a thermal Bose gas with a mean density of 1.3×10^{11} atoms/cm^3 and a temperature of 40.6 nK using magnetic-field sweeps across the 155 G zero-energy resonance of ^{85}Rb (Hodby *et al.*, 2005). For comparison, the dashed curve indicates the pairwise ensemble average over the transition probabilities $2p_{\rm ass}(\mathbf{k})$ with respect to the Maxwell distribution of relative velocities. This semiclassical estimate for the onset of molecule production in Bose gases is based on Eq. (142) and is therefore consistent with the limit of Eq. (145). Both solid and dashed curves are associated with the parameters $a_{\rm bg}$ and ΔB of Tables IV and V, respectively.

$$N_d^f = 2\pi N_1 N_2 \delta_{\rm LZ}. \tag{144}$$

We note that the two-body Landau-Zener coefficient, given explicitly by the right-hand side of Eq. (135), is inversely proportional to the volume $\mathcal{V}$ of the periodic box. The fraction of molecules N_d^f/N is therefore proportional to the density $N/\mathcal{V}$ which allows for an extension of Eq. (144) to inhomogeneous gases via the local-density approximation.

Given a balanced mixture of Zeeman states, i.e., $N_1=N_2=N/2$, Eqs. (144) and (131) show that the onset of molecule production in a Fermi gas is half as large as in a Bose-Einstein condensate of identical density and resonance parameters. In the limit of zero temperature, such a dilute, initially weakly interacting vapor of atoms may be approximately described by a pair of filled Fermi seas. As fast magnetic-field sweeps imply small atomic depletions, it may be argued intuitively that two-body cooling transitions leading into occupied modes below the Fermi energy are suppressed by the Pauli exclusion principle. This suggests a description of the two-spin-component Fermi sea in terms of a single level over a significant range of ramp speeds. The associated Landau-Zener approach (Chwedeńczuk *et al.*, 2004), consistent with the linear limit of Eq. (144), is illustrated in Fig. 21 in comparison with experiments on asymptotic magnetic-field sweeps across the 543 G zero-energy resonance of ^{6}Li (Strecker *et al.*, 2003). Accordingly, sup-

pression of cooling transitions gives an intuitive explanation for the onset of a substantial molecule production in two-spin-component Fermi gases.

In thermal Bose gases, each one of the N constituents can interact with all the other $N-1$ atoms to form a dimer Feshbach molecule. As opposed to the zero-energy mode of condensed pairs, diatomic wave functions in the presence of momentum spread need to be explicitly symmetrized, which enhances the association probability of Eq. (141) in the thermal average by a factor of 2 (Stoof *et al.*, 1989). As the number of interacting pairs is $N(N-1)/2 \approx N^2/2$, the fast sweep limit of the number of Feshbach molecules produced in a thermal Bose gas is given by

$$N_d^f = 2\pi N^2 \delta_{\mathrm{LZ}}. \tag{145}$$

This estimate is illustrated in the inset of Fig. 21 in comparison with experiments associated with thermal clouds of ^{85}Rb (Hodby *et al.*, 2005). We note that a similar enhancement of dimer formation in thermal Bose gases as compared to condensates was observed in the context of inelastic three-body recombination and reflects correlation properties (Kagan *et al.*, 1985; Burt *et al.*, 1997).

According to Eqs. (144), (131), and (145), the onsets of molecule production increase by factors of 2 between balanced two-spin-component Fermi gases, Bose-Einstein condensates, and thermal Bose gases of identical densities and resonance parameters. The validity of these statistical estimates based on two-body physics depends on the significance of multiple collisions of each atom during a magnetic-field sweep. This implies that the range of ramp speeds described by fast sweep limits depends on the density of the gas in addition to the specific nature of the Feshbach molecules associated with entrance- and closed-channel-dominated zero-energy resonances. Predictions accessing wider ranges of ramp speeds require many-body approaches (Javanainen *et al.*, 2004; Pazy *et al.*, 2004, 2005; Williams, Nikuni, *et al.*, 2004, Williams, Nygaard, and Clark, 2004).

3. Saturation of molecule production

Magnetic-field sweeps sufficiently slow to convert up to 88% of atoms into Feshbach molecules were employed to produce Bose-Einstein condensates of dimers from balanced two-spin-component mixtures of ^{40}K Fermi atoms (Greiner *et al.*, 2003). Figure 4 shows a typical density profile of such a final molecular cloud (right image) compared with a thermal distribution (left image). Motivated by the theory of ideal Bose gases, the conditions for condensation in these experiments are likely to depend on the phase space density $n_a^i \lambda_{\mathrm{th}}^3$ associated with the initial dilute atomic gas of density n_a^i and temperature T. Here $\lambda_{\mathrm{th}} = (2\pi\hbar^2/mk_{\mathrm{B}}T)^{1/2}$ is the thermal de Broglie wavelength. Given the experimental densities on the order of 10^{13} atoms/cm^3 and the 202 G zero-energy resonance parameters, magnetic-field sweeps with low ramp speeds of typically 160 G/s (Greiner *et al.*, 2003) may be considered to be adiabatic. Such processes smoothly alter diatomic wave functions but are not necessarily expected to change the occupation of states in phase space. It is therefore plausible that not only the condition for molecular condensation but also the saturated production efficiency $2N_d^f/N$ is determined just by the phase-space density rather than the number of atoms or their temperature individually.

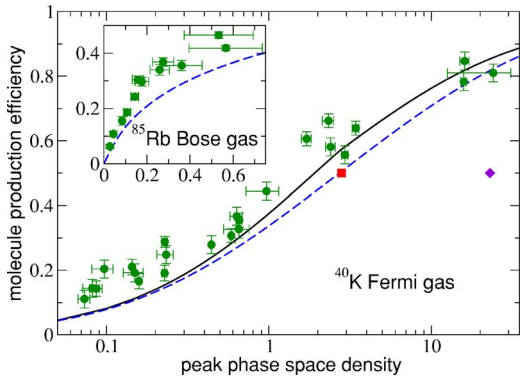

FIG. 22. (Color online) Molecular production efficiency $2N_d^f/N$ vs peak phase-space density of cold Bose as well as two-spin-component Fermi gases. Circles are dimer populations measured at the end of adiabatic magnetic-field sweeps across the zero-energy resonances of ^{85}Rb at 155 G (inset) and of ^{40}K at 202 G (Hodby *et al.*, 2005). Curves indicate predictions (Williams *et al.*, 2006) based on coupled Boltzmann equations including quantum statistical effects (solid curve) as well as their associated classical gas limit (dashed curves). For comparison, the square and diamond refer to molecular production efficiencies observed for the lowest ramp speeds in earlier sweep experiments using zero-energy resonances of ^{40}K at 224 G (Regal *et al.*, 2003a) and of ^{6}Li at 543 G (Strecker *et al.*, 2003), respectively.

Subsequent systematic studies of adiabatic magnetic-field sweeps in both two-spin-component Fermi gases of ^{40}K and thermal Bose gases of ^{85}Rb have supported this view (Hodby *et al.*, 2005). The measured molecule production efficiencies of Fig. 22 were analyzed in terms of a stochastic model assuming that the probability for two atoms to form a dimer depends solely on their proximity in phase space. Based on experimental data, the associated proximity conditions turned out to be virtually identical for both atomic species ^{40}K and ^{85}Rb. These observations can be understood from first principles using coupled Boltzmann equations for the Wigner functions associated with density matrices of separated atoms and pairs in the resonance state configuration (Williams *et al.*, 2006). Figure 22 illustrates the accuracy of this approach including quantum statistical effects (Bloch, 1928; Uehling and Uhlenbeck, 1933) as well as its classical gas limit.

Similar experiments using adiabatic magnetic-field sweeps across the 834 G zero-energy resonance in cold two-spin-component Fermi gases of ^{6}Li yielded up to 80% Feshbach molecular conversion (Cubizolles *et al.*, 2003). Such observations were analyzed in terms of theoretical approaches based on the assumption of thermal equilibrium throughout the sweep (Chin and Grimm, 2004; Kokkelmans *et al.*, 2004). In the magnetic-field

range of positive scattering lengths about B_0, the Feshbach molecular level gives rise to a local minimum of the many-particle action (Szymańska *et al.*, 2005) which is associated with a metastable state. As this state is energetically favorable to a gas of separated atoms, it may be argued intuitively that production of dimer molecules should also occur at a stationary magnetic-field strength when the system equilibrates. This principle has been employed to convert balanced incoherent two-spin-component mixtures of ^{6}Li atoms into dilute vapors of Feshbach molecules (Jochim *et al.*, 2003a). While energy conservation inevitably leads to components of comparatively hot atoms and dimers, the stability of universal Feshbach molecules discussed in Sec. III.E allows such gases to be cooled by evaporation. The associated increase in phase space density provides an alternative route to the Bose-Einstein condensation of $^6Li_2$ (Jochim *et al.*, 2003b; Zwierlein *et al.*, 2003) besides the approach of adiabatic magnetic-field sweeps.

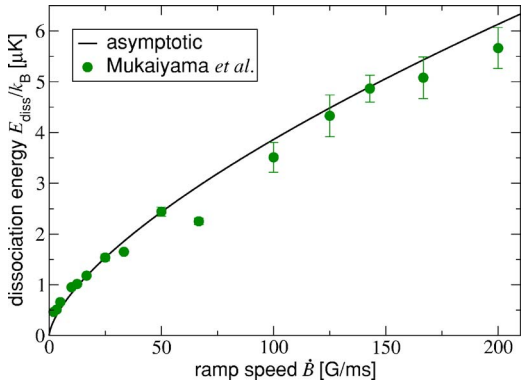

FIG. 23. (Color online) Mean energies of the atomic fragments of $^{23}Na_2$ Feshbach molecules dissociated by a linear upward sweep of the 907 G resonance level vs the ramp speed. Circles indicate experimental data (Mukaiyama *et al.*, 2003) while the solid curve refers to the predictions of Eq. (149) using the parameters a_{bg} and ΔB of Tables IV and V, respectively.

D. Dissociation of Feshbach molecules

Asymptotic upward sweeps of the resonance energy lead to the dissociation of Feshbach molecules, which often serves as a precursor to their detection. To this end, a molecular component is usually spatially separated from the environment of a remnant atomic gas using, for instance, the Stern-Gerlach technique illustrated in Sec. III.G. After this separation, dissociation allows fragments to be detected conventionally using probe lasers tuned to resonance with an atomic spectral line. The energy provided by the time-varying homogeneous magnetic field during the sweep is transferred to the relative motion of the atomic constituents of a Feshbach molecule. Such correlated atom pairs with a relative velocity depending on the ramp speed were detected in several experiments (Mukaiyama *et al.*, 2003; Dürr, Volz, and Rempe, 2004; Volz *et al.*, 2005). Their spectrum of kinetic energies of the relative motion is given by

$$n_{\rm diss}(\hbar^2k^2/m) = \frac{m\hbar k}{2}\int d\Omega |\langle \phi^f_{\hbar\mathbf{k}}|U_{2B}(t_f,t_i)|\phi^i_b\rangle|^2. \tag{146}$$

Here $d\Omega$ denotes the angular component of $d\mathbf{k}$ describing the direction of the momentum $\hbar\mathbf{k}$, while $|\phi^i_b\rangle$ and $|\phi^f_{\hbar\mathbf{k}}\rangle$ are bound and dressed continuum states associated with the initial and final magnetic-field strengths, respectively.

Similarly to the derivation of Eqs. (142) and (143), the energy spectrum of Eq. (146) can be determined analytically in the asymptotic limits $t_i \to -\infty$ and $t_f \to \infty$. As dissociation and association are related to each other by time reversal, their transition probability densities are identical. Typical energies $\hbar^2k^2/m$ of atomic fragments are on the order of μK in units of the Boltzmann constant which is usually inside the Wigner threshold law regime, i.e., $k|a_{bg}| \ll 1$. This implies that the matrix elements involving the interchannel coupling in Eqs. (142) and (143) can be evaluated at $\mathbf{k}=\mathbf{0}$ and $\mathbf{k}'=\mathbf{0}$, respectively. Consequently, the asymptotic dissociation spectrum of Eq. (146) is well approximated by (Mukaiyama *et al.*, 2003; Góral *et al.*, 2004)

$$n_{\rm diss}(E) = -\frac{\partial}{\partial E}\exp\left(-\frac{4}{3}\sqrt{\frac{mE}{\hbar^2}}\frac{|a_{bg}\Delta B|E}{\hbar|\dot{B}|}\right). \tag{147}$$

We note that the integral of Eq. (147) over all kinetic energies E of the relative motion gives unity. This implies that Feshbach molecules are dissociated with certainty in an asymptotic upward sweep of the resonance energy, provided that transitions to the highest excited entrance-channel vibrational level are negligible.

According to Eq. (147), the width of the dissociation spectrum increases with increasing ramp speeds. The associated single-particle kinetic energies are usually inferred from the velocities of the fragments, which constitute a radially expanding cloud of atoms. Their average $E_{\rm diss}$ amounts to one-half of the mean energy of the relative motion of all correlated pairs given in terms of Eq. (146) by

$$E_{\rm diss} = \frac{1}{2}\int_0^\infty dE E n_{\rm diss}(E). \tag{148}$$

Accordingly, the Wigner threshold law approximation of Eq. (147) determines $E_{\rm diss}$ to be

$$E_{\rm diss} = \frac{1}{3}\left(\frac{3}{4}\sqrt{\frac{\hbar^2}{ma_{bg}^2}}\frac{\hbar|\dot{B}|}{|\Delta B|}\right)^{2/3}\Gamma(2/3). \tag{149}$$

Figure 23 illustrates the accuracy of the predictions of Eq. (149) on average dissociation energies detected at the end of asymptotic magnetic-field sweeps across the 907 G zero-energy resonance of sodium (Mukaiyama *et al.*, 2003). While the solid curve refers to independently determined parameters a_{bg} and ΔB (Mies *et al.*, 2000), the good agreement with the measurements has motivated experiments using molecular dissociation to char-

acterize resonances (Dürr, Volz, and Rempe, 2004; Brouard and Plata, 2005).

We note that the asymptotic energy spectrum of Eq. (147) depends just on the product $a_{bg}\Delta B$, which, according to Eq. (39), determines near-resonant scattering lengths in the universal regime of magnetic-field strengths. A similar statement applies to Landau-Zener coefficients as well as the long-time asymptotic occupations predicted by the two-level mean-field approach (Góral *et al.*, 2004). In the limits $t_i \to -\infty$ and $t_f \to \infty$ the number of correlated atom pairs produced by linear magnetic-field sweeps is, therefore, insensitive to the parameters μ_{res} and $B_0 - B_{res}$ which directly refer to properties of the resonance level. This suggests that such populations can be inferred from any one of the single-channel approaches outlined in Secs. III.F and III.G, which give the correct magnetic-field dependence of the scattering length (Góral *et al.*, 2004; Köhler *et al.*, 2004). All derivations of the exact diatomic dynamics associated with linear magnetic-field sweeps of Sec. IV.A may be performed, for instance, using a single-channel Hamiltonian with a time-dependent separable potential. Despite the fact that such a two-body interaction is not suited to describe closed-channel-dominated Feshbach molecular states, it exactly recovers the asymptotic dissociation spectrum of Eq. (147).

In accordance with Eq. (122), the range of validity of the limits $t_i \to -\infty$ and $t_f \to \infty$ in applications to linear sweeps is determined by the accuracy of the stationary phase approach. Given a fixed ramp speed, this approximation is violated when the sweep starts or terminates too close to B_0 for the variation of the phases in Eq. (113) to produce sufficiently many oscillations of the complex exponential functions. We note that according to Eq. (119) the phase gradient with respect to the energy parameter is proportional to $1/\dot{B}$. This implies that slow sweeps tend to require smaller ranges of magnetic-field strengths about B_0 for the asymptotic limits to be applicable. Conversely, the faster a sweep, the more it resolves details of both the intermediate dynamics and the initial and final states.

In the idealized limit of a jump of the magnetic-field strength across B_0, the Feshbach molecular dissociation spectrum of Eq. (146) just probes the overlap of the dressed initial bound and final continuum states. Such a scenario has been realized using a narrow closed-channel-dominated zero-energy resonance of ^{87}Rb (Dürr, Volz, and Rempe, 2004). In these experiments, the initial magnetic-field strength was chosen such that the Feshbach molecule was virtually identical to the resonance state $|\phi_{res}, \mathrm{cl}\rangle$. According to Eq. (33), this implies that the dissociation spectrum is determined by the modulus squared of the amplitude of Eq. (34), i.e., $n_{diss}(p^2/m)2/mp = 4\pi |A(B_f, p^2/m)|^2$. Its resonance denominator gives rise to a sharp maximum at $E_{res}(B_f)$ (Dürr, Volz, and Rempe, 2004; Haque and Stoof, 2005) slightly shifted by the real part of Eq. (54), while the associated imaginary part yields the spectral width. Such dissociation jumps across B_0 using a resonance state of d-wave symmetry can populate several outgoing partial waves of the atomic fragments. This approach was employed, for instance, for the spectroscopy of a d-wave shape resonance (Dürr *et al.*, 2005; Volz *et al.*, 2005).

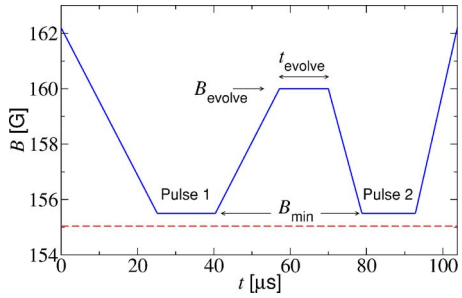

FIG. 24. (Color online) Typical magnetic-field pulse sequence (solid lines) used in experiments producing coherent oscillations between final atomic and molecular components in a ^{85}Rb Bose-Einstein condensate (Donley *et al.*, 2002). A pair of pulses with a minimum field strength $B_{min} = 155.5$ G is separated by an evolution period of variable duration t_{evolve} and field strength B_{evolve}. The zero-energy resonance position $B_0 \approx 155$ G is indicated by the dashed line.

V. ATOM-MOLECULE COHERENCE

Besides the production of Feshbach molecules via asymptotic linear sweeps across B_0, several approaches to date rely upon ramp sequences (Mark *et al.*, 2005; Yurovsky and Ben-Reuven, 2005) or resonant oscillating magnetic fields (Thompson *et al.*, 2005a). Such experimental techniques are designed to improve the efficiency of dimer formation in Bose gases mainly by avoiding the region of large scattering lengths and accordingly strong interatomic interactions. The associated nonlinear magnetic-field variations lead to dependences of the molecular population on properties of zero-energy resonances beyond those included in the Landau-Zener parameter.

A. Ramsey interferometry with atoms and molecules

Pulses starting and ending on the positive scattering length side of a zero-energy resonance (Claussen *et al.*, 2002) are of particular interest in this context. Their repeated application to a ^{85}Rb Bose-Einstein condensate gives rise to coherent oscillations between the final components of separated atoms and Feshbach molecules of Fig. 2 (Donley *et al.*, 2002; Claussen *et al.*, 2003).

1. Magnetic-field pulse sequence

A typical experimental pulse sequence (Donley *et al.*, 2002) is illustrated in Fig. 24. The associated magnetic-field strengths B are on the high-field side of the 155 G zero-energy resonance of ^{85}Rb where the scattering length is positive. Consequently, the interatomic potential supports a loosely bound dimer state whose energy as a function of B is shown in Fig. 12. Converting pairs of Bose-Einstein condensed atoms to Feshbach mol-

ecules in these experiments crucially depends on the intermediate order-of-magnitude variations of the scattering length $a(B)$ and, accordingly, of the dimer bond length $\langle r\rangle \approx a(B)/2$. The pulse sequence of Fig. 24 starts at the 162 G evaporation field strength at which a dilute ^{85}Rb Bose-Einstein condensate is usually produced (Cornish *et al.*, 2000) with a scattering length of about $200a_{\mathrm{Bohr}}$. Given the experimental mean interatomic distance of about $12\,000a_{\mathrm{Bohr}}$, the gas is initially therefore weakly interacting. Each pulse tunes the scattering length to $a(B_{\mathrm{min}}) \approx 9000a_{\mathrm{Bohr}}$ on time scales too short for the Bose-Einstein condensate to adjust its density. Consequently, at the magnetic-field strength B_{min} closest to the zero-energy resonance, the gas is driven into the regime of strong interatomic interactions. During the course of the experiments (Donley *et al.*, 2002; Claussen *et al.*, 2003), the stationary field B_{evolve} associated with the evolution period separating the pulses as well as the duration t_{evolve} were varied. The variation of B_{evolve} between 156 and 162 G corresponds to the range of Feshbach molecular binding energies displayed in the inset of Fig. 12 with associated scattering lengths between about $4000a_{\mathrm{Bohr}}$ and $200a_{\mathrm{Bohr}}$.

All measurements probing the densities of atoms were performed after each pulse sequence had terminated and therefore reflect the state of the weakly interacting gas with a final magnetic-field strength of about 162 G in Fig. 24. According to these observations, the fast magnetic-field variation gives rise to the three components of the atomic cloud illustrated in Fig. 2. The occupation numbers associated with the remnant Bose-Einstein condensate, burst component, and undetected atoms all oscillate with respect to each other as a function of the evolution time t_{evolve}. It turned out that their common angular frequency ω_e is accurately determined by the Feshbach molecular energy in the evolution period E_b^{evolve} via $\omega_e = |E_b^{\mathrm{evolve}}|/\hbar$. Donley *et al.* (2002) concluded that undetected atoms were transferred into Feshbach molecules whose fast phase evolution as compared to the atomic components leads to interference fringes in the final occupations.

In accordance with such an intuitive explanation, the first pulse provides overlap between the dimer size and the average distance between condensed atoms, which is crucial to molecular association. As this fast magnetic-field variation is not resonant with the binding energy, it inevitably leads to additional production of excited atom pairs which constitute a burst of atoms. During the evolution period, all components of the weakly interacting gas evolve independently and coherently and therefore accumulate a phase difference $\Delta\varphi = \omega_e t_{\mathrm{evolve}}$. Finally, the second pulse forces the Feshbach molecules and separated atoms to overlap once again and thereby probes $\Delta\varphi$ via an interference in their occupations. This intuitive scenario is analogous to a Ramsey interferometer using pairs of separated atoms and Feshbach molecules (Donley *et al.*, 2002; Zoller, 2002), as illustrated in Fig. 25.

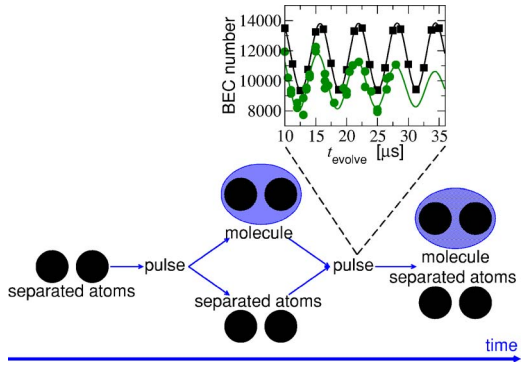

FIG. 25. (Color online) Schematic illustration of the Ramsey interferometry with ^{85}Rb atoms and Feshbach molecules associated with the magnetic-field pulse sequence of Fig. 24 (Donley *et al.*, 2002; Zoller, 2002). The first pulse drives the initial Bose-Einstein condensate into a coherent superposition of bound and unbound atom pairs. Between the pulses, the individual orthogonal components evolve independently. The second pulse forces the atomic and molecular states to overlap and thereby probes their phase difference. Inset: A typical interference fringe pattern at the end of the pulse sequence as a function of the evolution time t_{evolve}. Circles refer to measurements of the remnant Bose-Einstein condensate (Claussen *et al.*, 2003), while squares indicate theoretical predictions (Góral *et al.*, 2005).

2. Dynamics of a single atom pair

In analogy to Sec. IV.C, the observations of Fig. 2 can be qualitatively understood in terms of a single pair of atoms (Borca *et al.*, 2003; Góral *et al.*, 2005) in a periodic box of volume $\mathcal{V}$. To this end, the two-body time evolution operator of Eq. (98) associated with the magnetic-field variation of Fig. 24 may be split into its contributions of the first and second pulse as well as the evolution period. This yields

$$U_{2\mathrm{B}}(t_f,t_i) = U_2(t_f,t_2)U_{\mathrm{evolve}}(t_{\mathrm{evolve}})U_1(t_1,t_i). \tag{150}$$

Here the first pulse starts at the initial time t_i and terminates at t_1, while $t_2 = t_1 + t_{\mathrm{evolve}}$ indicates the beginning of the second pulse which ends at the final time of the sequence t_f. Accordingly, $U_1(t_1,t_i)$ and $U_2(t_f,t_2)$ describe the two-body dynamics during the first and second pulse, respectively. In between the pulses the magnetic-field strength is stationary, in accordance with Fig. 24. This implies that the associated time evolution operator $U_{\mathrm{evolve}}(t_{\mathrm{evolve}})$ depends just on the duration t_{evolve}. Its spectral decomposition in terms of dressed states of the relative motion of an atom pair exposed to the magnetic field of strength B_{evolve} is given by

$$U_{\mathrm{evolve}}(t_{\mathrm{evolve}}) = \sum_{v=-1}^{\infty} |\phi_v^{\mathrm{evolve}}\rangle e^{-iE_v^{\mathrm{evolve}}t_{\mathrm{evolve}}/\hbar} \times \langle \phi_v^{\mathrm{evolve}}|. \tag{151}$$

Here the index v labels the vibrational quantum numbers of the box states such that $|\phi_{-1}^{\mathrm{evolve}}\rangle$ correlates adiabatically, in the limit of infinite volume $\mathcal{V}$, with the Feshbach molecular dressed state $|\phi_b^{\mathrm{evolve}}\rangle$. Accordingly,

the associated vibrational energy levels are denoted by E_v^{evolve}, which implies the asymptotic behavior $E_{-1}^{\mathrm{evolve}} \sim E_{\mathrm{b}}^{\mathrm{evolve}}$ with increasing $\mathcal{V}$. The more tightly bound states associated with vibrational quantum numbers $v < -1$ contribute negligibly to the fringe pattern of Fig. 25 and are therefore omitted in Eq. (151).

Similarly to the treatment of Sec. IV.C, the interference fringes in the population of the remnant condensate component shown in the inset of Fig. 25 can be described in terms of the following transition probability:

$$p_{0,0} = |\langle \phi_0^f | U_{2\mathrm{B}}(t_f,t_i) | \phi_0^i \rangle|^2. \tag{152}$$

To this end, it is instructive to split the associated amplitude, in accordance with Eq. (151), into its contributions of the vibrational states with quantum numbers $v \geq 0$ and of the Feshbach molecule. This yields

$$\langle \phi_0^f | U_{2\mathrm{B}}(t_f,t_i) | \phi_0^i \rangle = D_{2\mathrm{B}} + A_{2\mathrm{B}}. \tag{153}$$

Due to the quasicontinuum of levels, the first term $D_{2\mathrm{B}}$ on the right-hand side of Eq. (153) tends to decay via phase diffusion as a function of t_{evolve}. Its explicit expression reads

$$D_{2\mathrm{B}} = \sum_{v=0}^{\infty} \langle \phi_0^f | U_2(t_f,t_2) | \phi_v^{\mathrm{evolve}} \rangle e^{-iE_v^{\mathrm{evolve}} t_{\mathrm{evolve}}/\hbar} \times \langle \phi_v^{\mathrm{evolve}} | U_1(t_1,t_i) | \phi_0^i \rangle. \tag{154}$$

The magnitude of the second term $A_{2\mathrm{B}}$ on the right-hand side of Eq. (153) depends on the product of the amplitudes for Feshbach molecular association during the first pulse and dissociation into the zero mode due to the second pulse. Its evolution as a function of t_{evolve} stems from the phase shift associated with the energy E_{-1}^{evolve}, in accordance with

$$A_{2\mathrm{B}} = \langle \phi_0^f | U_2(t_f,t_2) | \phi_{-1}^{\mathrm{evolve}} \rangle e^{-iE_{-1}^{\mathrm{evolve}} t_{\mathrm{evolve}}/\hbar} \times \langle \phi_{-1}^{\mathrm{evolve}} | U_1(t_1,t_i) | \phi_0^i \rangle. \tag{155}$$

The modulus squared of the sum of interfering amplitudes $D_{2\mathrm{B}}$ and $A_{2\mathrm{B}}$ therefore leads to the anticipated fringe pattern in its usual form,

$$p_{0,0} = |D_{2\mathrm{B}}|^2 + |A_{2\mathrm{B}}|^2 + 2|D_{2\mathrm{B}}||A_{2\mathrm{B}}| \sin(\omega_e t_{\mathrm{evolve}} + \varphi), \tag{156}$$

in agreement with Fig. 25. Here the angular frequency $\omega_e = |E_{-1}^{\mathrm{evolve}}|/\hbar$ is determined by the Feshbach molecular binding energy. The absolute phase φ is associated with both amplitudes $A_{2\mathrm{B}}$ and $D_{2\mathrm{B}}$ and depends sensitively on the exact shape of each pulse. A similar statement applies to the efficiency of dimer production and dissociation which are both crucial to the fringe visibility, according to Eqs. (155) and (156).

Populations of Feshbach molecules as well as the burst spectrum composed of excited dressed levels at the final magnetic-field strength may be inferred from the associated transition probabilities, similarly to Eq. (156). Their pairwise averages in a volume $\mathcal{V}$ in addition to a subsequent local-density approximation give a good account of the magnitudes of all gas components shown in Fig. 2 (Góral *et al.*, 2005). The range of validity of such a two-body estimate is set by the requirement that B_{evolve} is sufficiently far from B_0 that the mean distance between atoms is much larger than the scattering length during the evolution period. As the 155 G zero-energy resonance of ^{85}Rb is entrance-channel-dominated, the two-body dynamics is well described in terms of both the effective two- and single-channel approaches of Sec. III.G (Köhler, Gasenzer, and Burnett, 2003; Góral *et al.*, 2005). We note, however, that the contact pseudointeraction is insufficient. This is immediately apparent, for instance, from the inaccuracy of the universal estimate of the binding energy in the inset of Fig. 12, whose experimental data were determined using measured fringe frequencies (Claussen *et al.*, 2003). The interference experiments are therefore sensitive to the van der Waals tail of the interatomic potential, which is not accounted for in the Landau-Zener parameter associated with asymptotic linear magnetic-field sweeps.

B. Number of dimers produced in Bose and Fermi gases

Another significant difference in the descriptions of linear sweep and magnetic-field pulse techniques is associated with the Feshbach molecular state. The results of Sec. IV.A suggest that the number of dimers produced via asymptotic magnetic-field sweeps may be inferred from two-level approaches effectively identifying dressed Feshbach molecules with bare resonance states. For the Ramsey interference experiments (Donley *et al.*, 2002; Claussen *et al.*, 2003) operating just in the vicinity of the zero-energy resonance, a maximum final molecular conversion of about 16% was reported under the conditions referred to in Fig. 2. The closed-channel admixture to the dressed bound state, however, is approximately 25% at the final magnetic-field strength of 162 G (Köhler *et al.*, 2004) and even smaller throughout the pulse sequence (Braaten *et al.*, 2003; Köhler, Gasenzer, Julienne, and Burnett, 2003). In order to predict the observed number of dimers, it is therefore necessary to include the long-range nature of Feshbach molecules produced in the description of their detection.

An associated generic approach suitable for both magnetic-field sweeps and pulse sequences may be based on the following observable for the population of any diatomic state $|\phi_d\rangle$ in a gas consisting of N atoms (Köhler, Gasenzer, and Burnett, 2003):

$$\mathsf{N}_d = \frac{1}{2} \sum_{\substack{i,j=1 \\ i \neq j}}^{N} |\phi_{ij}^d\rangle\langle\phi_{ij}^d|. \tag{157}$$

Here the indices i and j label the atoms, $|\phi_{ij}^d\rangle$ refers to the two-body state $|\phi_d\rangle$ associated with the atoms i and j, and the factor of $1/2$ on the right-hand side of Eq. (157) prevents double counting of pairs. Given any state of the gas generally described by a density matrix $\rho_{N\mathrm{B}}$, the number of atomic pairs in the state $|\phi_d\rangle$ is consequently determined by the following expectation value:

$$N_d = \langle \mathsf{N}_d \rangle = \mathrm{Tr}(\mathsf{N}_d \rho_{\mathrm{NB}}). \tag{158}$$

Here the symbol Tr refers to the trace over the degrees of freedom of all atoms constituting the gas.

Many-body systems consisting of identical atoms are usually described using the approach of second quantization (Fetter and Walecka, 1971). Accordingly, any N-particle state is constructed by repeated application of creation operators to the vacuum $|\Omega\rangle$, which refers to the absence of atoms. The associated field operators $\psi_\alpha(\mathbf{x})$ and $\psi_\beta^\dagger(\mathbf{y})$ annihilating and creating single atoms at the positions $\mathbf{x}$ and $\mathbf{y}$, respectively, fulfill the following (anti)commutation relations:

$$\psi_\alpha(\mathbf{x})\psi_\beta^\dagger(\mathbf{y}) \mp \psi_\beta^\dagger(\mathbf{y})\psi_\alpha(\mathbf{x}) = \delta_{\alpha\beta}\delta(\mathbf{x}-\mathbf{y}). \tag{159}$$

Here the minus sign is associated with bosons while the plus sign refers to fermions, and the greek labels α and β indicate their Zeeman states. Given the diatomic wave function of the relative motion $\phi^d_{\alpha\beta}(\mathbf{r}) = \langle \mathbf{r};\alpha,\beta|\,\phi_d\rangle$, the second quantized representation of the number operator of Eq. (157) reads

$$\mathsf{N}_d = \frac{1}{2}\sum_{\alpha,\beta,\alpha',\beta'} \int d\mathbf{R} \int d\mathbf{r} \int d\mathbf{r}'\, \phi^d_{\alpha\beta}(\mathbf{r})[\phi^d_{\alpha'\beta'}(\mathbf{r}')]^* \times \psi_\alpha^\dagger(\mathbf{x})\psi_\beta^\dagger(\mathbf{y})\psi_{\beta'}(\mathbf{y}')\psi_{\alpha'}(\mathbf{x}'). \tag{160}$$

Here the single-particle coordinates are given in terms of the center of mass and relative positions by $\mathbf{x}=\mathbf{R}+\mathbf{r}/2$, $\mathbf{y}=\mathbf{R}-\mathbf{r}/2$, $\mathbf{x}'=\mathbf{R}+\mathbf{r}'/2$, and $\mathbf{y}'=\mathbf{R}-\mathbf{r}'/2$.

The approach of Eq. (160) was introduced in the context of simulations of the Ramsey fringes given in Fig. 2 (Köhler, Gasenzer, and Burnett, 2003; Köhler, Gasenzer, Julienne, and Burnett, 2003) and subsequently applied to the molecule production via magnetic-field sweeps in Bose (Góral *et al.*, 2004) and Fermi gases (Perali *et al.*, 2005). In accordance with Eq. (160), the expectation value of Eq. (158) depends on the two-body correlation function,

$$G^{(2)}_{\alpha'\beta',\alpha\beta}(\mathbf{x}',\mathbf{y}';\mathbf{x},\mathbf{y}) = \langle \psi_\alpha^\dagger(\mathbf{x})\psi_\beta^\dagger(\mathbf{y})\psi_{\beta'}(\mathbf{y}')\psi_{\alpha'}(\mathbf{x}')\rangle. \tag{161}$$

Here the average refers to the final state of the gas $\rho_{\mathrm{NB}}(t_f)$. In the context of the dimer production via fast magnetic-field sweeps of Sec. IV.C, for instance, the dynamics of $G^{(2)}$ is determined simply by the two-body evolution operator $U_{2\mathrm{B}}(t_f,t_i)$ in the limit of short interaction times. Given an ideal gas initial state $\rho_{\mathrm{NB}}(t_i)$ associated with either Bose or Fermi atoms, the exact form of the initial two-body correlation function can be inferred from Wick's theorem of statistical mechanics (Wick, 1950; Matsubara, 1955; Fetter and Walecka, 1971). In the single resonance approach, the diatomic channel wave functions of the Feshbach molecular state occurring in Eq. (160) are determined in terms of the entrance- and closed-channel components by

$$\sum_{\alpha,\beta} |\alpha,\beta\rangle \phi^b_{\alpha\beta}(\mathbf{r}) = |\mathrm{bg}\rangle \phi_b^{\mathrm{bg}}(\mathbf{r}) + |\mathrm{cl}\rangle \phi_b^{\mathrm{cl}}(\mathbf{r}). \tag{162}$$

Based on these assumptions, the number of Feshbach molecules predicted by Eq. (160) strictly confirms the fast sweep limits of Eqs. (144), (131), and (145), in particular, their coefficients associated with the identical nature of the atoms. Besides these statistical estimates, the general observable of Eq. (160) may be applied to a variety of dynamical magnetic-field variations as well as physical quantities. Given the associated two-body correlation function, it recovers, for instance, not only the measured maximum conversion into bound dimers of about 16% in Fig. 2 but also the populations of correlated pairs in continuum levels which constitute the burst of atoms (Köhler, Gasenzer, and Burnett, 2003). It turns out that due to the nonlinear magnetic-field variation of Fig. 24, the determination of the time dependence of $G^{(2)}$ requires a description via techniques beyond the two-level mean-field approach of Sec. IV.B.

C. Dynamics of partially condensed Bose gases

The precise many-body dynamics underlying all observations of Fig. 2 can be derived from the time-dependent Schrödinger equation determined by the general Hamiltonian (Fetter and Walecka, 1971),

$$H = \sum_\alpha \int d\mathbf{x}\,\psi_\alpha^\dagger(\mathbf{x})\left[-\frac{\hbar^2}{2m}\nabla^2 + E^a_\alpha + V^{\mathrm{ho}}_\alpha(\mathbf{x})\right]\psi_\alpha(\mathbf{x}) + H_{\mathrm{int}}. \tag{163}$$

Here E^a_α refers to an atomic Zeeman energy whose typical magnetic-field dependence is illustrated in Fig. 17 for the example of ^{87}Rb, and $V^{\mathrm{ho}}_\alpha(\mathbf{x})$ describes the harmonic confinement due to an atom trap. For dilute gases, interatomic interactions are predominantly pairwise which implies the following potential energy contribution:

$$H_{\mathrm{int}} = \frac{1}{2}\sum_{\alpha,\beta,\alpha',\beta'} \int d\mathbf{x} \int d\mathbf{y} V_{\alpha\beta,\alpha'\beta'}(\mathbf{x}-\mathbf{y}) \times \psi_\alpha^\dagger(\mathbf{x})\psi_\beta^\dagger(\mathbf{y})\psi_{\beta'}(\mathbf{y})\psi_{\alpha'}(\mathbf{x}). \tag{164}$$

Here $V_{\alpha\beta,\alpha'\beta'}(\mathbf{x}-\mathbf{y})$ denotes the two-body potential associated with the incoming and outgoing spin channels $|\alpha',\beta'\rangle$ and $|\alpha,\beta\rangle$, respectively. We note that Eqs. (163) and (164) are formulated sufficiently generally to treat interatomic interactions on a microscopic level, similarly to the coupled-channels theory of Sec. III.A. As a consequence, the atomic Zeeman levels E^a_α appear separately in Eq. (163), while in the two-body Hamiltonian of Eq. (16) the dissociation threshold energy associated with the closed channel is included in the potential $V_{\mathrm{cl}}(B,r)$. Accordingly, all interactions $V_{\alpha\beta,\alpha'\beta'}(\mathbf{x}-\mathbf{y})$ vanish in the limit of infinite distances $r=|\mathbf{x}-\mathbf{y}|\to\infty$, similarly to the interaction matrix $V_{\mathrm{int}}(r)$ of Eq. (11).

1. Beyond mean-field approaches

Several techniques were employed in treatments of the many-body dynamics of dilute gases beyond the Gross-Pitaevskii and two-level mean-field approaches of Sec. IV.B. These methods involve the Schwinger-Keldysh formalism (Schwinger, 1961; Keldysh, 1965) suitable for descriptions of phenomena associated with the evolution toward thermal equilibrium, such as the dimer production via adiabatic magnetic-field sweeps of Fig. 22 (Williams, Nikuni, *et al.*, 2004; Williams, Nygaard, and Clark, 2004, 2005). Practical approaches describing equilibration on even longer time scales, i.e., beyond the range of validity of the generalized Boltzmann equations derived from the Schwinger-Keldysh theory, may be based on the two-particle irreducible action (Luttinger and Ward, 1960; Baym, 1962; Cornwall *et al.*, 1974). For the dynamics of cold gases, such techniques have been implemented, to date, using the contact pseudointeraction in a single spatial dimension (Gasenzer *et al.*, 2005; Rey *et al.*, 2005). While the Ramsey fringes of Fig. 2 are sensitive to parameters of the interatomic potential besides the scattering length, the associated typical pulse sequence of Fig. 24 involves time scales sufficiently short for equilibration phenomena to be negligible. This implies that the gas dynamics is captured by extensions of mean-field theory, which account for the two-body time evolution beyond the Markov approximation (Proukakis *et al.*, 1998; Holland *et al.*, 2001; Köhler and Burnett, 2002; Naidon and Masnou-Seeuws, 2006).

The usual quantities of interest in these short-time quantum kinetic approaches may be expressed in terms of correlation functions, i.e., expectation values of normal ordered products of field operators, such as $G^{(2)}$ of Eq. (161). Their general expression reads $\langle\psi_\beta^\dagger(\mathbf{y})\cdots\psi_\alpha(\mathbf{x})\rangle_t$, where all creation operators appear to the left of all annihilation operators, and the average refers to the many-body state at time t. The number of field operators constituting the product shall be referred to as the order of the correlation function. Based on the Schrödinger equation, the associated dynamics is determined by

$$i\hbar\frac{\partial}{\partial t}\langle\psi_\beta^\dagger(\mathbf{y})\cdots\psi_\alpha(\mathbf{x})\rangle_t=\langle[\psi_\beta^\dagger(\mathbf{y})\cdots\psi_\alpha(\mathbf{x}),H]\rangle_t. \quad (165)$$

Here H is the Hamiltonian of Eq. (163), and the symbol $[A,B]=AB-BA$ indicates the commutator of the operators A and B. Due to the potential-energy contribution of Eq. (164), the commutator on the right-hand side of Eq. (165) gives rise to products containing two more field operators than the expectation value to the left. This implies that the dynamics of any one correlation function is determined by a coupled set of equations involving all the others. Approximate solutions to Eq. (165), therefore, often rely on schemes for the truncation of the associated infinite hierarchy of dynamical equations. The range of validity of such approaches is sensitive to the initial state of the many-body system.

For weakly interacting gases close to thermal equilibrium, an approximate form of all correlation functions may be determined using Wick's theorem of statistical mechanics (Wick, 1950; Matsubara, 1955; Fetter and Walecka, 1971). To this end, it is instructive to introduce the connected correlation functions (Weinberg, 1996), sometimes referred to as cumulants. These quantities may be inferred recursively from a decomposition of each correlation function into a sum of all possible products of cumulants which preserve the order of appearance of the operators. Given a set of Bose field operators A, B, and C, for instance, the first three cumulants, denoted by $\langle A\rangle^c$, $\langle BA\rangle^c$, and $\langle CBA\rangle^c$, are determined implicitly by

$$\langle A\rangle=\langle A\rangle^c, \quad (166)$$

$$\langle BA\rangle=\langle BA\rangle^c+\langle A\rangle^c\langle B\rangle^c, \quad (167)$$

$$\langle CBA\rangle=\langle CBA\rangle^c+\langle BA\rangle^c\langle C\rangle^c+\langle CA\rangle^c\langle B\rangle^c+\langle CB\rangle^c\langle A\rangle^c+\langle A\rangle^c\langle B\rangle^c\langle C\rangle^c. \quad (168)$$

The cumulants associated with Fermi field operators may be inferred from expressions similar to Eqs. (166)–(168). In accordance with the anticommutation relation of Eq. (159), however, the number of commutations of field operators in the decompositions needs to be accounted for by an appropriate sign of each contribution. In both cases, Bose and Fermi atoms, Wick's theorem reduces to the statement that all cumulants containing more than two field operators vanish provided that the gas is ideal and in thermal equilibrium. The magnitude of higher-order cumulants, therefore, provides a measure of the deviations of the state from the grand-canonical density matrix in the absence of interatomic interactions.

This suggests that for dilute, weakly interacting gases, a reasonable quantum kinetic approach may be based on the transformation of Eq. (165) into the associated set of dynamical equations for cumulants. In accordance with Wick's theorem, this coupled system allows for an approximate truncation at any order of correlation usually determined by external driving fields as well as the initial state (Fricke, 1996). The dilute gas of ^{85}Rb atoms in the Ramsey interferometry experiments illustrated in Fig. 25 was prepared as a Bose-Einstein condensate in the $(f=2, m_f=-2)$ Zeeman level. Such a coherent initial state gives rise to a mean field $\Psi_\alpha(\mathbf{x},t)=\langle\psi_\alpha(\mathbf{x})\rangle_t$ describing the density associated with the macroscopically occupied mode via its modulus squared (Dalfovo *et al.*, 1999). In accordance with Fig. 2, the condensate is depleted due to the near-resonant magnetic-field variation of Fig. 24. This implies that, in addition to the mean field, a minimum set of cumulants describing this experiment is given, respectively, by the pair function and the one-body density matrix of the noncondensed component,

$$\Phi_{\alpha\beta}(\mathbf{x},\mathbf{y},t)=\langle\psi_\beta(\mathbf{y})\psi_\alpha(\mathbf{x})\rangle_t-\Psi_\alpha(\mathbf{x},t)\Psi_\beta(\mathbf{y},t), \quad (169)$$

$$\Gamma_{\alpha\beta}(\mathbf{x},\mathbf{y},t)=\langle\psi_\beta^\dagger(\mathbf{y})\psi_\alpha(\mathbf{x})\rangle_t-\Psi_\alpha(\mathbf{x},t)\Psi_\beta^*(\mathbf{y},t). \quad (170)$$

Accordingly, at any time t the density of atoms in the Zeeman state with index α is given by $|\Psi_\alpha(\mathbf{x},t)|^2$

$+\Gamma_{\alpha\alpha}(\mathbf{x},\mathbf{x},t)$. Due to the weak interactions in the gas at the beginning of the magnetic-field pulse sequence, the second-order cumulants of Eqs. (169) and (170) are initially negligible i.e., $\Phi_{\alpha\beta}(\mathbf{x},\mathbf{y},t_i)=0=\Gamma_{\alpha\beta}(\mathbf{x},\mathbf{y},t_i)$.

To a first approximation, the dynamical equations (165) may be transformed and truncated such that they just include products of normal-ordered cumulants containing at most three field operators (Köhler and Burnett, 2002). This yields the following relation for the time derivative of the condensate mean field:

$$i\hbar\,\dot{\Psi}_\alpha(\mathbf{x},t)=H_\alpha^{1B}\Psi_\alpha(\mathbf{x},t)+\sum_{\alpha,\alpha',\beta'}\int d\mathbf{y}V_{\alpha\beta,\alpha'\beta'}(\mathbf{r})\times\Psi_\beta^*(\mathbf{y},t)\langle\psi_{\beta'}(\mathbf{y})\psi_{\alpha'}(\mathbf{x})\rangle_t. \quad (171)$$

Here $\mathbf{r}=\mathbf{x}-\mathbf{y}$ refers to the relative coordinates of a pair of atoms at the positions $\mathbf{x}$ and $\mathbf{y}$, and the one-body Hamiltonian H_α^{1B} consists of the kinetic and Zeeman energies as well as the trap potential of Eq. (163). The correlation function $\langle\psi_{\beta'}(\mathbf{y})\psi_{\alpha'}(\mathbf{x})\rangle_t$ on the right-hand side of Eq. (171) is determined in terms of cumulants by Eq. (169). In addition to Eq. (171), the dynamical equation associated with the pair function reads

$$i\hbar\,\dot{\Phi}_{\alpha\beta}(\mathbf{x},\mathbf{y},t)=\sum_{\alpha',\beta'}[H^{2B}_{\alpha\beta,\alpha'\beta'}\Phi_{\alpha'\beta'}(\mathbf{x},\mathbf{y},t)+V_{\alpha\beta,\alpha'\beta'}(\mathbf{r})\Psi_{\alpha'}(\mathbf{x},t)\Psi_{\beta'}(\mathbf{y},t)]. \quad (172)$$

Here $H^{2B}_{\alpha\beta,\alpha'\beta'}$ denotes the two-body Hamiltonian matrix associated with the incoming and outgoing spin channels $|\alpha',\beta'\rangle$ and $|\alpha,\beta\rangle$, respectively, describing both the center of mass and relative motions of an atom pair.

Given this first-order truncation scheme, Eqs. (171) and (172) determine the condensate mean field as well as the pair function. It turns out that the dynamical equation associated with the one-body density matrix of the noncondensed component may be solved implicitly in terms of the pair function. This yields

$$\Gamma_{\alpha\beta}(\mathbf{x},\mathbf{y},t)=\sum_\gamma\int d\mathbf{z}\Phi_{\alpha\gamma}(\mathbf{x},\mathbf{z},t)[\Phi_{\beta\gamma}(\mathbf{y},\mathbf{z},t)]^*. \quad (173)$$

In accordance with the general expression for the associated observable $\mathsf{N}=\Sigma_\alpha\int d\mathbf{x}\psi_\alpha^\dagger(\mathbf{x})\psi_\alpha(\mathbf{x})$, the expectation value of the number of atoms N is strictly conserved by Eqs. (171)–(173) at all times, i.e.,

$$\sum_\alpha\int d\mathbf{x}[|\Psi_\alpha(\mathbf{x},t)|^2+\Gamma_{\alpha\alpha}(\mathbf{x},\mathbf{x},t)]=N. \quad (174)$$

In addition, Eqs. (170) and (173) preserve the positivity of the one-body density matrix $\langle\psi_\beta^\dagger(\mathbf{y})\psi_\alpha(\mathbf{x})\rangle_t$, a consequence of the unitary time evolution, which is not necessarily recovered by higher-order approximation schemes.

In the context of dimer formation in partially condensed Bose gases, similar extensions of mean-field theory are based on the Hartree-Fock-Bogoliubov approach (Holland *et al.*, 2001) as well as the reduced pair wave-function approximation (Cherny and Shanenko, 2000; Naidon and Masnou-Seeuws, 2003,2006). Since these methods originate from Eq. (165), their short-time asymptotic limits agree with the exact result given by the perturbation expansion of the dynamical many-body Schrödinger equation. In addition, the correlation functions predicted with any of these approaches (Holland *et al.*, 2001; Köhler and Burnett, 2002; Naidon and Masnou-Seeuws, 2003, 2006) are free of secular long-time asymptotic behavior, a common artifact of perturbation theory associated with a spurious polynomial time dependence. Both the cumulant (Köhler and Burnett, 2002) and reduced pair wave-function approach (Naidon and Masnou-Seeuws, 2003, 2006) were formulated in such a way that they are compatible with the use of microscopic potentials beyond contact pseudo-interactions.

Most current implementations of quantum kinetic approaches to dimer production via Feshbach resonances are based on single-channel or two-channel single-resonance binary interactions illustrated in Sec. III.B. This implies that the Bose-Einstein condensate mode is described by a single mean field $\Psi(\mathbf{x},t)$ associated with the Zeeman level in which the gas is prepared. In addition, the entrance- and closed-channel components of the pair function may be inferred, similarly to Eq. (162), from

$$\sum_{\alpha,\beta}|\alpha,\beta\rangle\Phi_{\alpha\beta}(\mathbf{x},\mathbf{y},t)=|\mathrm{bg}\rangle\Phi_{\mathrm{bg}}(\mathbf{x},\mathbf{y},t)+|\mathrm{cl}\rangle\Phi_{\mathrm{cl}}(\mathbf{x},\mathbf{y},t). \quad (175)$$

The resonance mean field of Sec. IV.B is determined by $\Phi_{\mathrm{cl}}(\mathbf{x},\mathbf{y},t)=\Psi_{\mathrm{res}}(\mathbf{R},t)\phi_{\mathrm{res}}(r)$. Here $\mathbf{R}=(\mathbf{x}+\mathbf{y})/2$ refers to the center-of-mass coordinates of atom pairs and $r=|\mathbf{x}-\mathbf{y}|$ denotes their relative distance. Based on a two-channel implementation of Eqs. (171) and (172), the two-level mean-field approach (Drummond *et al.*, 1998; Tommasini *et al.*, 1998; Timmermans *et al.*, 1998, 1999a) may be recovered by formally solving the dynamical equation associated with the entrance-channel component of the pair function. A subsequent elimination of $\Phi_{\mathrm{bg}}(\mathbf{x},\mathbf{y},t)$ from the coupled equations (171) and (172) yields the functional form of the right-hand sides of Eqs. (136) and (137). The coupling constants of Eq. (134) and entrance-channel contact pseudo-interaction are determined by the Markov approximation (Góral *et al.*, 2004).

We note that truncation schemes of higher order than Eqs. (171) and (172) can involve cross-coupling terms that give rise to pair functions beyond the two-channel decomposition of Eq. (175). Such a scenario occurs in quantum kinetic approaches associated with both Bose and Fermi gases provided that one and the same atomic Zeeman state is shared between the two-body entrance and closed channels (Bruun *et al.*, 2005; Parish *et al.*, 2005). This, in turn, restricts the applicability of the current model Hamiltonians (Ranninger and Robaszkiewicz, 1985; Friedberg and Lee, 1989) which separate out the resonance state in descriptions of Feshbach molecule production.

2. Remnant Bose-Einstein condensate

The dynamics of the condensate mean field associated with Ramsey interferometry experiments (Donley *et al.*, 2002) was described using the Hartree-Fock-Bogoliubov method (Kokkelmans and Holland, 2002) and related techniques (Mackie, Suominen, and Javanainen, 2002), as well as the first-order cumulant approach of Eqs. (171) and (172) (Köhler, Gasenzer, and Burnett, 2003). Such studies involving beyond mean-field theories can often be simplified by eliminating the pair function from the set of dynamical or associated eigenvalue equations, respectively (Burnett, 1999). In the context of Eqs. (171) and (172), this procedure yields (Köhler and Burnett, 2002)

$$i\hbar\,\dot{\Psi}(\mathbf{x},t) = H_{1\mathrm{B}}\Psi(\mathbf{x},t) - \Psi^{*}(\mathbf{x},t)\int_{t_{\mathrm{i}}}^{\infty} dt'\,\Psi^{2}(\mathbf{x},t')\frac{\partial}{\partial t'}h(t,t'). \quad (176)$$

Here $H_{1\mathrm{B}}$ is the one-body Hamiltonian associated with the initial Zeeman state of condensed atoms. The coupling function on the right-hand side of Eq. (176),

$$h(t,t') = \theta(t-t')(2\pi\hbar)^{3}\langle 0,\mathrm{bg}|VU_{2\mathrm{B}}(t,t')|0,\mathrm{bg}\rangle, \quad (177)$$

is determined by the two-body time evolution operator given by Eq. (150). Here $\langle\mathbf{r}|0\rangle = 1/(2\pi\hbar)^{3/2}$ denotes the zero momentum plane wave of the relative motion of an atom pair and V is the microscopic potential matrix of Eq. (164).

The representation of Eqs. (176) and (177) shows that all findings of Sec. V.A about the two-body time evolution and physical origin of the Ramsey fringes are included in the quantum kinetic approach. Its degree of accuracy in comparison with experimental data of the condensate component remaining at the end of a magnetic-field pulse sequence (Claussen *et al.*, 2003) is illustrated in the inset of Fig. 25. The associated theory curve is based on an implementation of the two-channel single-resonance approach of Sec. III.G using a separable background scattering potential (Góral *et al.*, 2005).

3. Feshbach molecule and burst components

In accordance with Eq. (174), the total number of atoms can be decomposed into a mean-field contribution as well as a noncondensed component $N_{\mathrm{nc}}(t)$ described by the density matrix of Eq. (170). The physical significance of $N_{\mathrm{nc}}(t)$ in the Ramsey interferometry experiments (Donley *et al.*, 2002) may be inferred from Eq. (173). To this end, it is instructive to replace the spatial average of Eq. (173) using the completeness of the set of dressed bound and continuum energy states associated with the magnetic-field strength at time t. This leads to

$$N_{\mathrm{nc}}(t) = \int d\mathbf{R}\left[\int d\mathbf{p}|\langle\mathbf{R},\phi_{\mathbf{p}}|\Phi(t)\rangle|^{2} + |\langle\mathbf{R},\phi_{b}|\Phi(t)\rangle|^{2}\right]. \quad (178)$$

Here $\mathbf{R}$ may be interpreted in terms of the center-of-mass position of an atom pair and $|\Phi(t)\rangle$ refers to the pair function whose channel components in the spatial representation are given by Eq. (169). For simplicity, the spectral decomposition of Eq. (178) includes just the dressed continuum states $|\phi_{\mathbf{p}}\rangle$ and the Feshbach molecular state $|\phi_{b}\rangle$. More deeply bound levels are neglected.

Equation (178) suggests that the continuum contribution may be interpreted in terms of correlated atom pairs associated with relative momenta $\mathbf{p}$, while the bound-state part yields the number of atoms converted into dimers. An analysis based on the observable given by Eq. (160) confirms this view (Köhler, Gasenzer, and Burnett, 2003). Its practical implementation based on Eqs. (171) and (172) involves a cumulant expansion of the two-body correlation function in accordance with the first-order truncation scheme. This yields

$$G^{(2)}_{\alpha'\beta',\alpha\beta}(\mathbf{x}',\mathbf{y}';\mathbf{x},\mathbf{y};t) = \langle\psi^{\dagger}_{\alpha}(\mathbf{x})\psi^{\dagger}_{\beta}(\mathbf{y})\rangle_{t} \times\langle\psi_{\beta'}(\mathbf{y}')\psi_{\alpha'}(\mathbf{x}')\rangle_{t}. \quad (179)$$

Here the correlation functions on the right-hand side can be expressed in terms of pair functions and condensate mean fields via Eq. (169). Using Eqs. (162) and (179), it turns out that the diatomic number operator given by Eq. (160) gives rise to a dimer mean field,

$$\Psi_{b}(\mathbf{R},t) = \frac{1}{\sqrt{2}}\left\{\langle\mathbf{R},\phi_{b}|\Phi(t)\rangle + \int d\mathbf{r}[\phi_{b}^{\mathrm{bg}}(\mathbf{r})]^{*}\Psi(\mathbf{x},t)\Psi(\mathbf{y},t)\right\}, \quad (180)$$

which determines the number of Feshbach molecules produced via $N_{d}(t) = \int d\mathbf{R}\,|\Psi_{b}(\mathbf{R},t)|^{2}$.

The first term on the right-hand side of Eq. (180) recovers the bound-state contribution given by Eq. (178). In accordance with the long-range $^{85}Rb_{2}$ entrance-channel wave functions of Fig. 11, the second term may be interpreted in terms of the overlap between dimers produced and the surrounding gas. Its magnitude is determined by the dilute gas parameter squared $n_{c}(t)a^{3}$, where $n_{c}(t)$ is the average condensate density and a is the scattering length associated with the magnetic-field strength at time t (Köhler, Gasenzer, Julienne, and Burnett, 2003). Consequently, the existence of this overlap term reflects the breakdown of the concept of diatomic molecules in the environment of a strongly interacting gas. This breakdown occurs when the bond length $\langle r\rangle = a/2$ of the universal dimer wave function given by Eq. (2) is comparable to the mean interatomic distance $n_{c}^{-1/3}$ of the condensate. Similar phenomena are visible in Figs. 13–15.

At the end of the magnetic-field pulse sequence of Fig. 24, the gas is weakly interacting and the second, overlap term on the right-hand side of Eq. (180) is negligible. Based on Eqs. (176) and (180), the predicted number of atoms converted into dimers recovers the 16% maximum fraction of missing atoms in Fig. 2 as well as its modulation as a function of t_{evolve} (Köhler, Gasenzer, and Burnett, 2003). In accordance with Fig. 15, the

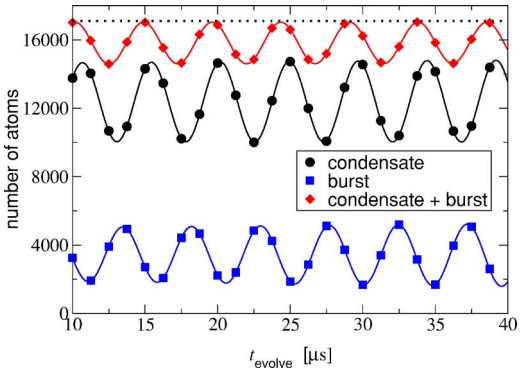

FIG. 26. (Color online) Predicted Ramsey fringes between three components of a dilute gas of ^{85}Rb (Góral *et al.*, 2005) at the end of the magnetic-field pulse sequence of Fig. 24 vs the evolution time t_{evolve}. Circles are the remnant Bose-Einstein condensate, while squares indicate the final population of correlated atom pairs constituting the burst component. The remnant condensate and burst add up to the number of detectable atoms (diamonds). Its difference to the total number of $N=17\,100$ atoms (dotted line) in the experiments (Donley *et al.*, 2002) determines the population of Feshbach molecules. The magnetic-field strength in the evolution period of $B_{evolve}=159.84$ G associated with these predictions refers to the conditions of the measured fringes of Fig. 2.

fact that these Feshbach molecules were not detected reflects their lifetime with respect to spin relaxation on the order of only 100 μs at the final 162 G magnetic-field strength (Köhler *et al.*, 2005; Thompson *et al.*, 2005b). An analysis based on Eqs. (160) and (179) also shows that the continuum contribution on the right-hand side of Eq. (178) is associated with correlated atom pairs that constitute the measured burst component in Fig. 2 (Köhler, Gasenzer, and Burnett, 2003).

4. Three-component Ramsey fringes

The physical origin of the Ramsey fringes (Donley *et al.*, 2002) was the subject of several theoretical works (Kokkelmans and Holland, 2002; Mackie, Suominen, and Javanainen, 2002; Köhler, Gasenzer, and Burnett, 2003; Góral *et al.*, 2005) using different beyond mean-field approaches. Figure 26 shows such a prediction (Góral *et al.*, 2005) referring to the magnetic-field pulse sequence and number of atoms reported for the measurements of Fig. 2. The overall picture indicates that the quantum kinetic approaches support the interpretation of Sec. V.A, provided that the gas is weakly interacting during the evolution period.

Some measurements were also performed in the regime of near-resonant evolution fields, $B_{evolve}<157$ G. Under these conditions, the scattering length as well as the spatial extent of the Feshbach molecule are comparable to the mean interatomic distance of the gas. As the atomic and dimer components are no longer orthogonal during the evolution period, the classic concept of a Ramsey interferometer is expected to break down when B_{evolve} approaches B_0 (Góral *et al.*, 2005). Such a phenomenon was observed in terms of a pronounced damping of the fringe pattern accompanied by an upward shift of its frequency with respect to the two-body prediction of $|E_b^{evolve}|/h$ (Claussen *et al.*, 2003). This shift was subsequently attributed to genuinely many-particle corrections to the intuitive viewpoint illustrated in Fig. 25 (Duine and Stoof, 2003b; Góral *et al.*, 2005).

VI. CONCLUSIONS AND OUTLOOK

This article has given an overview of a variety of concepts associated with the description of the properties of Feshbach molecules as well as techniques for their production in the environment of a cold atomic gas. The conclusions can be summarized as follows: Coupled-channels theory provides the foundation for an accurate understanding of the diatomic molecular and collision physics. Its predictions can be recovered, in an experimentally relevant energy range near the dissociation threshold, with two-channel approaches characterized in terms of just a few measurable quantities. These involve the resonance position and width, the background scattering length, and the van der Waals dispersion coefficient, as well as the difference in magnetic moments associated with the resonance state and a pair of asymptotically separated atoms. Universal properties of Feshbach molecules and the low-energy collision physics are directly related to Wigner's threshold law. Such concepts associated with two-body physics treat identical bosons and fermions in different Zeeman states as well as distinguishable atoms in essentially the same manner. The fundamental transition amplitudes for Feshbach molecular association of an atom pair via linear magnetic-field sweeps can be represented analytically in the context of two-channel single-resonance approaches. Such an exact treatment provides the foundation of the Landau-Zener approach to dimer production in tight traps, such as optical lattice sites, as well as in cold gases in the fast sweep limit. While these limits including their quantum statistical phenomena can be understood largely in terms of classical probability theory, the saturation of molecule production involves the many-body dynamics of thermalization. Given sufficiently short time scales, beyond mean-field approaches can provide quantitative descriptions of Feshbach molecule production in Bose-Einstein condensates also in the context of nonlinear magnetic-field variations.

Closely related to the enhancement of the s-wave scattering cross sections discussed in this review are similar magnetically tunable Feshbach resonance phenomena involving finite angular momentum quantum numbers, $\ell>0$. Associated scattering amplitudes $f_\ell(p)$ are usually negligible compared to the s-wave contribution in cold collision physics due to their $p^{2\ell}$ scaling with the relative momentum of an atom pair. In gases of identical Fermi atoms involving a single Zeeman state, however, only odd partial waves contribute to diatomic scattering in accordance with the Pauli exclusion principle. In such cases, p-wave ($\ell=1$) resonances have been observed in both ^{40}K (Regal *et al.*, 2003b) and ^{6}Li gases

(Zhang *et al.*, 2004; Schunck *et al.*, 2005), providing possibilities of magnetically tuning interactions as well as associating dimers.

Optical Feshbach resonances (Fedichev *et al.*, 1996; Bohn and Julienne, 1997, 1999) provide an alternative approach to tune *s*-wave scattering cross sections in cold gases. This technique relies on coupling the internal states of separated atom pairs to a closed channel using laser light instead of a homogeneous magnetic field. According to experimental studies in cold gases of ^{23}Na (Fatemi *et al.*, 2000) and ^{87}Rb Bose-Einstein condensates (Theis *et al.*, 2004), significant changes to the scattering length tend to cause substantial atom loss due to spontaneous photon emission. Recent predictions indicate, however, that such loss may be suppressed in applications to cold gases of alkaline earth metal atoms, such as bosonic calcium, as well as ytterbium (Ciurylo *et al.*, 2005). As these atoms lack hyperfine structure due to the absence of nuclear spin, magnetic Feshbach resonances are ruled out. Their optical counterpart may therefore provide the only possibility of tuning interactions in such gases.

Interspecies magnetic Feshbach resonances were observed in boson-fermion mixtures consisting of cold ^{6}Li and ^{23}Na (Stan *et al.*, 2004) as well as ^{40}K and ^{87}Rb gases (Inouye *et al.*, 2004). Their binary physics can be described using the approaches outlined in this review, whereas the collisional stability of interspecies Feshbach molecules requires special attention (Petrov *et al.*, 2005a). Producing such diatomic molecules is of particular interest because of a possible polar character of their bonds (Doyle *et al.*, 2004). Cold polar molecules composed of Bose atoms have been produced via photoassociation (Kerman *et al.*, 2004; Wang *et al.*, 2004). According to predictions (Baranov *et al.*, 2002), the long range, anisotropy, and magnitude of dipole-dipole interactions give rise to a host of new features in the associated fermionic and bosonic superfluids. Arrays of polar molecules in optical lattices may provide an opportunity to study supersolid phases (Góral *et al.*, 2002). It is hoped that heavy polar molecules will enable us to improve tests of fundamental physical symmetries, including measurements of the electron dipole moment (Sandars, 1975; Hudson *et al.*, 2002). Stabilization with respect to collisional relaxation of excited molecular states may be achieved via transfer to their vibrational ground states, an approach also demonstrated in the context of photoassociation (Sage *et al.*, 2005). Such deexcitation, in turn, tends to enhance the polar character of their bonds.

Few-body scattering phenomena, such as dimer-dimer resonances recently observed in cold gases of $^{133}Cs_2$ (Chin *et al.*, 2005), may provide possibilities of extending existing techniques of Feshbach molecule production to more complex species. One of the long-standing goals is an experimental confirmation of predictions associated with Efimov's effect in the three-body energy spectrum of identical Bose particles (Efimov, 1970, 1971). The Efimov spectrum consists of an infinite sequence of isotropic three-body bound states accumulating at the dissociation threshold, which occurs in the limit of infinite *s*-wave scattering length of each two-body subsystem. This scenario is therefore directly related to the long-range nature of weakly bound two-particle halo states (Jensen *et al.*, 2004) and may be realized via magnetic Feshbach resonances in cold gases. Signatures of the emergence of such Efimov states are predicted to occur in terms of a modulation of three-body recombination loss rates as a function of the near-resonant magnetic-field strength (Esry *et al.*, 1999; Nielsen and Macek, 1999; Braaten and Hammer, 2001). Recently, the first experimental evidence for this phenomenon was reported (Kraemer *et al.*, 2006). Such inelastic-scattering resonances may be exploited to associate metastable three-body Efimov molecules from cold Bose gases loaded into optical lattices, using the magnetic-field sweep technique discussed in this review (Stoll and Köhler, 2005).

ACKNOWLEDGMENTS

We are grateful to Johannes Hecker Denschlag, Stephan Dürr, Rudi Grimm, Tom Hanna, Eleanor Hodby, Randy Hulet, Debbie Jin, Wolfgang Ketterle, Servaas Kokkelmans, Tobias Kraemer, Takashi Mukaiyama, Christoph Nägerl, Nicolai Nygaard, Cindy Regal, Gregor Thalhammer, Sarah Thompson, Boudewijn Verhaar, Carl Wieman, Jamie Williams, and Kaiwen Xu for providing their experimental and theoretical data to us. We thank Keith Burnett, Cheng Chin, Thomas Gasenzer, Josh Milstein, Bill Stwalley, Marzena Szymańska, and Eite Tiesinga for valuable discussions. This review was supported by the Royal Society (T.K. and K.G.). P.S.J. gratefully acknowledges support from the Office of Naval Research.

REFERENCES

Abraham, E. R. I., W. I. McAlexander, J. M. Gerton, R. G. Hulet, R. Côté, and A. Dalgarno, 1997, Phys. Rev. A **55**, R3299.

Anderson, M. H., J. R. Ensher, M. R. Matthews, C. E. Wieman, and E. A. Cornell, 1995, Science **269**, 5221.

Arimondo, E., M. Inguscio, and P. Violino, 1977, Rev. Mod. Phys. **49**, 31.

Balakrishnan, N., R. C. Forrey, and A. Dalgarno, 1997, Chem. Phys. Lett. **280**, 1.

Baranov, M., L. Dobrek, K. Góral, L. Santos, and M. Lewenstein, 2002, Phys. Scr., T **102**, 74.

Bartenstein, M., A. Altmeyer, S. Riedl, R. Geursen, S. Jochim, C. Chin, J. H. Denschlag, R. Grimm, A. Simoni, E. Tiesinga, C. J. Williams, and P. S. Julienne, 2005, Phys. Rev. Lett. **94**, 103201.

Bartenstein, M., A. Altmeyer, S. Riedl, S. Jochim, C. Chin, J. H. Denschlag, and R. Grimm, 2004, Phys. Rev. Lett. **92**, 120401.

Baym, G., 1962, Phys. Rev. **127**, 1391.

Bender, P. L., 1963, Phys. Rev. **132**, 2154.

Bethe, H. A., 1949, Phys. Rev. **76**, 38.

Blatt, J. M., and V. F. Weisskopf, 1952, *Theoretical Nuclear Physics* (Wiley, New York).
Bloch, F., 1928, Z. Phys. **52**, 555.
Blume, D., and C. H. Greene, 2002, Phys. Rev. A **65**, 043613.
Bohn, J. L., and P. S. Julienne, 1997, Phys. Rev. A **56**, 1486.
Bohn, J. L., and P. S. Julienne, 1999, Phys. Rev. A **60**, 414.
Bolda, E. L., E. Tiesinga, and P. S. Julienne, 2002, Phys. Rev. A **66**, 013403.
Borca, B., D. Blume, and C. H. Greene, 2003, New J. Phys. **5**, 111.
Bose, S. N., 1924, Z. Phys. **26**, 178.
Bourdel, T., L. Khaykovich, J. Cubizolles, J. Zhang, F. Chevy, M. Teichmann, L. Tarruell, S. J. J. M. F. Kokkelmans, and C. Salomon, 2004, Phys. Rev. Lett. **93**, 050401.
Braaten, E., and H.-W. Hammer, 2001, Phys. Rev. Lett. **87**, 160407.
Braaten, E., H.-W. Hammer, and M. Kusunoki, 2003, e-print cond-mat/0301489.
Bradley, C. C., C. A. Sackett, and R. G. Hulet, 1997, Phys. Rev. Lett. **78**, 985.
Bradley, C. C., C. A. Sackett, J. J. Tollett, and R. G. Hulet, 1995, Phys. Rev. Lett. **75**, 1687.
Bransden, B. H., and C. J. Joachain, 2003, *Physics of Atoms and Molecules* (Pearson Education, Harlow).
Breit, G., and I. I. Rabi, 1931, Phys. Rev. **38**, 2082.
Brouard, S., and J. Plata, 2005, Phys. Rev. A **72**, 023620.
Bruun, G. M., A. D. Jackson, and E. E. Kolomeitsev, 2005, Phys. Rev. A **71**, 052713.
Bruun, G. M., and C. J. Pethick, 2004, Phys. Rev. Lett. **92**, 140404.
Burke, J. P., C. H. Greene, and J. L. Bohn, 1998, Phys. Rev. Lett. **81**, 3355.
Burnett, K., 1999, in *Bose-Einstein Condensation in Atomic Gases*, edited by M. Inguscio, S. Stringari, and C. E. Wieman, International School of Physics Enrico Fermi (IOS, Amsterdam), p. 265.
Burt, E. A., R. W. Ghrist, C. J. Myatt, M. J. Holland, E. A. Cornell, and C. E. Wieman, 1997, Phys. Rev. Lett. **79**, 337.
Busch, T., B.-G. Englert, K. Rzążewski, and M. Wilkens, 1998, Found. Phys. **28**, 549.
Cherny, A. Y., and A. A. Shanenko, 2000, Phys. Rev. E **62**, 1646.
Child, M. S., 1974, *Molecular Collision Theory* (Academic, London).
Chin, C., 2005, e-print cond-mat/0506313.
Chin, C., M. Bartenstein, A. Altmeyer, S. Riedl, S. Jochim, J. H. Denschlag, and R. Grimm, 2004, Science **305**, 1128.
Chin, C., and R. Grimm, 2004, Phys. Rev. A **69**, 033612.
Chin, C., A. J. Kerman, V. Vuletic, and S. Chu, 2003, Phys. Rev. Lett. **90**, 033201.
Chin, C., T. Kraemer, M. Mark, J. Herbig, P. Waldburger, H.-C. Nägerl, and R. Grimm, 2005, Phys. Rev. Lett. **94**, 123201.
Chin, C., V. Vuletic, A. J. Kerman, S. Chu, E. Tiesinga, P. J. Leo, and P. S. Julienne, 2004, Phys. Rev. A **70**, 032701.
Chwedeńczuk, J., K. Góral, T. Köhler, and P. S. Julienne, 2004, Phys. Rev. Lett. **93**, 260403.
Ciurylo, R., E. Tiesinga, and P. S. Julienne, 2005, Phys. Rev. A **71**, 030701(R).
Claussen, N. R., E. A. Donley, S. T. Thompson, and C. E. Wieman, 2002, Phys. Rev. Lett. **89**, 010401.
Claussen, N. R., S. J. J. M. F. Kokkelmans, S. T. Thompson, E. A. Donley, E. Hodby, and C. E. Wieman, 2003, Phys. Rev. A **67**, 060701(R).
Cornish, S. L., N. R. Claussen, J. L. Roberts, E. A. Cornell, and C. E. Wieman, 2000, Phys. Rev. Lett. **85**, 1795.
Cornwall, J. M., R. Jackiw, and E. Tomboulis, 1974, Phys. Rev. D **10**, 2428.
Courteille, P., R. S. Freeland, D. J. Heinzen, F. A. van Abeelen, and B. J. Verhaar, 1998, Phys. Rev. Lett. **81**, 69.
Cubizolles, J., T. Bourdel, S. J. J. M. F. Kokkelmans, G. V. Shlyapnikov, and C. Salomon, 2003, Phys. Rev. Lett. **91**, 240401.
Cvitas, M. T., P. Soldán, J. M. Hutson, P. Honvault, and J.-M. Launay, 2002, Phys. Rev. Lett. **89**, 153201.
Cvitas, M. T., P. Soldán, J. M. Hutson, P. Honvault, and J.-M. Launay, 2005a, Phys. Rev. Lett. **94**, 200402.
Cvitas, M. T., P. Soldán, J. M. Hutson, P. Honvault, and J.-M. Launay, 2005b, Phys. Rev. Lett. **94**, 033201.
Dalfovo, F., S. Giorgini, L. P. Pitaevskii, and S. Stringari, 1999, Rev. Mod. Phys. **71**, 463.
Dalgarno, A., and M. R. H. Rudge, 1965, Proc. R. Soc. London, Ser. A **286**, 519.
Dalibard, J., 1999, in *Bose-Einstein Condensation in Atomic Gases*, edited by M. Inguscio, S. Stringari, and C. E. Wieman, International School of Physics Enrico Fermi (IOS, Amsterdam), p. 463.
Davis, K. B., M.-O. Mewes, M. R. Andrews, N. J. van Druten, D. S. Durfee, D. M. Kurn, and W. Ketterle, 1995, Phys. Rev. Lett. **75**, 3969.
Demkov, Y. N., and V. I. Osherov, 1968, Sov. Phys. JETP **26**, 916.
Derevianko, A., W. R. Johnson, M. S. Safronova, and J. F. Babb, 1999, Phys. Rev. Lett. **82**, 3589.
Donley, E. A., N. R. Claussen, S. L. Cornish, J. L. Roberts, E. A. Cornell, and C. E. Wieman, 2001, Nature (London) **412**, 295.
Donley, E. A., N. R. Claussen, S. T. Thompson, and C. E. Wieman, 2002, Nature (London) **417**, 529.
Doyle, J., B. Friedrich, R. V. Krems, and F. Masnou-Seeuws, 2004, Eur. Phys. J. D **31**, 149.
Drummond, P. D., and K. V. Kheruntsyan, 2004, Phys. Rev. A **70**, 033609.
Drummond, P. D., K. V. Kheruntsyan, and H. He, 1998, Phys. Rev. Lett. **81**, 3055.
Duine, R. A., and H. T. C. Stoof, 2003a, Phys. Rev. A **68**, 013602.
Duine, R. A., and H. T. C. Stoof, 2003b, Phys. Rev. Lett. **91**, 150405.
Duine, R. A., and H. T. C. Stoof, 2004, Phys. Rep. **396**, 115.
Dürr, S., T. Volz, A. Marte, and G. Rempe, 2004, Phys. Rev. Lett. **92**, 020406.
Dürr, S., T. Volz, and G. Rempe, 2004, Phys. Rev. A **70**, 031601(R).
Dürr, S., T. Volz, N. Syassen, G. Rempe, E. van Kempen, S. Kokkelmans, B. Verhaar, and H. Friedrich, 2005, Phys. Rev. A **72**, 052707.
Eagles, D. M., 1969, Phys. Rev. **186**, 456.
Eckart, C., 1930, Rev. Mod. Phys. **2**, 305.
Efimov, V., 1970, Phys. Lett. **33**, B563.
Efimov, V. N., 1971, Sov. J. Nucl. Phys. **12**, 589.
Einstein, A., 1924, Sitzungsber. Preuss. Akad. Wiss., Phys. Math. Kl. **22**, 261.
Einstein, A., 1925, Sitzungsber. Preuss. Akad. Wiss., Phys. Math. Kl. **1**, 3.
Esry, B. D., C. H. Greene, and J. P. Burke, 1999, Phys. Rev.

Lett. **83**, 1751.
Fano, U., 1935, Nuovo Cimento **12**, 154, translation edited by G. Pupillo, A. Zannoni, and C. W. Clark, e-print cond-mat/0502210.
Fano, U., 1961, Phys. Rev. **124**, 1866.
Fatemi, F. K., K. M. Jones, and P. D. Lett, 2000, Phys. Rev. Lett. **85**, 4462.
Fedichev, P. O., Y. Kagan, G. V. Shlyapnikov, and J. T. M. Walraven, 1996, Phys. Rev. Lett. **77**, 2913.
Feshbach, H., 1958, Ann. Phys. (N.Y.) **5**, 357.
Feshbach, H., 1962, Ann. Phys. (N.Y.) **19**, 287.
Fetter, A. L., and J. D. Walecka, 1971, *Quantum Theory of Many-Particle Systems* (McGraw-Hill, New York).
Fioretti, A., D. Comparat, A. Crubellier, O. Dulieu, F. Masnou-Seeuws, and P. Pillet, 1998, Phys. Rev. Lett. **80**, 4402.
Flambaum, V. V., G. F. Gribakin, and C. Harabati, 1999, Phys. Rev. A **59**, 1998.
Folman, R., P. Krüger, J. Schmiedmayer, J. Denschlag, and C. Henkel, 2002, Adv. At., Mol., Opt. Phys. **48**, 263.
Fricke, J., 1996, Ann. Phys. (N.Y.) **252**, 479.
Friedberg, R., and T. D. Lee, 1989, Phys. Rev. B **40**, 6745.
Gao, B., 1996, Phys. Rev. A **54**, 2022.
Gao, B., 1998a, Phys. Rev. A **58**, 4222.
Gao, B., 1998b, Phys. Rev. A **58**, 1728.
Gao, B., 2004, J. Phys. B **37**, 4237.
Gao, B., E. Tiesinga, C. J. Williams, and P. S. Julienne, 2005, Phys. Rev. A **72**, 042719.
Gasenzer, T., J. Berges, M. G. Schmidt, and M. Seco, 2005, Phys. Rev. A **72**, 063604.
Góral, K., M. Gajda, and K. Rzażewski, 2001, Phys. Rev. Lett. **86**, 1397.
Góral, K., T. Köhler, and K. Burnett, 2005, Phys. Rev. A **71**, 023603.
Góral, K., T. Köhler, S. A. Gardiner, E. Tiesinga, and P. S. Julienne, 2004, J. Phys. B **37**, 3457.
Góral, K., L. Santos, and M. Lewenstein, 2002, Phys. Rev. Lett. **88**, 170406.
Greiner, M., C. A. Regal, and D. S. Jin, 2003, Nature (London) **426**, 537.
Gribakin, G. F., and V. V. Flambaum, 1993, Phys. Rev. A **48**, 546.
Grisenti, R. E., W. Schöllkopf, J. P. Toennies, G. C. Hegerfeldt, T. Köhler, and M. Stoll, 2000, Phys. Rev. Lett. **85**, 2284.
Gross, E. P., 1961, Nuovo Cimento **20**, 454.
Haque, M., and H. T. C. Stoof, 2005, Phys. Rev. A **71**, 063603.
Herbig, J., T. Kraemer, M. Mark, T. Weber, C. Chin, H.-C. Nägerl, and R. Grimm, 2003, Science **301**, 1510.
Hinds, E. A., C. J. Vale, and M. G. Boshier, 2001, Phys. Rev. Lett. **86**, 1462.
Hodby, E., S. T. Thompson, C. A. Regal, M. Greiner, A. C. Wilson, D. S. Jin, E. A. Cornell, and C. E. Wieman, 2005, Phys. Rev. Lett. **94**, 120402.
Holland, M., J. Park, and R. Walser, 2001, Phys. Rev. Lett. **86**, 1915.
Houbiers, M., H. T. C. Stoof, W. I. McAlexander, and R. G. Hulet, 1998, Phys. Rev. A **57**, R1497.
Hudson, J. J., B. E. Sauer, M. R. Tarbutt, and E. A. Hinds, 2002, Phys. Rev. Lett. **89**, 023003.
Inouye, S., M. R. Andrews, J. Stenger, H.-J. Miesner, D. M. Stamper-Kurn, and W. Ketterle, 1998, Nature (London) **392**, 151.
Inouye, S., J. Goldwin, M. L. Olsen, C. Ticknor, J. L. Bohn, and D. S. Jin, 2004, Phys. Rev. Lett. **93**, 183201.
Ishkhanyan, A., M. Mackie, A. Carmichael, P. L. Gould, and J. Javanainen, 2004, Phys. Rev. A **69**, 043612.
Jaksch, D., V. Venturi, J. I. Cirac, C. J. Williams, and P. Zoller, 2002, Phys. Rev. Lett. **89**, 040402.
Javanainen, J., M. Kostrun, Y. Zheng, A. Carmichael, U. Shrestha, P. J. Meinel, M. Mackie, O. Dannenberg, and K.-A. Suominen, 2004, Phys. Rev. Lett. **92**, 200402.
Jensen, A. S., K. Riisager, D. V. Fedorov, and E. Garrido, 2004, Rev. Mod. Phys. **76**, 215.
Jochim, S., M. Bartenstein, A. Altmeyer, G. Hendl, C. Chin, J. H. Denschlag, and R. Grimm, 2003a, Phys. Rev. Lett. **91**, 240402.
Jochim, S., M. Bartenstein, A. Altmeyer, G. Hendl, S. Riedl, C. Chin, J. H. Denschlag, and R. Grimm, 2003b, Science **302**, 2101.
Julienne, P. S., and F. H. Mies, 1989, J. Opt. Soc. Am. B **6**, 2257.
Julienne, P. S., E. Tiesinga, and T. Köhler, 2004, J. Mod. Opt. **51**, 1787.
Kagan, Y., B. V. Svistunov, and G. V. Shlyapnikov, 1985, JETP Lett. **42**, 209.
Keldysh, L. V., 1965, Sov. Phys. JETP **20**, 1018.
Kerman, A. J., J. M. Sage, S. Sainis, T. Bergeman, and D. DeMille, 2004, Phys. Rev. Lett. **92**, 033004.
Kharchenko, P., J. F. Babb, and A. Dalgarno, 1997, Phys. Rev. A **55**, 3566.
Kinast, J., S. L. Hemmer, M. E. Gehm, A. Turlapov, and J. E. Thomas, 2004, Phys. Rev. Lett. **92**, 150402.
Köhler, T., and K. Burnett, 2002, Phys. Rev. A **65**, 033601.
Köhler, T., T. Gasenzer, and K. Burnett, 2003, Phys. Rev. A **67**, 013601.
Köhler, T., T. Gasenzer, P. S. Julienne, and K. Burnett, 2003, Phys. Rev. Lett. **91**, 230401.
Köhler, T., K. Góral, and T. Gasenzer, 2004, Phys. Rev. A **70**, 023613.
Köhler, T., E. Tiesinga, and P. S. Julienne, 2005, Phys. Rev. Lett. **94**, 020402.
Kokkelmans, S. J. J. M. F., 2002, private communication, quoted by E. A. Donley *et al.* (Donley *et al.*, 2002).
Kokkelmans, S. J. J. M. F., and M. J. Holland, 2002, Phys. Rev. Lett. **89**, 180401.
Kokkelmans, S. J. J. M. F., J. N. Milstein, M. L. Chiofalo, R. Walser, and M. J. Holland, 2002, Phys. Rev. A **65**, 053617.
Kokkelmans, S. J. J. M. F., G. V. Shlyapnikov, and C. Salomon, 2004, Phys. Rev. A **69**, 031602(R).
Kotochigova, S., E. Tiesinga, and P. S. Julienne, 2001, Phys. Rev. A **63**, 012517.
Kraemer, T., M. Mark, P. Waldburger, J. G. Danzl, C. Chin, B. Engeser, A. D. Lange, K. Pilch, A. Jaakkola, H.-C. Nägerl, and R. Grimm, 2006, Nature (London) **440**, 315.
Landau, L. D., 1932, Phys. Z. Sowjetunion **2**, 46.
Leggett, A. J., 1980, in *Modern Trends in the Theory of Condensed Matter*, edited by A. Pekalski and R. Przystawa (Springer-Verlag, Berlin), p. 13.
Leo, P. J., C. J. Williams, and P. S. Julienne, 2000, Phys. Rev. Lett. **85**, 2721.
Loftus, T., C. Regal, C. Ticknor, J. Bohn, and D. Jin, 2002, Phys. Rev. Lett. **88**, 173201.
Long, R., T. Steinmetz, P. Hommelhoff, W. Hänsel, T. W. Hänsch, and J. Reichel, 2003, Philos. Trans. R. Soc. London, Ser. A **361**, 1375.
Lovelace, C., 1964, Phys. Rev. **135**, B1225.
Luo, F., G. C. McBane, G. Kim, C. F. Giese, and W. R. Gentry,

1993, J. Chem. Phys. **98**, 3564.
Luttinger, J. M., and J. C. Ward, 1960, Phys. Rev. **118**, 1417.
Macek, J. H., and M. J. Cavagnero, 1998, Phys. Rev. A **58**, 348.
Mackie, M., A. Carmichael, M. Kostrun, R. J. Perkins, C. Xu, Y. Zhen, K.-A. Suominen, and J. Javanainen, 2002, e-print physics/0210131.
Mackie, M., K.-A. Suominen, and J. Javanainen, 2002, Phys. Rev. Lett. **89**, 180403.
Marcelis, B., E. G. M. van Kempen, B. J. Verhaar, and S. J. J. M. F. Kokkelmans, 2004, Phys. Rev. A **70**, 012701.
Mark, M., T. Kraemer, J. Herbig, C. Chin, H.-C. Nägerl, and R. Grimm, 2005, Europhys. Lett. **69**, 706.
Marte, A., T. Volz, J. Schuster, S. Dürr, G. Rempe, E. G. M. van Kempen, and B. J. Verhaar, 2002, Phys. Rev. Lett. **89**, 283202.
Matsubara, T., 1955, Prog. Theor. Phys. (Kyoto) **14**, 351.
Mies, F. H., P. S. Julienne, C. J. Williams, and M. Krauss, 1996, J. Res. Natl. Inst. Stand. Technol. **101**, 521.
Mies, F. H., and M. Raoult, 2000, Phys. Rev. A **62**, 012708.
Mies, F. H., and M. Raoult, 2004, Phys. Rev. A **70**, 012710.
Mies, F. H., E. Tiesinga, and P. S. Julienne, 2000, Phys. Rev. A **61**, 022721.
Mitra, A. N., 1962, Phys. Rev. **127**, 1342.
Moerdijk, A. J., B. J. Verhaar, and A. Axelsson, 1995, Phys. Rev. A **51**, 4852.
Moritz, H., T. Stöferle, K. Günter, M. Köhl, and T. Esslinger, 2005, Phys. Rev. Lett. **94**, 210401.
Mukaiyama, T., J. R. Abo-Shaeer, K. Xu, J. K. Chin, and W. Ketterle, 2003, Phys. Rev. Lett. **92**, 180402.
Müller, D., D. Z. Anderson, R. J. Grow, P. D. D. Schwindt, and E. A. Cornell, 1999, Phys. Rev. Lett. **83**, 5194.
Naidon, P., and F. Masnou-Seeuws, 2003, Phys. Rev. A **68**, 033612.
Naidon, P., and F. Masnou-Seeuws, 2006, Phys. Rev. A **73**, 043611.
Nielsen, E., and J. H. Macek, 1999, Phys. Rev. Lett. **83**, 1566.
Nikolov, A. N., E. E. Eyler, X. T. Wang, J. Li, H. Wang, W. C. Stwalley, and P. L. Gould, 1999, Phys. Rev. Lett. **82**, 703.
Nozières, P., and S. Schmitt-Rink, 1985, J. Low Temp. Phys. **59**, 195.
Nygaard, N., B. I. Schneider, and P. S. Julienne, 2006, Phys. Rev. A **73**, 042705.
O'Hara, K. M., S. L. Hemmer, M. E. Gehm, S. R. Granade, and J. E. Thomas, 2002, Science **298**, 2179.
Orso, G., L. P. Pitaevskii, S. Stringari, and M. Wouters, 2005, Phys. Rev. Lett. **95**, 060402.
Parish, M. M., B. Mihaila, B. D. Simons, and P. B. Littlewood, 2005, Phys. Rev. Lett. **94**, 240402.
Partridge, G. B., K. E. Strecker, R. I. Kamar, M. W. Jack, and R. G. Hulet, 2005, Phys. Rev. Lett. **95**, 020404.
Pauling, L., 1939, *The Nature of the Chemical Bond and the Structure of Molecules and Crystals* (Cornell University Press, Ithaca, NY).
Pazy, E., I. Tikhonenkov, Y. B. Band, M. Fleischhauer, and A. Vardi, 2005, Phys. Rev. Lett. **95**, 170403.
Pazy, E., A. Vardi, and Y. B. Band, 2004, Phys. Rev. Lett. **93**, 120409.
Perali, A., P. Pieri, and G. C. Strinati, 2005, Phys. Rev. Lett. **95**, 010407.
Petrov, D. S., 2004, Phys. Rev. Lett. **93**, 143201.
Petrov, D. S., C. Salomon, and G. V. Shlyapnikov, 2004, Phys. Rev. Lett. **93**, 090404.
Petrov, D. S., C. Salomon, and G. V. Shlyapnikov, 2005a, J. Phys. B **38**, S645.
Petrov, D. S., C. Salomon, and G. V. Shlyapnikov, 2005b, Phys. Rev. A **71**, 012708.
Pitaevskii, L. P., 1961, Sov. Phys. JETP **13**, 451.
Proukakis, N. P., K. Burnett, and H. T. C. Stoof, 1998, Phys. Rev. A **57**, 1230.
Randeria, M., 1995, in *Bose-Einstein Condensation*, edited by A. Griffin, D. W. Snoke, and S. Stringari (Cambridge University Press, Cambridge), p. 355.
Ranninger, J., and S. Robaszkiewicz, 1985, Physica B & C **135**, 468.
Regal, C. A., M. Greiner, and D. S. Jin, 2004a, Phys. Rev. Lett. **92**, 083201.
Regal, C. A., M. Greiner, and D. S. Jin, 2004b, Phys. Rev. Lett. **92**, 040403.
Regal, C. A., M. Greiner, and D. S. Jin, 2004c, Phys. Rev. Lett. **92**, 040403.
Regal, C. A., and D. S. Jin, 2003, Phys. Rev. Lett. **90**, 230404.
Regal, C. A., C. Ticknor, J. L. Bohn, and D. S. Jin, 2003a, Nature (London) **424**, 47.
Regal, C. A., C. Ticknor, J. L. Bohn, and D. S. Jin, 2003b, Phys. Rev. Lett. **90**, 053201.
Rey, A. M., B. L. Hu, E. Calzetta, and C. W. Clark, 2005, Phys. Rev. A **72**, 023604.
Rice, O. K., 1933, J. Chem. Phys. **1**, 375.
Roberts, J. L., N. R. Claussen, J. P. Burke, C. H. Greene, E. A. Cornell, and C. E. Wieman, 1998, Phys. Rev. Lett. **81**, 5109.
Roberts, J. L., N. R. Claussen, S. L. Cornish, E. A. Donley, E. A. Cornell, and C. E. Wieman, 2000a, Phys. Rev. Lett. **86**, 4211.
Roberts, J. L., N. R. Claussen, S. L. Cornish, and C. E. Wieman, 2000b, Phys. Rev. Lett. **85**, 728.
Sage, J. M., S. Sainis, T. Bergeman, and D. DeMille, 2005, Phys. Rev. Lett. **94**, 203001.
Sandars, P. G. H., 1975, in *Atomic Physics 4*, edited by G. zu Putlitz (Plenum, New York), p. 71.
Schöllkopf, W., and J. P. Toennies, 1994, Science **266**, 1345.
Schrieffer, J. R., 1964, *Theory of Superconductivity* (Benjamin, New York).
Schunck, C. H., M. W. Zwierlein, C. A. Stan, S. M. F. Raupach, W. Ketterle, A. Simoni, E. Tiesinga, C. J. Williams, and P. S. Julienne, 2005, Phys. Rev. A **71**, 045601.
Schwinger, J., 1947a, Harvard lecture notes, quoted by H. A. Bethe (Bethe, 1949).
Schwinger, J., 1947b, Phys. Rev. **72**, 738.
Schwinger, J., 1961, J. Math. Phys. **2**, 407.
Simonucci, S., P. Pieri, and G. C. Strinati, 2005, Europhys. Lett. **69**, 713.
Stan, C. A., M. W. Zwierlein, C. H. Schunck, S. M. F. Raupach, and W. Ketterle, 2004, Phys. Rev. Lett. **93**, 143001.
Stenger, J., S. Inouye, M. R. Andrews, H.-J. Miesner, D. M. Stamper-Kurn, and W. Ketterle, 1999, Phys. Rev. Lett. **82**, 2422.
Stoll, M., and T. Köhler, 2005, Phys. Rev. A **72**, 022714.
Stoof, H. T. C., A. M. L. Janssen, J. M. V. A. Koelman, and B. J. Verhaar, 1989, Phys. Rev. A **39**, 3157.
Stoof, H. T. C., J. M. V. A. Koelman, and B. J. Verhaar, 1988, Phys. Rev. B **38**, 4688.
Strecker, K. E., G. B. Partridge, and R. G. Hulet, 2003, Phys. Rev. Lett. **91**, 080406.
Stwalley, W. C., 1976, Phys. Rev. Lett. **37**, 1628.
Szymańska, M. H., K. Góral, T. Köhler, and K. Burnett, 2005, Phys. Rev. A **72**, 013610.

Takekoshi, T., B. M. Patterson, and R. J. Knize, 1999, Phys. Rev. A **59**, R5.
Tang, K. T., J. P. Toennies, and C. L. Yiu, 1995, Phys. Rev. Lett. **74**, 1546.
Taylor, J. R., 1972, *Scattering Theory* (Wiley, New York).
Thalhammer, G., K. Winkler, F. Lang, S. Schmid, R. Grimm, and J. H. Denschlag, 2006, Phys. Rev. Lett. **96**, 050402.
Theis, M., G. Thalhammer, K. Winkler, M. Hellwig, G. Ruff, R. Grimm, and J. H. Denschlag, 2004, Phys. Rev. Lett. **93**, 123001.
Thompson, S., E. Hodby, and C. Wieman, 2005a, Phys. Rev. Lett. **95**, 190404.
Thompson, S. T., E. Hodby, and C. E. Wieman, 2005b, Phys. Rev. Lett. **94**, 020401.
Thywissen, J. H., R. M. Westervelt, and M. Prentiss, 1999, Phys. Rev. Lett. **83**, 3762.
Tiesinga, E., B. J. Verhaar, and H. T. C. Stoof, 1993, Phys. Rev. A **47**, 4114.
Tiesinga, E., C. J. Williams, F. H. Mies, and P. S. Julienne, 2000, Phys. Rev. A **61**, 063416.
Timmermans, E., P. Tommasini, R. Côté, M. Hussein, and A. Kerman, 1998, e-print cond-mat/9805323.
Timmermans, E., P. Tommasini, R. Coté, M. Hussein, and A. Kerman, 1999a, Phys. Rev. Lett. **83**, 2691.
Timmermans, E., P. Tommasini, M. Hussein, and A. Kerman, 1999b, Phys. Rep. **315**, 199.
Tommasini, P., E. Timmermans, M. Hussein, and A. Kerman, 1998, e-print cond-mat/9804015.
Uang, Y. H., R. F. Ferrante, and W. C. Stwalley, 1981, J. Chem. Phys. **74**, 6267.
Uang, Y.-H., and W. C. Stwalley, 1980, Phys. Rev. Lett. **45**, 627.
Uehling, E. A., and G. E. Uhlenbeck, 1933, Phys. Rev. **43**, 552.
van Abeelen, F. A., and B. J. Verhaar, 1998, unpublished, quoted by S. Inouye *et al.* (Inouye *et al*, 1998).
van Abeelen, F. A., and B. J. Verhaar, 1999, Phys. Rev. Lett. **83**, 1550.
van Kempen, E. G. M., S. J. J. M. F. Kokkelmans, D. J. Heinzen, and B. J. Verhaar, 2002, Phys. Rev. Lett. **88**, 093201.
van Kempen, E. G. M., and B. J. Verhaar, 2004, private communication, quoted by S. Dürr *et al.* (Dürr *et al.*, 2004a).
Volz, T., S. Dürr, S. Ernst, A. Marte, and G. Rempe, 2003, Phys. Rev. A **68**, 010702(R).
Volz, T., S. Dürr, N. Syassen, G. Rempe, E. van Kempen, and S. Kokkelmans, 2005, Phys. Rev. A **72**, 010704.
Vuletic, V., A. J. Kerman, C. Chin, and S. Chu, 1998, Phys. Rev. Lett. **82**, 1406.
Wang, D., J. Qi, M. F. Stone, O. Nikolayeva, H. Wang, B. Hattaway, S. D. Gensemer, P. L. Gould, E. E. Eyler, and W. C. Stwalley, 2004, Phys. Rev. Lett. **93**, 243005.
Weber, T., J. Herbig, M. Mark, H.-C. Nägerl, and R. Grimm, 2003, Science **299**, 232.
Weinberg, S., 1996, *The Quantum Theory of Fields* (Cambridge University Press, Cambridge, England).
Weiner, J., V. S. Bagnato, S. Zilio, and P. S. Julienne, 1999, Rev. Mod. Phys. **71**, 1.
Weinstein, J. D., and K. G. Libbrecht, 1995, Phys. Rev. A **52**, 4004.
Wick, G. C., 1950, Phys. Rev. **80**, 268.
Wigner, E. P., 1927, Z. Phys. **43**, 624.
Wigner, E. P., 1948, Phys. Rev. **73**, 1002.
Williams, J. E., T. Nikuni, N. Nygaard, and C. W. Clark, 2004, J. Phys. B **37**, 351.
Williams, J. E., N. Nygaard, and C. W. Clark, 2004, New J. Phys. **6**, 123.
Williams, J. E., N. Nygaard, and C. W. Clark, 2006, New J. Phys. **8**, 150.
Wouters, M., and G. Orso, 2006, Phys. Rev. A **73**, 012707.
Wynar, R., R. S. Freeland, D. J. Han, C. Ryu, and D. J. Heinzen, 2000, Science **287**, 1016.
Xu, K., T. Mukaiyama, J. R. Abo-Shaeer, J. K. Chin, D. E. Miller, and W. Ketterle, 2003, Phys. Rev. Lett. **91**, 210402.
Yamaguchi, Y., 1954, Phys. Rev. **95**, 1628.
Yan, Z.-C., J. F. Babb, A. Dalgarno, and G. W. F. Drake, 1996, Phys. Rev. A **54**, 2824.
Yurovsky, V. A., and A. Ben-Reuven, 1998, J. Phys. B **31**, 1.
Yurovsky, V. A., and A. Ben-Reuven, 2003a, J. Phys. B **36**, 335.
Yurovsky, V. A., and A. Ben-Reuven, 2003b, Phys. Rev. A **67**, 043611.
Yurovsky, V. A., and A. Ben-Reuven, 2004, Phys. Rev. A **70**, 013613.
Yurovsky, V. A., and A. Ben-Reuven, 2005, Phys. Rev. A **72**, 053618.
Yurovsky, V. A., A. Ben-Reuven, P. S. Julienne, and Y. B. Band, 1999a, J. Phys. B **32**, 1845.
Yurovsky, V. A., A. Ben-Reuven, P. S. Julienne, and C. J. Williams, 1999b, Phys. Rev. A **60**, R765.
Yurovsky, V. A., A. Ben-Reuven, P. S. Julienne, and C. J. Williams, 2000, Phys. Rev. A **62**, 043605.
Zener, C., 1932, Proc. R. Soc. London, Ser. A **137**, 696.
Zhang, J., E. G. M. van Kempen, T. Bourdel, L. Khaykovich, J. Cubizolles, F. Chevy, M. Teichmann, L. Tarruell, S. J. J. M. F. Kokkelmans, and C. Salomon, 2004, Phys. Rev. A **70**, 030702(R).
Zoller, P., 2002, Nature (London) **417**, 493.
Zwierlein, M. W., J. R. Abo-Shaeer, A. Schirotzek, C. H. Schunck, and W. Ketterle, 2005, Nature (London) **435**, 1047.
Zwierlein, M. W., C. A. Stan, C. H. Schunck, S. M. F. Raupach, S. Gupta, Z. Hadzibabic, and W. Ketterle, 2003, Phys. Rev. Lett. **91**, 250401.
Zwierlein, M. W., C. A. Stan, C. H. Schunck, S. M. F. Raupach, A. J. Kerman, and W. Ketterle, 2004, Phys. Rev. Lett. **92**, 120403.